Molecular interactions of ErbB receptor tyrosine kinases – with an outlook on their therapeutic targeting

Elza Friedländer

DEBRECENI EGYETEM
ORVOS ÉS EGÉSZSÉGTUDOMÁNYI CENTRUM
BIOFIZIKAI ÉS SEJTBIOLÓGIAI INTÉZET

DEBRECEN, 2008.

Table of Contents

1. Introduction 4
2. Background 5
2.1. The ErbB family 5
2.2. Structure and function of ErbB kinases 5
2.2.1 Mechanisms of ErbB receptor activation 6
2.2.2. Distinct molecular properties of ErbB2 8
2.2.3. Homo- and heterodimers and the central role of ErbB2 in heterodimerization 9
2.2.4. Intracellular regulation of ErbB activation 10
2.3. Intracellular signaling pathways 10
2.3.1. The Phosphatidylinositol 3-kinase/ Akt pathway 12
2.3.2. Phospholipase Cγ 12
2.3.3. Signal transducers and activators of transcription (Stat) proteins 13
2.3.4. Role of Src kinase in ErbB-signaling 13
2.4. Role of ErbBs in carcinogenesis 13
2.4.1. ErbB1 13
2.4.2. ErbB2 14
2.4.3. ErbB3 and ErbB4 14
2.5. Molecular mechanisms of ErbB targeted antibody therapy – trastuzumab as an example 15
2.5.1. Trastuzumab (rhu4D5, Herceptin®) – the first humanized monoclonal antibody against ErbB2 15
2.5.2. ErbB2 activation, internalization and degradation via trastuzumab binding 16
2.5.3 Antibody mediated cellular cytotoxicity – an important mechanism of trastuzumab action *in vitro* 17
2.5.4. Inhibition of cell cycle progression, angiogenesis and migration 17
2.6. Other ErbB targeted antibodies 18
2.6.1. Antibodies targeting ErbB1 18
2.6.2. Antibodies targeting ErbB2 19
2.6.3. Engineered immunological tools against ErbBs 19
2.7. Trastuzumab resistance – a major clinical problem 21
2.7.1. Steric hindrance 21
2.7.2. Overexpression and cross-talk with the interaction partners of ErbB2 21
2.7.3. Ineffectiveness of ADCC 22
3. Aims 24
4. Materials and Methods 25
4.1. Cells 25
4.2. Western blot 25
4.3. Ca^{2+} measurements 26
4.4. Fluorescence Correlation Spectroscopy (FCS) 27
4.4.1. Origin and analysis of the autocorrelation function in fluctuation measurements 27

4.4.2 Measurement of fluorescence autocorrelation in ErbB1-eGFP expressing CHO cells 30
4.5 Fluorescence recovery after photobleaching (FRAP) 31
4.6. Antibodies 33
4.7. Determination of receptor numbers and trastuzumab dissociation constants 34
4.8. Immunofluorescent labeling 34
4.9. Preparation of chemically coupled trastuzumab and EGF microspheres 35
4.10. Cell stimulation with derivatized paramagnetic microbeads 35
4.11. Confocal Laser Scanning Microscopy 36
4.12. Image Analysis 36
5. Results and Discussion 38
5.1. Fluorescence correlation spectroscopy gives new insight into the activation mechanism of ErbB1 38
5.1.1. The ErbB1-eGFP fluorescent chimera created for FCS measurements is functionally active 38
5.1.2 Diffusion rate of ErbB1 decreases upon EGF stimulation 40
5.1.3 ErbB1 could exist also as pre-formed di- or oligomers 45
5.1.4. Complementarity of Fluorescence Recovery After Photobleaching and FCS in resolving the mobility of ErbB1 48
5.2. Derivatized microbeads as a novel tool for assessing ErbB activation 50
5.2.1. EGF and trastuzumab conjugated microspheres efficiently evoke ErbB autophosphorylation 51
5.2.2. Focal stimulation by EGF and trastuzumab microspheres yields a well-localized activation process without lateral signal spreading 51
5.2.3. EGF-bound ErbB1 transactivates ErbB2 but trastuzumab-bound ErbB2 does not transactivate ErbB1 53
5.2.4. Transactivation of ErbB2 via ligand bound ErbB1 depends on receptor density 55
5.3. Steric hindrance: a possible trastuzumab resistance mechanism 58
5.3.1. ErbB2 expression and affinity for trastuzumab in trastuzumab sensitive and resistant cell lines 58
5.3.2. Trastuzumab microspheres are effective even if trastuzumab in solution has no effect 59
5.3.3. Membrane-associated mucin, MUC4, can be one cause of decreased trastuzumab binding and efficiency 61
6. Conclusions 64
7. References 66
8. Acknowledgements 82
10. Publications 83
10.1. Related In extenso publications 83
10.2. Other publications 84
10.3. Lectures and posters 84

1. Introduction

Gene amplification, overexpression or mutation of growth factor receptors, including members of the ErbB family, can cause increased signaling activity and are associated with poor prognosis in most of the human cancers. ErbB molecules have high affinity for other members of the family and are proposed to form homo- or heterodimers when activated. Ligand binding can be a necessary condition or enhancer of activation, resulting in receptor transphosphorylation on tyrosine residues of the activation loop leading to significantly enhanced kinase activity. Subsequent phosphorylation of tyrosine residues on the carboxy terminal domain of ErbB molecules enables recruitment and consequential activation of intracellular signaling molecules containing phosphotyrosine binding and Src homology domains. Heterodimerization of ErbBs compared to homodimerization results in additional phosphotyrosine residues for the recruitment of binding partners yielding to more potent mitogenic signals. Interrupting these signaling pathways by antibodies or tyrosine kinase inhibitors have good perspectives in personalized therapies because of their selectivity, and better tolerable side effects. At the same time, these targeted therapies require an intimate knowledge of the molecular details of activation ErbB receptor activation as well as transactivation between the family members.

The action of therapeutic antibodies is complex and in addition to their target specificity it is based on their structure. They can manipulate signaling by stimulating transmembrane receptors resulting in their down regulation, or by interrupting their interactions with adjacent signaling partners. As immunologically active molecules, they can evoke complement-dependent or antibody-mediated cellular cytotoxicity. Trastuzumab, targeting ErbB2, was the first humanized antibody approved against a human solid tumor. Clinical experiences with this IgG1 antibody are diverse. A major problem is trastuzumab resistance, which occurs in 60 to 80% of ErbB2 overexpressing breast cancers. Information on molecular interactions of ErbB2 with members of the ErbB family or with other cell surface molecules such as syalomucine complexes may shed light on certain mechanisms of trastuzumab resistance.

2. Background

2.1. The ErbB family

In 1984, Downward and colleagues have discovered that the oncogene v-erbB encoded by the avian erythroblastosis virus shows high similarity to the human epidermal growth factor receptor (EGFR, consequently also termed ErbB1) [1]. Other publications have reported close relation between the neu gene that was identified from chemically induced rat neuroglioblastoma and the gene of EGFR [2,3]. Independent groups have isolated human EGFR related genes, HER2 [4] and c-erbB2 [5], and discovered that a gene related to EGFR is amplified in human breast cancer cell lines [6]. All of these were found to be homologous to the rat neu gene, and thus members of the ErbB family.

The ErbB family of class I growth factor receptor tyrosine kinases consists of four members, EGFR (ErbB1, HER1) ErbB2 (HER2, neu), ErbB3 (HER3) and ErbB4 (HER4).

Ligands of the ErbB receptor family members can regulate cellular functions in auto-, para-, and endocrine ways; they can be intramembrane proteins, or proteolytic products of intramembrane proteins circulating in the blood plasma. ErbB ligands can be divided into three groups:

- epidermal growth factor-like ligands (epidermal growth factor, transforming growth factor α, amphiregulin) binding mostly to ErbB1
- neuregulins (or heregulins, NRGα, NRGβ) binding to ErbB3 and ErbB4
- heparin binding EGF (HB-EGF) binding to ErbB1, ErbB3 and ErbB4

ErbB2 does not have a known soluble ligand.

2.2. Structure and function of ErbB kinases

ErbB kinases are large glycoproteins with an extracellular domain, a single-chain membrane spanning domain, and an intracellular tyrosine kinase domain which is flanked by non-catalytic regulatory regions [7]. The extracellular domain consists of four (sub)domains designated L1, CR1, L2 and CR2, or - in another nomenclature -domains I-IV. L domains (I and III) form six turn right handed β sheets that are capped at each end by an α helix and a disulphide bond, whereas CR domains (II and IV) form laminin-like folds [8].

Domains I and III serve as ligand binding sites. By binding simultaneously to both domains, the ligand may alter their relative orientation leading to conformational change of domain II [9]. This latter holds a dimerization arm that plays an essential role in ErbB homo- and heterodimerization. In all ErbB proteins except ErbB2, a direct intramolecular interaction between the cysteine reach regions of domains II and IV restrains the interaction between domains II and III, which is characteristic for the inactive state [10,11]. More than that, the intramolecular tether formed by domains II and IV buries the dimerization arm at domain II, so that the tethered form cannot dimerize and appears to be autoinhibited [10-12]. The tethered form has only low affinity for ligands, as the ligand binding areas are too far in the tethered configuration, so a single ligand cannot bind to both sides. After ligand binding, the extracellular domain of the molecule becomes "extended" - the conformational state required for the high affinity to its ligand - exposing both ligand binding areas and also the dimerization arm (Fig. 1. A, B) [13].

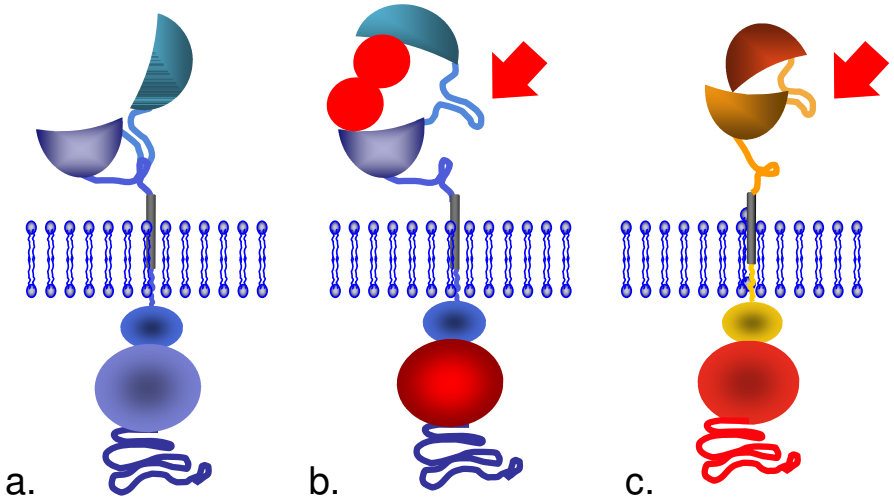

Fig. 1. Structure of ErbB1 and ErbB2 molecules
Extracellular domains of ErbB1 show a tethered conformation (a) hiding the dimerization arm. Upon EGF binding (b), the dimerization arm (arrow) is exposed, and the receptor is ready to interact with and transphosphorylate another ErbB. (c) The ligand binding site of ErbB2 is buried, and the dimerization arm (arrow) is exposed without any stimulation.

2.2.1 Mechanisms of ErbB receptor activation

According to a commonly accepted theory, dimerization is necessary for ErbB receptor autophosphorylation, and leads to significant enhancement of the kinase domain activity [14].

ErbB3 is the only exception as it has an impaired kinase unit and can transmit signals only when a dimerization partner is present [15].

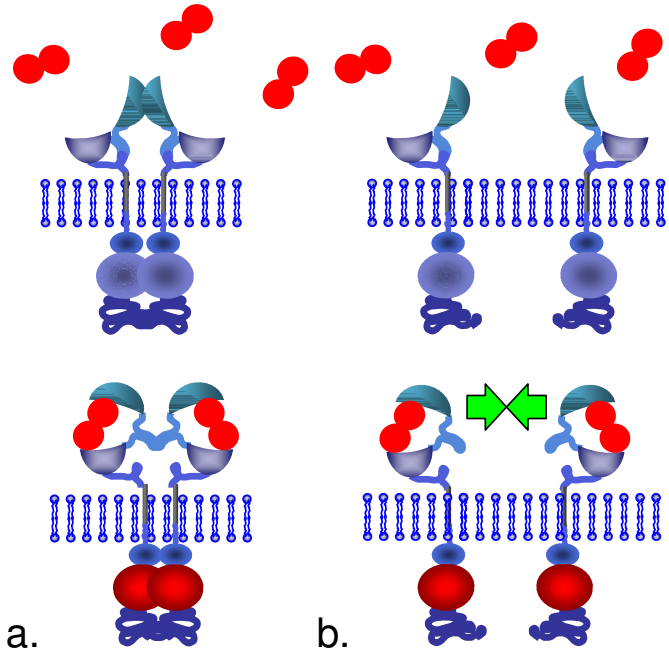

Fig. 2. Mechanisms of ErbB activation
Two models of ErbB receptor activation have been proposed. The first suggests preformed ErbB dimers on the cell surface (a) that undergo conformational change(s) and become activated in the presence of EGF, whereas the second predicts di- or multimerization of activated receptors after ligand binding (b)

The precise process of ErbB1 activation is not yet known in detail. Two models have been proposed [16], which are illustrated in Fig. 2. The first underlines the role of ligand binding and a still uncharacterized consequential conformational change in the transmembrane domain leading to activation of already pre-dimerized receptors. This theory seems to be supported by the observation that some point mutations of the transmembrane domain led to increased kinase activity without EGF stimulation [17], as well as the presence of high affinity preformed dimers shown by FRET measurements [16]. Extracted ErbB1 molecules have also shown spontaneous activation when diluted in detergents or during affinity chromatography studies [18]. The theory of allosteric oligomerization [19,20] is more generally accepted. Here, intramolecular interactions evoked upon EGF binding are proposed to result in aggregation of ErbB molecules leading to higher affinity for the ligand and to kinase domain activation.

Several independent experimental results support this theory. An electron microscopic study has proven that ErbB1 molecules labeled with immunogold are aggregated upon EGF stimulation [21]. Immunohistochemical studies using bivalent antibodies with the ability to cross-link the receptor could evoke ErbB1 activation without the presence of EGF [22], although in this case the possibility of conformational change caused by the antibody cannot be excluded. Activation kinetics of dissolved ErbB1 receptors were a secondary function of concentration [19], and chemical cross-linking also activated the kinase domain of ErbB1 [23].

EGF functionalized microbead studies on ErbB1 overexpressing cells have shown contradictory results. Verveer et al. [24] reported that focal stimulation generated phosphorylated ErbB1 patches with rapid lateral spreading of ErbB1 activation over the entire cell. The latter phenomenon was attributed to dissociation of activated ErbB1 from the dimers and activation of ErbB1 molecules in the absence of ligand, i.e., via re-dimerization outside of the microsphere-stimulated area. In contrast, others have reported focal ErbB1 activation induced by EGF-linked microspheres and Shc translocation to these sites [25,26]. On ErbB1/green fluorescent protein transfected Chinese hamster ovary and A431 cells, the internalization of the EGF coated microspheres occurred rapidly but required ErbB1 activation. These latter observations appear to be more consistent with the presence of preformed dimers or clusters – which are likely localized to membrane lipid rafts [27] – as signaling units than with the idea of single ErbB1 molecules, however, the presence of hindered diffusion by membrane boundaries limiting the lateral signal spreading cannot be excluded either.

2.2.2. Distinct molecular properties of ErbB2

ErbB2 has unique properties as it has no known ligand, suggesting that it may function only as a dimerization partner or a co-receptor for the other members of the family [15,28]. Moreover, even without binding a ligand, the extracellular domain of ErbB2 shows extended configuration exposing the dimerization arm (see Fig. 1.C) suggesting that it may be autoactivated, and the ligand binding areas of its domains I and III are in contact similar to the conformation of these same sites in the case of ligand-bound ErbB1 [13]. This property suggests that ErbB2 alone can cause transformation if overexpressed, however, biophysical studies failed to detect significant ErbB2 homodimerization in solution [29]. On the other hand, in the cellular environment where ErbB2 may be regulated in manifold intricate ways, ErbB2 homodimerization [27,30] and autophosphorylation [31] is often detected in tumor cells overexpressing this protein.

2.2.3. Homo- and heterodimers and the central role of ErbB2 in heterodimerization

After EGF binding, ErbB1 can form a dimer with the ligandless ErbB2. Members of this ligand-induced (primary) dimer possess high tyrosine kinase activity, transphosphorylate each other starting intracellular signaling cascades, then dissociate. The activated ErbB2 may form a secondary dimer with the kinase domain impaired ErbB3 or another ErbB2, and by phosphorylating it, activate other, distinct signaling pathways. When neuregulins bind to ErbB3 or ErbB4, these form a primary dimer with ErbB2, while ErbB2 thus activated can form secondary dimers with ErbB1 or other members of the family. Intracellular activation patterns of the three primary dimers are different, and this is also true for the secondary dimers, which greatly diversifies the signaling capacity of the ErbB family [32].

Ligand affinities also differ among the dimerization partners. ErbB3 homodimers have higher affinity to NRGs than ErbB4 containing ones, and heterodimerization of both with ErbB2 further increases ligand affinity. Presence of ErbB1/ErbB3 and ErbB1/ErbB4 heterodimers have been also described, but they appeared only on cells where no ErbB2 was available, and these associations were rare. ErbB2 has a central role in heterodimer formation. On cells where ErbB2 is expressed together with other members of the ErbB family, ErbB2 is the preferred dimerization partner [33]. Dimers containing ErbB2 are more stable; they have higher affinity to ligands and owe more potent tyrosine kinase activity. It is important to note that ErbB2 containing dimers are able to avoid degradation after internalization and they readily recirculate to the cell membrane. As opposed to this, ErbB1 containing dimers are down-regulated very fast after EGF activation. ErbB1 down-regulation after activation by EGF may be an important negative feedback in the control of epithelial cell proliferation. On cells with ErbB2 overexpression, spontaneous homodimerization of ErbB2 molecules can be observed because of the high receptor density [34]. ErbB2 homodimers are also present on cells if the transmembrane domain is mutated as it was shown in nitrosourea induced neuroblastoma cells [35], but similar mutations in human cancers have not been detected.

ErbB2/ErbB3 is the most mitogenic ErbB dimer, because ErbB2 enhances the ligand affinity by modulating the rate of ligand dissociation and widens the ligand spectrum of ErbB3 towards EGF-like ligands. Phosphorylated ErbB2 serves activation sites for Shc coupling to the MAPK pathway, whereas ErbB3 if activated is able to recruit PI3K, and thus to signal via the Akt pathway [15]. This capacity of signaling through the MAPK pathway leading to proliferation and through the PI3K/Akt pathway leading to survival, combined with

the prolonged signaling caused by evaded internalization [36] explains why the presence of the ErbB2/ErbB3 heterodimer is a bad prognostic factor.

2.2.4. Intracellular regulation of ErbB activation

The intracellular kinase domain lacks autoinhibitory regulation [37], as most kinase domains of receptor tyrosine kinases are inactive until ligand-induced dimerization and auto/transphosphorylation occurs [38]. This latter normally induces significant conformational changes in the kinase domain that allow substrate binding and promote phosphotransfer. As an exception, the kinase domain of ErbB1 does not require such phosphorylation of its activation loop, and assumes a constitutively active conformation, implying that ligand mediated dimerization (or a conformational change upon ligand binding) could be a key event in regulating ErbB1 kinase activity by delivering the substrate – the intracellular domain of another ErbB1 – for transphosphorylation [13].

Activated ErbB family homo- or heterodimers and multimers are internalized to endosomes where the ligand dissociates from the receptor, and the receptor either recycles back to the cell surface, or, after c-Cbl mediated ubiquitination, is degraded in lysosomes [39-41]. ErbB2 appears to be resistant to internalization [42] and ErbB2 containing heterodimer or heteromultimer complexes are preferentially recycled to the cell membrane and thus they can send prolonged proliferation signals to the cell nucleus [34].

2.3. Intracellular signaling pathways

The intracellular ErbB-triggered pathway system is highly complex [28] (Fig. 3.). Activation of an ErbB kinase leads to the phosphorylation of key tyrosine residues within its carboxy terminal portion and thereby provides specific docking sites for cytoplasmic proteins. The main signal transmitting pathways are (Fig. 3):

- Ras/Raf/mitogen-activated protein kinase (MAPK) pathway.
- Phosphatidylinositol 3-kinase/Akt pathway.
- Phospholipase Cγ pathway.
- Signal transducers and activators of transcription (STAT) pathway.

In addition, Src [43] and Rho kinase [44,45] may also be important in ErbB-based signaling.

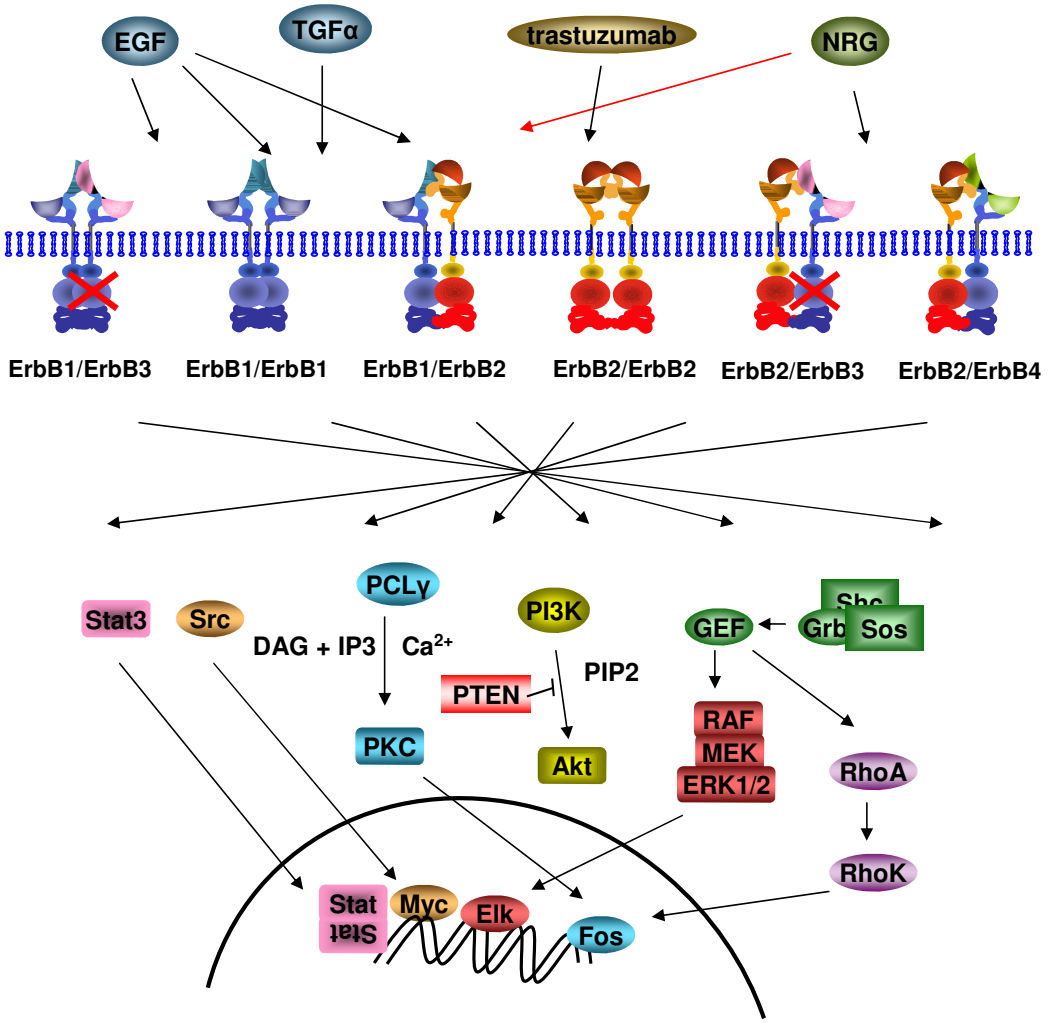

Fig. 3. The ErbB network
The figure shows the most potent homo- and heterodimers of the members of ErbB family. Activated receptors cross-phosphorylate their intracellular domains. To the phosphorylated sites, small intracellular kinases like PI3K or Src, phospholipases like PLCγ, or adapter proteins can dock, and transmit the signal into the cell nucleus. Stat-3, ERK1/2, Akt, Src and PKC molecules are key activators, with direct effect on cell survival and proliferation.

2.3.1. The Ras/Raf/MAPK pathway

Ras/Raf/MAPK pathway [46] is a critically important route that regulates cell proliferation and survival. Following ErbB trans-phosphorylation, a complex formed by adaptor proteins Grb2 and Sos binds either directly, or through another adaptor molecule Shc, to specific phosphorylated ErbB docking sites. This interaction leads to a conformational change of Sos,

now able to recruit Ras-GDP, resulting in Ras activation (Ras-GTP). Ras-GTP activates Raf-1 that, through intermediate steps, phosphorylates ERK1/2 (extracellular signal-regulated kinases 1 and 2). Activated ERK1/2 initiate a signaling cascade leading to the phosphorylation of transcription factors (like Elk-1 or c-myc) involved in cell proliferation.

2.3.2. The Phosphatidylinositol 3-kinase/ Akt pathway

ErbB activated Akt is involved in cell growth, invasion and migration [47]. Moreover, activation of this pathway leads to anti-apoptotic processes. Phosphatidylinositol 3-kinase (PI3K) is a dimeric enzyme composed of a regulatory p85 subunit, responsible for binding to specific docking sites on ErbB receptors, and a catalytic p110 subunit that generates the second messenger phosphatidylinositol 3,4,5-trisphosphate, which is necessary for serine/threonine phosphorylation, thus, the activation of the Akt kinase. The principal mechanism that drives ErbB-dependent PI3K activation is predominantly the dimerization of ErbB2 with ErbB3 [48]. In fact, direct docking sites for p85 are absent on ErbB1. In contrast, docking sites for p85 are abundant on ErbB3. ErbB1, however, can activate the p85 subunit through the docking protein Gab-1. PTEN (Phosphatase and tensin homolog deleted on chromosome TEN), a major tumor suppressor phosphatase in human, is also an important element of this pathway as it dephosphorylates phosphatidylinositol 3,4,5-triphosphate [49]. PTEN is differentially expressed in a wide group of cancers and may be involved in trastuzumab responsiveness [49,50].

2.3.3. Phospholipase Cγ

Phospholipase Cγ (PLCγ) [51] has been described to directly interact with activated ErbB1. PLCγ hydrolyzes phosphatidylinositol 4,5-bisphosphate (PIP_2) to inositol-1,4,5-trisphosphate (IP_3), a second messenger inducing intracellular calcium release leading to short and long term cellular events, and 1,2-diacylglycerol, a cofactor in protein kinase C (PKC) activation. PKCβII and PKCε activation has effects on cell proliferation and survival [52], and can, in turn, result in ERK1/2 activation, whereas other isoforms of PKC, like PKCα, PKCβI and PKCδ are considered to mediate growth inhibitory and apoptotic signals [52].

2.3.4. Signal transducers and activators of transcription (Stat) proteins

Stats interact with phosphotyrosine residues via their Src homology 2 (SH2) domains and, on dimerization, translocate to the nucleus where occupation of specific DNA sites results in transcription [53,54]. Constitutive activation of Stat proteins and especially Stat3 has been found in numerous primary cancers and tumor-derived cell lines [55]. Augmented activity of transmembrane tyrosine kinases, such as ErbB1 and ErbB2, promotes persistent Stat3 activation, which contributes to oncogenesis and tumor progression.

2.3.5. Role of Src kinase in ErbB-signaling

Src is the archetypal non-receptor tyrosine kinase that plays a critical role in the regulation of cell proliferation, migration, adhesion and angiogenesis [56]. Src, which is located in the cytosol but is membrane-anchored, interacts with a series of signal transducers, including Focal Adhesion Kinase (FAK), PI3K, and Stat proteins [57]. Although Src functions independently, it also cooperates with other receptor tyrosine kinases. The interaction between ErbB receptors and Src is complex. On the one hand, Src serves as a signal transducer and an enhancer of ErbB-activation. On the other, it may be involved in resistance to ErbB targeted therapies via independent activation or association with other receptors [58].

2.4. Role of ErbBs in carcinogenesis

Growth factors and their receptors are important and sensitive regulatory elements of the growth and differentiation processes of cells, tissues and the whole organism. Damage to their signaling pathways at any level can lead to malignant transformation. ErbB proteins often play an important role in the first steps of malignant transformation. In addition to deregulation of their signaling pathways, both mutations causing constitutive or ligand-independent activation and overexpression – mostly based on gene amplification – of ErbB proteins are prominent causes of human tumors [59].

2.4.1. ErbB1

Overexpression of ErbB1 was shown in various cancers like ovarian [60], cervical [61], esophageal [62] bladder [63] and lung cancer [64]. ErbB1 is also overexpressed in breast cancer [65]. It is generally accepted that overexpression of ErbB1 drives cell survival and proliferation pathways similar to those activated by the regularly expressed receptor.

Mutations, however, also appear to play a distinct role in carcinogenesis. The most frequent class III mutants (ErbB1vIII, delta2-7 EGFR) contain a deletion within the extracellular domain leading to a conformational change resulting in constitutive kinase activation [66]. This form is a frequent genomic variant in brain, breast and non small cell lung cancers [67,68], and its importance is underlined by the finding that the ErbB1-specific tyrosine kinase inhibitors gefitinib and erlotinib are largely ineffective in tumors expressing ErbB1vIII [69]. ErbB1vIII and also the wild type ErbB1 is also frequent in glioblastomas [70], and its presence is thought to confer radiation resistance to the tumor [71].

2.4.2. ErbB2

ErbB2 is well known for its oncological relevance, as its overexpression can be demonstrated in many tumor types. Amplification of the ErbB2 gene was first described in human breast and ovarian cancer [72], but often occurs in other human malignancies. ErbB2 is overexpressed in 60% of the inflammatory and in 25% of the non-inflammatory ductal invasive breast cancers [73], in 60% of Wilm's tumors and in 44% of the carcinomas of the bladder [74]. In the case of tumors of various other origins, the level and occurrence of overexpression is not that high, but also significant, like in colon, pancreas, ovarian, lung and head-neck tumors and non small cell lung cancer. [74-77]. In neural tumors, especially in glioblastomas, the presence of ErbB2 applies to the peripheral phenotype [78], and in some cases, ErbB2/ErbB3 heterodimer – neuregulin-1 autocrin loops lead to constitutive activation of the signaling cascade [79]. ErbB2/ErbB3 complexes were also shown in non-small cell lung cancer [80] and breast cancer [81].

ErbB2 overexpression is a relatively early event in cancer pathogenesis according to immunohistological studies that show its frequent occurrence in pre-invasive lesions and *in situ* ductal carcinomas [82,83]. This uncontrolled ErbB2 expression can drive tumor proliferation, and play an important role in aggressive tumor behavior associated with poor clinical outcome, thus substantiating the importance of early stage anti-ErbB2 therapies.

2.4.3. ErbB3 and ErbB4

In lung cancer patients, overexpression of both ErbB2 and ErbB3 decreased survival [84], while in bi-transgenic ErbB2/ErbB3 mice spontaneous lung cancer formation was observed [85]. The presence of ErbB2/ErbB3 heterodimers was also shown in breast [81,86], prostate [87], lung [80], and colorectal cancer [88].

The physiological and pathological role of ErbB4 is not yet clear. Its overexpression was found in breast [89] and bladder cancers [90].

2.5. Molecular mechanisms of ErbB targeted antibody therapy – trastuzumab as an example

The observation by Sato et al. that some of the monoclonal antibodies against ErbB1 inhibited the binding of the natural ligand to its receptor and thus inhibited receptor phosphorylation and downstream signaling [91] encouraged scientists to develop high affinity antibodies against the extracellular domain of ErbB proteins. Although ErbB2 overexpression is a bad prognostic factor in breast cancer, ErbB2 is also a good target of personalized molecular therapies, as it is present in large amounts in the membrane of the tumor cells compared to healthy adult tissues [92]. While the extracellular domain of ErbB2 molecules offers many epitopes to target with therapeutic antibodies and many monoclonal antibodies against ErbB2 can inhibit the growth of cancer cells, it was reported that some antibodies had no effect on cell growth, moreover, antibodies were found which have tumor stimulatory effect *in vitro* or both *in vitro* and *in vivo* via inducing strong ErbB2 phosphorylation [93-96]. These observations suggest that the identification of those epitopes on ErbB2 to which the binding of antibodies can inhibit tumor growth is crucial in the design of effective anti-ErbB2 antibody-drugs [97]. The most obvious target is the dimerization arm at domain II itself, where the homo- or heterodimerization and thus the activation can be prevented. Domain IV includes a cleavage site for metalloproteinases that is important in the release of the 110 kDa extracellular domain from the cell membrane. Once it is removed from ErbB2, the remaining part of the protein achieves increased potential for homodimerization and interaction with uncleaved ErbB2 molecules resulting in constitutive activation [98], and blocking this site by an antibody could prevent this unfavorable effect.

2.5.1. Trastuzumab (rhu4D5, Herceptin®) – the first humanized monoclonal antibody against ErbB2

Of the murine monoclonal antibodies, 4D5, targeting the extracellular cysteine-rich juxtamembrane region in domain IV of ErbB2 [99] showed very potent, dose dependent antiproliferative effect on cell lines overexpressing ErbB2 [100]. It was also found to be an

effective inhibitor of the growth of human breast cancer xenografts and was selected for clinical studies. For this purpose, a recombinant humanized monoclonal antibody, trastuzumab (type IgG1, rhuMAb-HER2, Herceptin®, Genentech, South San Francisco, CA) was developed, with an approximately three times greater binding affinity to purified ErbB2 extracellular domain than its murine predecessor 4D5 [101].

Trastuzumab is approved for the treatment of patients with ErbB2 overxpressing metastatic breast cancer who have received one or more chemotherapy regimens. Trastuzumab is also applied in combination with doxorubicin, cyclophosphamide, and paclitaxel and indicated for patients with ErbB2 overexpressing metastatic breast cancer who have not received chemotherapy for their metastatic disease (source: www.FDA.org). Phase II studies with ErbB2 positive ovarian cancer are in progress but results so far have shown a relatively low rate of objective response [102]. In studies where trastuzumab was applied alone or in combination with cisplatine or gemcitabine, patients with non-small cell lung cancer showed no significant clinical benefit; even though patients with ErbB2 overexpression are theoretically a prospective target, this subset of the patient population was too small [103]. Although trastuzumab alone did not evoke significant responses in hormone refractory prostate cancer patients, a need for studies on trastuzumab in combination with other agents was suggested [104]. Preclinical studies on gastric cancer models [105,106] showed promising results.

2.5.2. ErbB2 activation, internalization and degradation via trastuzumab binding

The mechanism of action of trastuzumab is still not fully elucidated, although several models have been proposed. First, on ErbB2 overexpressing cells, trastuzumab causes ErbB2 activation, internalization and down-regulation, which has previously been postulated as the primary mechanism of direct growth inhibition [107,108]. C-Cbl catalyzed ubiquitination in the endosomal compartment may be one factor controlling the recycling/degradation pathways of ErbB molecules [109]. One theory suggests that ErbB2 specific antibodies, like trastuzumab, could favor the mono-ubiquitination of ErbB2 through recruiting C-Cbl to ErbB2, and thus accelerate the endocytotic removal from the cell surface and intracellular degradation via C-Cbl and other pathways [109-111]. In contrast to these observations, recent publications suggest that down-regulation is not the main mechanism of the action of trastuzumab *in vivo*. It has been reported that trastuzumab does not down-regulate cell surface ErbB2, but instead recycles with ErbB2 after endocytosis [112]. Furthermore, when

trastuzumab down-regulated ErbB2 from the cell surface, down-regulation was unrelated to the action of trastuzumab *in vivo*: trastuzumab IgG and trastuzumab-F(ab')2 were equally effective in down-regulating ErbB2, but trastuzumab-F(ab')2 had no inhibitory effect on tumor growth while trastuzumab caused a significant inhibition [113]. Also, *in vitro* experiments have demonstrated that even though cross-linking of lipid rafts with cholera toxin B subunit prevented trastuzumab-evoked ErbB2 internalization, cholera toxin B and trastuzumab proved to be synergistic in their growth inhibitory effect [27].

2.5.3 Antibody mediated cellular cytotoxicity – an important mechanism of trastuzumab action *in vitro*

Antibody dependent cellular cytotoxicity (ADCC) seems to have a key role in the *in vivo* effect of trastuzumab: Clynes et al. inoculated ErbB2-positive, *in vitro* trastuzumab-sensitive BT-474 cells into knockout mice lacking activating FcRγIII receptors (CD16). In this model system, the anti-tumor activity of trastuzumab was reduced but not ablated: about 25% of the effect was retained. In the same manner, treatment of wild-type mice with the mutated form of 4D5, the parent antibody of trastuzumab, which was made unable to bind to Fc receptors, had a similar partial effect only [114].

2.5.4. Inhibition of cell cycle progression, angiogenesis and migration

The role of p27kip and cyclin D1 leading to disorders in G1/S phase transition was demonstrated in ErbB2 overexpressing tumors. Trastuzumab was shown to down-regulate cyclin D1, and increase p27 protein levels via inhibiting PI3K and Akt in BT-474 and SKBR-3 human breast cancer cells [115]. By inhibiting ErbB2 kinase activity, growth arrest in G1/S could be achieved, and this could be abrogated by applying p27kip antisense RNA [116]. Decreased expression level of p27kip was also suggested to affect trastuzumab response [117].

Trastuzumab was also shown to inhibit angiogenesis [118] possibly by reducing the expression of angiogenic factors like vascular endothelial growth factor (VEGF), causing the reduction of the diameter, volume and permeability of tumor blood vessels, which underscores the importance of tumor-matrix interactions in the angiogenic process. The role of angiopoietin-2 was also implicated in ErbB2 induced tumor vascularization [120], and its expression could be effectively decreased by trastuzumab treatment [121]. In cells treated with the combination of trastuzumab and paclitaxel, not only the production of VEGF was

diminished, but also decreased cellular migration was shown, with decreased activity of the PI3K/Akt pathway in the background [122].

2.6. Other ErbB targeted antibodies

Paralel to trastuzumab, many other antibodies against ErbB1 and ErbB2 have been developed (Table 1.).

2.6.1. Antibodies targeting ErbB1

The two main mechanisms of antibodies against ErbB1 are inhibition of ligand binding, and, in the case of IgG1 type antibodies, ADCC. Cetuximab is a monoclonal chimeric type IgG1 antibody against ErbB1, approved for colorectal and head and neck cancer in combination with chemotherapy and is already in phase II/III clinical trials for other ErbB1 overexpressing tumors. Cetuximab interacts exclusively with domain III of the extracellular domain of ErbB1, partially occluding the ligand-binding region and sterically preventing the receptor from adopting the extended conformation required for dimerization [123]. Cetuximab also induces ErbB1 internalization and degradation, blocks the cell cycle in G1, inhibits proliferation, and induces programmed cell death [124]. Cetuximab also sensitizes the cells to conventional DNA damaging chemotherapeutic agents by inhibiting the activation of a DNA-repair kinase DNA-PK via ErbB1 [125]. Matuzumab (EMD 72000) is also a humanized IgG1 antibody that competitively inhibits EGF binding and inhibits signaling by ErbB1 without altering its expression level, but compared to cetuximab it has a prolonged half life [126]. Nimotuzumab (h-R3, TheraCIM®) blocks ligand binding to ErbB1 by interacting with its extracellular domain thus inhibiting signaling, however, growth inhibition or apoptosis during *in vitro* experiments were not confirmed. The main effect of nimotuzumab on ErbB1 positive tumor cells is to inhibit VEGF production, thus inhibiting the tumor driven angiogenesis [127]. Panitumumab (ABX-EGF, Vectibix®) is the first fully humanized monoclonal antibody against ErbB1 [128-130], inhibiting EGF and TGFα binding, resulting in inhibition of cell growth and decreased production of growth factors such as VEGF or interleukin-8. As a completely humanized antibody, it was well tolerated in all of the clinical trials.

2.6.2. Antibodies targeting ErbB2

Regarding ErbB2 targeted antibodies, ways of trastuzumab action have already been discussed. However, other antibodies in this group possess yet other modes of action. Pertuzumab, the humanized form of mouse 2C4 binds extracellularly to the dimerization arm near the junctions of domain I, II and III of ErbB2 and thus inhibits dimerization both of ErbB2 homodimers and ErbB2 containing heterodimers, such as the highly mitogenic ErbB2/ErbB3 and ErbB1/ErbB2 dimers. Pertuzumab was also shown to disrupt ErbB2/IGF-IR interactions in trastuzumab resistant cells [131]. It also mediates ADCC [114], but it does not block shedding [132]. Unlike in the case of trastuzumab, this effect of pertuzumab does not strictly require ErbB2 overexpression [133]. In cells where ErbB2 was activated but not overexpressed, the Fab fragment of pertuzumab was just as effective in inhibiting ErbB2 mediated signaling as the intact antibody [131], suggesting that its biological activity is not dependent on bivalence or the presence of the Fc region. This is in sharp contrast to trastuzumab, explaining why pertuzumab may be a better choice against tumors expressing ErbB2 at a low level but adjacent to other members of ErbB family. On ErbB2 overexpressing cells that have not been treated with trastuzumab, pertuzumab and trastuzumab had a synergistic effect and induced apoptosis. However, on trastuzumab resistant cell lines pertuzumab, either alone or in combination with trastuzumab, had no significant antiproliferative effect suggesting that in these cases alterations of intracellular signaling pathways were also involved in trastuzumab resistance, leading to cross-resistance to various ErbB2 targeted agents [50].

A unique approach is to use single chain variable fragment (scFv) antibodies with the sole purpose of targeting ErbB kinases but avoiding any own biological effect. In this setting, unexpected interactions of the antibody's own effects and the actually intended effect of the cargo can be avoided. FRP5, a mouse monoclonal antibody targeting the extracellular domain of ErbB2 has been one of the first to construct a single chain variable domain antibody fragment (scFvFRP5) and is currently used to deliver peptide toxins [134,135]. A similar scFv against ErbB2, F5, has been successfully applied to target and mediate internalization of sterically stabilized liposomes enclosing doxorubicin [136]

2.6.3. Engineered immunological tools against ErbBs

Bispecific, multifunctional antibodies against both ErbB1 and ErbB2 are under development. MDX-447 and MDX-H210 bind to ErbB1 and ErbB2 respectively, and, with another valence,

to FcγRI, thus bridging tumor and effector cells. Both of them are in phase I trials, whereas the antibody 2B1 binding to ErbB2 and FcγRIII was cancelled in phase I because it caused a severe cytokine storm. Ertumaxomab bridges ErbB2 to CD3, but its Fc domain is also present, thus, it is tri-functional, and showed promising results in phase II studies.

Agent	Type	Target	Status
cetuximab (Erbitux) [137-142]	IgG1	ErbB1	Approved for colorectal and head and neck cancer; in trials for non-small cell lung cancer, pancreas, breast and cervical cancer.
ICR62 [143,144]	IgG1	ErbB1	Preclinical
panitumumab (Vectibix) [145,146]	IgG2	ErbB1	Approved for metastatic colorectal cancer in combination with chemotherapy, in trial for non-small cell lung cancer
matuzumab [124,126]	IgG2	ErbB1	In phase II trial for ovarian, peritoneal, gastric and non-small cell lung cancer
nimotuzumab (TheraCim) [147] Spicer, 2005 #197}	IgG2a	ErbB1	Approved for head and neck cancer; in phase I for pancreatic cancer
ch806 [148]	IgG1	ErbB1	In phase I for mutant ErbB1 positive tumors
L8A4 [149]	IgG2	ErbB1	Boronated L8A4 is in preclinical phase
MDX-447 [150]	bispecific antibody	ErbB1/ FcγRI	In phase I
trastuzumab (Herceptin) [151]	IgG1	ErbB2	Approved for breast cancer
pertuzumab (Omnitarg®) [152-155]	IgG1	ErbB2	In Phase II/III for ovarian, breast and non-small cell lung cancer and low ErbB2 expressing tumors
MDX-H210 [156]	bispecific antibody	ErbB2/ FcγRI	In phase I
2B1 [157]	bispecific antibody	ErbB2/ FcγRIII	Cancelled in Phase I
C6.5xscFv(NM3E2) [158]	bispecific antibody without Fc domain	ErbB2/ FcγRIII	Unknown
ertumaxomab [159]	IgG2b based trifunctional antibody	ErbB2/CD3	In Phase II against advanced metastatic breast cancer
scFvFRP5 [134,160]	scFv fragment	ErbB2	ScFv(FRP5)-ETA or -GrB are in Phase I/II trials for metastatic breast, prostate, head and neck, NSCLC and transitional cell carcinoma

Table 1. Therapeutic antibodies against ErbB1 ad ErbB2

2.7. Trastuzumab resistance – a major clinical problem

Although ErbB2 overexpression identifies patients who are likely to respond to therapy with trastuzumab, the occurrence of trastuzumab resistance is frequent. In contrast to the tight prognostic correlation and specific therapeutic opportunities, trastuzumab seems to be effective only in 20-50% of ErbB2 overexpressing breast tumor patients, and many of the initial responders have a relapse after a few months [161]. The background of resistance is probably versatile and may differ from case to case. Being the first of its class amenable to passaging *in vitro*, the JIMT-1 cell line isolated from a clinically trastuzumab resistant breast cancer patient vastly improved our possibilities of understanding resistance mechanisms [162].

2.7.1. Steric hindrance

Since trastuzumab initiates a series of ErbB2-mediated events including ErbB2 phosphorylation and internalization, the interaction of ErbB2 with other molecules and its distribution on the cell surface may influence the trastuzumab responsiveness of a cell. The simplest cause of resistance is the disruption of interaction between trastuzumab and ErbB2. One group of candidates for masking ErbB2 could be overexpressed sialomucin complexes, among them MUC4, which is often found on the surface of malignant tumor cells. In addition to hindering ErbB2-trastuzumab interactions, MUC4 could also hide tumor cells from immune surveillance, promote tumor progression and metastasis, suppress apoptosis, and potentially even activate ErbB2 via its EGF homologue domains, resulting in increased tyrosine phosphorylation [163,164].

CD44, a hyaluronan receptor is an important factor in lymphocyte homing and cancer progression, but its interaction with ErbB2 was also shown [165]. Activation of CD44 leads to cell survival via PI3K/Akt signaling [166], as well as to cytoskeletal rearrangements, this latter suggesting the role of CD44 in cellular adhesion, migration and invasion [167]. The presence of overexpressed CD44 inhibits trastuzumab binding and increases trastuzumab clearance from the cell surface[168].

2.7.2. Overexpression and cross-talk with the interaction partners of ErbB2

Overexpression of Insulin-like Growth Factor-I Receptor (IGF-IR) is also associated with trastuzumab resistance, as this cell surface receptor physically interacts with and

phosphorylates ErbB2 [169]. In this process, PI3K/Akt and MAPK pathways are also involved, and with inhibition of IGF-IR, trastuzumab responsiveness can be restored. Other studies on the interaction of IGF-IR and ErbB2 have suggested that p27kip1 is a critical element of trastuzumab response, and its down regulation by the increased signaling of growth factor receptors can promote trastuzumab resistance. The decreased expression or activity of the tumor suppressor PTEN involved in the PI3K/Akt pathway can be also responsible for trastuzumab resistance; in this case, PI3K inhibitors might be considered to remedy the situation [170].

On the intracellular side, a significant level of compensatory 'cross-talk' among ErbB kinases within a signaling network, as well as with other pathways regulating cell growth, proliferation, and survival might be involved in and responsible for therapy resistance [171,172]. The molecular basis of signal diversification and specification in the intracellular compartments involving the pathways mentioned above is incompletely understood but its elucidation is highly important for specific therapeutic targeting.

2.7.3. Ineffectiveness of ADCC

Although Clynes et al. suggested that the effect of trastuzumab is mainly mediated via ADCC [114], only a few works have investigated the role of impaired ADCC in trastuzumab resistance. Mimura et al. reported that trastuzumab-mediated ADCC against transforming growth factor-β (TGF-β) producing esophageal cancer cells was enhanced by treatment with a selective inhibitor of TGF-β [173]. Kono et al. showed that capability of trastuzumab-mediated ADCC was significantly reduced in NK cells from advanced gastric cancer patients compared to healthy individuals. NK cell dysfunction was correlated to the down-regulation of CD16ζ, whose phosphorylation has a key role in NK cell-mediated ADCC. Furthermore, *in vitro* interleukin-2 treatment of NK cells could normalize CD16ζ expression and increase trastuzumab-mediated ADCC [174].

In vivo experiments have shown that trastuzumab does actually inhibit the growth of JIMT-1 xenografts in SCID mice if its administration is started at small xenograft size, or at the time of tumor cell inoculation, despite the *in vitro* resistance of these cells to trastuzumab. The growth inhibitory effect was mediated via ADCC, but resistance developed after 5-7 weeks. A subline, JIMT-X+, generated from a trastuzumab-resistant xenograft, did not differ from the parental JIMT-1 cells in an *in vitro* ADCC assay and was equally sensitive to trastuzumab when re-grafted to mice [113]. Furthermore, trastuzumab significantly reduced

the number of circulating and disseminated tumor cells at a time when the primary tumor was already unresponsive to trastuzumab, suggesting that ErbB2 positive circulating and disseminated tumor cells could be sensitive to trastuzumab-mediated ADCC even when the primary tumor is already non-responsive [175]. Taken together, it is likely that single tumor cells or smaller clusters are sensitive to trastuzumab-mediated ADCC, but lose their sensitivity to ADCC when cell-cell and cell-matrix junctions are formed and the cells develop into a 3 dimensional tumor tissue.

3. Aims

The interactions of ErbB kinases with each other and with various membrane proteins define their signaling activity and accessibility as therapeutic targets. Our aim was to contribute to the understanding of mechanisms behind ErbB1 and ErbB2 activation and transactivation, and compare, in this respect, trastuzumab resistant and sensitive breast tumor cell lines. In this context, the following questions were posed:

- Can fluorescence correlation spectroscopy (FCS) be used to detect the diffusion properties of ErbB1 in the membrane of living cells and reveal new information about the mechanism of ErbB1 activation?
- How do FCS and fluorescence recovery after photobleaching (FRAP) data on the mobility of ErbB1 correlate in the same cellular system?
- Does local activation of ErbB1 and ErbB2 by derivatized paramagnetic microspheres give rise to localized or laterally spreading signals?
- Can EGF and trastuzumab, binding to their targets, evoke transactivation of ErbB2 and ErbB1, respectively?
- On trastuzumab resistant JIMT-1 cells, is it the lack of function, or the diminished accessibility of ErbB2 to trastuzumab that causes resistance?
- In case of diminished accessibility, can the MUC4 sialomucin complex be responsible for the masking of ErbB2 on JIMT-1 cells?

4. Materials and Methods

4.1. Cells

CHO cells, CHO transfected with ErbB1-eGFP (sub-clones F1-4 and F1-10 expressing ErbB1 with a C-terminally fused eGFP), A431 epidermoid carcinoma, its sub-clone A4-ErbB2-mYFP stably transfected with the ErbB2-mYFP fusion gene (expressing in addition to ErbB1 also ErbB2 with a C-terminal monomeric YFP fusion) SKBR-3 breast tumor cells (American Type Culture Collection, Rockville, MD), and JIMT-1 trastuzumab resistant breast tumor cells (kind gift of Jorma Isola, [162]) were cultured in Dulbecco's Modified Eagle's Medium (DMEM, Sigma, Schnelldorf, Germany) supplemented with 10% fetal calf serum (FCS, GIBCO BRL), and antibiotics (0.5mg/ml gentamycin, Chinoin) in humid atmosphere containing 5% CO_2. The line F1-4 expressed 10^6 ErbB1-eGFP per cell, while F1-10 2×10^4 per cell on average, but with considerable variation among cells. Both were kept under selection pressure using 1 mg/ml G418 (Gibco BRL). Culture medium of JIMT-1 was supplemented with F12 (1:1 with DMEM; Sigma and 60 NE/L insulin). The cultures were propagated every 3-4 days. For microscopic and fluorescence correlation spectroscopy measurements cells were seeded onto 12 mm diameter cover slips, or cover slip based chamber slides (Nunc), and used at sub-confluence (50-80% density). Before stimulation experiments, cultures were starved in serum-free DMEM for 12 or 24 h.

4.2. Western blot

Sub-confluent cultures grown in 50 cm^2 area culture dishes were starved for 12 hours in serum free DMEM, then stimulated with 8 or 50 nM EGF (recombinant human epidermal growth factor, IC Chemikalien GmbH) for 5 minutes. Stimulation was stopped by applying 300 µl of lysis buffer containing 1% Triton-X-100, 50mM Tris-HCl, 25 mM KCl, 5 mM $MgCl_2$, 1 mM EGTA, 0.4 mM phenyl-methyl-sulphonyl-fluoride (Merck), 2 mg/ml aprotinin (Sigma), 10 mg/ml leupeptin (BioMol), 500 mM benzamidin (Sigma), and 2 mg/ml pepstatin (Merck). Samples were then added to 150 µl 3× SDS sample buffer and boiled for 10 minutes at 100 °C, then ran on 10% polyacrylamide gels (BioRad Mini Gel System, 40mA, 120V) for 90 minutes [176]. Proteins were blotted to PVDF Immobilon P membrane (Millipore) for 100

minutes at room temperature with 60 mA current, the membrane was blocked with 1% BSA-PBST (0,1% Tween-20 in PBS-ben pH= 7.4 with 1% BSA) for 30 minutes, and phospho-tyrosine was labeled with horse radish peroxidase conjugated anti-phospho-tyrosine antibody (SC-508-HRP, 10 ng/ml, overnight at 4ºC in 1% BSA-PBST). After washing in PBST, membranes were incubated with ECL reagent (Amersham Pharmacia Biotech), luminescence was detected on Fuji X-Ray films and digitized at 1200 dpi. Protein content of the membrane was detected with Amido black staining; remaining protein content in the gel after blotting was stained with Coomassie Brilliant Blue.

4.3. Ca^{2+} measurements

Intracellular Ca^{2+} concentrations were measured by fluorescence microscopy using the calcium indicator dye Fura-2 (Molecular Probes, Eugene, OR) [177]. The ratio I_{340}/I_{380} of the fluorescence intensities excited at 340 and 380 nm is independent of dye concentration and is a monotonously increasing function of $[Ca^{2+}]$. F1-10, A431 and CHO cells were grown on 25 mm diameter round cover-slips in DMEM. Before the experiment, cells were starved for 12 hours in serum-free medium. Cells were loaded with 2 μg/ml Fura-2-AM for 30 minutes at 37 ˚C, washed twice with HBS (containing, in mM: 135 NaCl, 5 KCl, 1 $MgCl_2$, 1.8 $CaCl_2$, 5 glucose, 10 HEPES, pH 7.4) and imaged with an Attofluor Digital Ratio Imaging System (Atto Instruments, Rockville, MD) with a time resolution of 0.2 frames per second. Spectral ranges were 340 ± 12.5 nm and 380 ± 12.5 nm for excitation and larger than 520 nm for emission. After 100 seconds 0, 8 or 50 nM EGF was administered, and at 400 seconds 2 μg/ml of ionomycin (Sigma) was added to permeabilize the plasma membranes for Ca^{2+}. To display activation-induced temporal changes in Ca^{2+} concentration ratio images (I_{334}/I_{380}) corrected for field flatness were calculated, and the average ratio of regions-of-interest (ROIs) covering the inside of each cell were graphed versus time.

4.4. Fluorescence Correlation Spectroscopy (FCS)

4.4.1. Origin and analysis of the autocorrelation function in fluctuation measurements

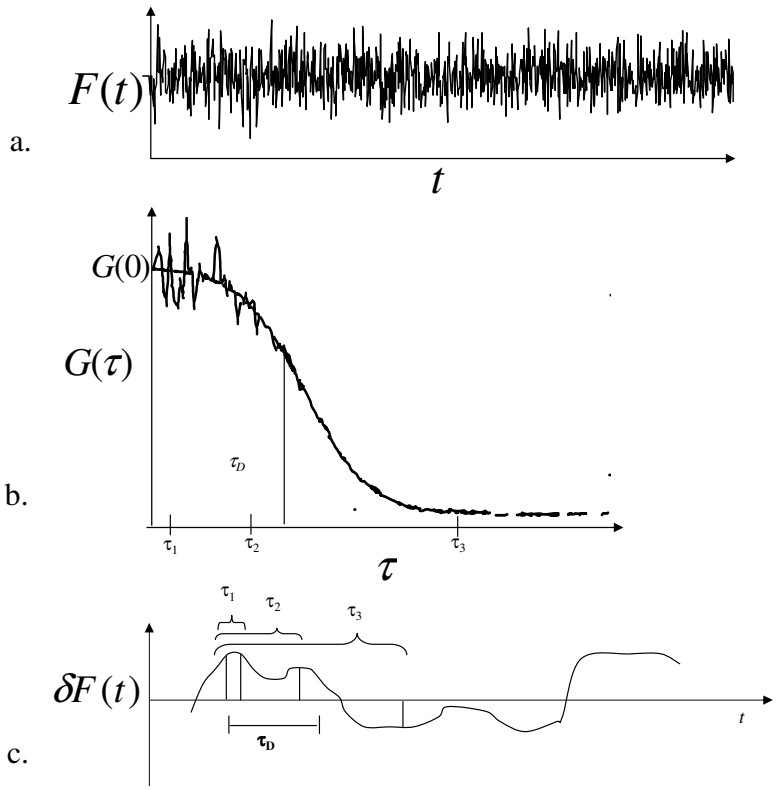

Fig. 4. Mathematical background of FCS
Fluorescence intensity fluctuation (a), autocorrelation curve derived from it (b.) and a sketch (c) explaining the shape of the autocorrelation curve are shown on this figure. Within τ values smaller than the diffusion time (in this example τ_1 and τ_2), the amount of fluorescent molecules in the confocal volume does not change significantly, thus, the product of two δF intensities separated by time τ is positive. For τ values greater than the diffusion time (in this case τ_3), the two fluorescence intensities are independent from the each other, since any molecule which has been inside the observation volume at time t and be either inside the volume or outside the volume at time t+τ. Thus, either of the two δF values can be positive or negative independent of each other. Consequently, the average of their products will converge to zero.

In fluorescence correlation spectroscopy measurements, fluctuation of fluorescence intensity is followed in a sub-femtoliter confocal volume using sensitive detection with an avalanche photodiode. This fluctuation is dependent on photophysical processes and diffusion of the molecules in and out of the measuring volume.

The intensity time trace of the fluorescence signal is analyzed for its time-wise autocorrelation using

$$G(\tau) = \frac{\langle \delta F(t) \cdot \delta F(t+\tau) \rangle}{\langle F \rangle^2} \tag{1}$$

and

$$\delta F(t) = F(t) - \langle F \rangle \tag{2}$$

where $F(t)$ is the intensity of fluorescence at any time point, t, $\langle F \rangle$ is the average intensity obtained during the whole time of observation and $\delta F(t)$ is the deviation of fluorescence at this time point from $\langle F \rangle$, the average. The brackets $\langle\ \rangle$ in the formulas denote time averages of the appropriate terms. The $\delta F(t)$ values are used to obtain the $G(\tau)$ autocorrelation function by averaging the products of all possible ordered pairs of $\delta F(t)$ and $\delta F(t+\tau)$, where all possible τ time-differences are considered. Fig. 4a. shows a typical trace and Fig. 4b. the resulting autocorrelation function; Fig. 4c. helps explain how interdependence of two fluorescence fluctuation values separated by various time lags yields positive or close to zero correlation values as a function of the average time the particle spends in the observation volume. In our experiments, the component of the autocorrelation function originating from the diffusion of fluorescent molecules was of major interest, but other factors – dissociation-association and physicochemical processes – can contribute as well.

We have analyzed our data using the Levenberg-Marquardt non-linear least-squares method implemented in the LabView programming environment to fit to a single- or multi-component, free or anomalous diffusion model. Additional terms often need to be included to take into consideration the fluctuations due to triplet state formation characteristic of many widely used fluorophores; as well as dark state formation (blinking) exhibited by most GFP derivatives. This latter can result either from protonation [178,179] or from light-induced conformational transition to a non-fluorescent state [180]. We have used the fit function:

$$\mathrm{G}(\tau) = a_0 + \frac{1}{<\mathrm{N}>} \cdot G_{tr} . G_{bl} . \cdot \sum_i^n \left[w_i \left(1 + \left(\frac{\tau}{\tau_{d,i}} \right)^{2/d_{w,i}} \right)^{-1} \left(1 + \frac{1}{S^2} \left(\frac{\tau}{\tau_{d,i}} \right)^{2/d_{w,i}} \right)^{-1/2} \right] \tag{3}$$

where the triplet state correction is given by

$$G_{tr}(\tau) = \frac{\left(1 - T + Te^{-\tau/\tau_{tr}}\right)}{1 - T} \tag{4}$$

and the blinking correction by

$$G_{bl}(\tau) = \frac{\left(1 - \Theta_{bl} + \Theta_{bl}.e^{-\tau/\tau_{bl}}\right)}{1 - \Theta_{bl}} \tag{5}$$

In Eq. (3) ⟨N⟩ is the average number of molecules in the detection volume, which is a great asset, since by fitting the autocorrelation function the concentration of labeled molecules can be obtained. The diffusion autocorrelation time, $\tau_{d,i}$ of the i^{th} diffusing species is also obtained from fitting; it represents the average time it takes for this species (of a weight fraction w_i) to traverse the detection volume. The detection volume is the space inside the surface where the detection efficiency, described by a 3D Gaussian function, falls to e^{-2} times the maximal value present at the center of this volume. This volume is a rotational ellipsoid, which is characterized by the structure parameter, $S = \omega_z/\omega_{xy}$ (ratio of axial radius ω_z to the lateral radius ω_{xy} of the ellipsoid, usually a value between 4-7, or in the case of 2D diffusion in the membrane $S \to \infty$). $d_{w,i}$ denotes the anomaly parameters of the diffusing components: a value of 2 is characteristic of free Brownian diffusion, while values larger than 2 hint at possible obstacles in the way of diffusing molecules – barriers, binding sites temporarily slowing down diffusion, etc., and values below 2 result from facilitated or guided diffusion, which, obviously, is also a sign of molecular interactions. Less importantly, a_0 is an offset to compensate for the nonzero baseline of the autocorrelation function arising from drifts in the fluorescence signal, such as photobleaching.

In the triplet term, G_{tr}, T denotes the equilibrium molar fraction of fluorophores in the triplet state and τ_{tr} is the triplet lifetime. The "blinking term", G_{bl} accounts for the conformational fluctuations between fluorescent and dark state formation. Θ_{bl} is the fraction of fluorophores in the detection volume in the dark state and τ_{bl} is the corresponding relaxation time. Measurements can also be complicated by photobleaching, which, although it can be accounted for in the fitting algorithms, can bias the assessment of the more slowly or the faster diffusing molecular species.

The diffusional autocorrelation times, $\tau_{d,i}$ can be converted to a diffusion coefficient (D) using the equation:

$$D_i = \frac{\omega_{xy}^2}{4\tau_{d,i}} \tag{6}$$

The radii ω_{xy} and ω_z are obtained by calibrating the system with a dilute solution of a dye of known concentration and diffusion coefficient. Rh6G of molecular mass 0.479 kDa is commonly used for its small size and photostability. In a dilute solution (~10 nM), for the Brownian diffusion of a single species that has a triplet state Eq. (3) then simplifies to

$$G(\tau) = a_0 + \frac{1}{<N>} \cdot G_{tr} \cdot \left(1 + \frac{\tau}{\tau_d}\right)^{-1} \left(1 + \frac{1}{S^2}\frac{\tau}{\tau_d}\right)^{-1/2} \tag{7}$$

The diffusion time, τ_d obtained from a Levenberg-Marquardt non-linear least-squares fit to Eq. (7) and the diffusion coefficient of a standard, e.g. Rh6G (280 $\mu m^2/s$ at 25°C) are used in Eq. (6) to obtain ω_{xy}. An estimate of ω_z can then be obtained from the fit result of S, or rigorously determined from measurements of a series of dilute concentrations of the dye. For a given concentration of dye, the average number of molecules in the detection volume can be expressed in terms of the dimensions of the ellipsoidal sensitive volume in the optical plane and the molar concentration *c*:

$$N = N_A c \pi^{3/2} \omega_{xy}^2 \omega_z \tag{8}$$

N_A is Avogadro's number. Thus, $\omega_{xy}^2 \omega_z$ can be derived from the slope of a plot of the apparent number of particles, N vs. dye concentration. In our case, typical dimensions for the setup used were ω_{xy} = 0.34 ± 0.04 µm and ω_z = 2.43 ± 0.58 µm.

4.4.2 Measurement of fluorescence autocorrelation in ErbB1-eGFP expressing CHO cells

For the measurement of fluorescence autocorrelation, the instrument described in [181-183] was used. Cells were grown on 12 mm diameter round cover slips in DMEM, washed twice in HBSS with 0.1% BSA and allowed to equilibrate at 25°C for 30 min. FCS measurements were performed using a water immersion objective (C-Apochromat 40×, NA 1.2, Carl Zeiss, Göttingen, Germany) at defined positions of the plasma membrane. Cells were visualized by the camera in transmission and wide-field fluorescence mode, and the cell was positioned in the x- and y-dimension with respect to the laser focus using a high-precision motorized x-y stage (Märzhäuser, Wetzlar, Germany). Transmission and wide-field fluorescence images were recorded. Positioning of the focal volume along the optical axis (z) was achieved by a

Pifoc piezoelectric lens positioner (Physik Instrumente, Waldbronn, Germany). In cells expressing the ErbB1-eGFP fusion protein, the plasma membrane was apparent as peaks proximal and distal to the coverslip in the z-profile of the fluorescence intensity. Measurements were carried out in the upper (distal) cell membrane over 60-200 seconds. A series of 3-10 consecutive measurements were acquired at each position. After about every fifth measurement the focal position was confirmed by recording a fluorescence profile. For assessing the effect of receptor stimulation on autocorrelation functions, EGF was added at a final concentration of 50 nM by carefully pipetting 200 µl of 250 nM stock solution to the 800 µl buffer already on the cells. Data are presented for those experiments only (~30% of total), where no significant displacement of the membrane with respect to the confocal detection volume took place during the series of measurements. For excitation, the 488 nm line of an Ar ion laser (2313-150MLYV, Uniphase, Eching, Germany) at laser power densities of ~1 kW/cm^2 was used. Emission was detected through a 515-545 nm bandpass filter.

Control measurements were done on a Zeiss LSM510-Conforcor 2 combi instrument in dual channel mode to observe co-diffusion of the GFP tag on ErbB1 and AlexaFluor647 labeled 528-Fab on F1-10 cells. In these measurements the fluorophores were excited with the 488 and 633 nm laser lines of the microscope, and emission was detected through 80 µm diameter (1 Airy unit) pinholes and 500-550 nm bandpass and 650 nm longpass filters, respectively.

4.5 Fluorescence recovery after photobleaching (FRAP)

FRAP measurements were performed using a custom-made instrument based on a Leica fluorescence microscope. The beam of a 488 nm argon ion laser was splitted with a half-mirror and focused to a diffraction-limited spot with a 40× (N.A. = 0.5) dry objective. The beam radius was determined to be 375 nm by comparing the e^{-2} diameter of the intensity profile of the beam to the image of microbeads of known diameter projected to a screen. Laser output was 40 mW, with 10^4× attenuation of the beam for monitoring. The monitoring excitation power density in the illuminated spot was <0.5 kW/cm^2. An electromechanical shutter wheel was used to block the main beam path during monitoring. Bleaching time was 200 ms, preceded and followed by 200 ms dead time for protecting the cooled photomultiplier used for sampling the recovery kinetics at 5 - 50 Hz. Emission was detected through the half-mirror and a 500 nm longpass filter. Data were fitted with a custom-written LabVIEW

program employing a nonlinear Levenberg-Marquardt algorithm for the general model accounting for both free and anomalous (hindered) diffusion [184]. Assuming that there is no directional flow and that recovery after bleaching is due to diffusion of a single component only, the fluorescence intensity *f(t)* at any time *t* for a Gaussian laser beam is given by the equation:

$$f(t) = \frac{f_0 + f_\infty \left(t/t_{1/2}\right)^\alpha}{1 + \left(t/t_{1/2}\right)^\alpha} \tag{9}$$

where f_0 is the fluorescence intensity immediately after photobleaching, f_∞ is the maximum recovered intensity attainable after a long time, $t_{1/2}$ is the time of recovery to $(f_\infty + f_0)/2$, and α is the anomaly parameter [184], which in the FRAP formalism has a value of 1 for free diffusion, and <1 for hindered diffusion. The mobile fraction (percentage recovery of fluorescence) is determined by

$$R = \frac{f_\infty - f_0}{f^0 - f_0} \tag{10}$$

and the diffusion constant by

$$D = \frac{\gamma\omega^2}{4t_{1/2}} \tag{11}$$

where f^0 is the fluorescence intensity before bleaching, ω is the radius of the laser beam at e^{-2} height of the Gaussian beam at the point of focus on the membrane and the correction factor γ (a function of bleaching) was determined to be 1.147±0.073 according to [185]. A typical FRAP curve and its fit can be seen on Fig. 5.

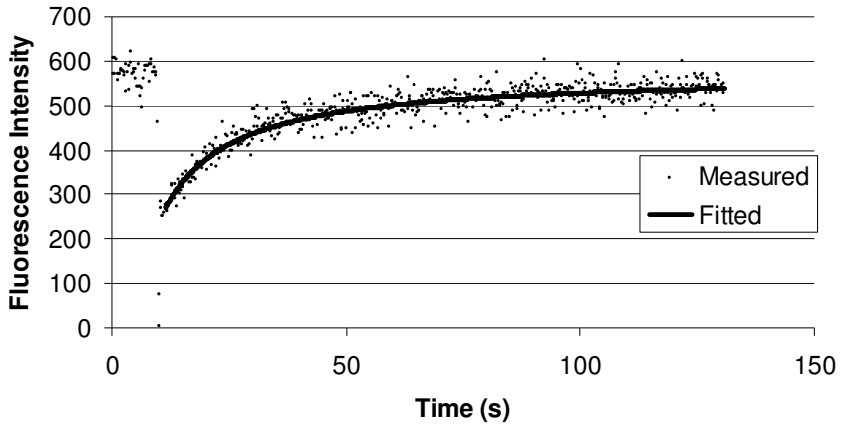

Fig. 5. A typical FRAP curve and its fit
Fluorescence of the eGFP is photobleached at the 10th second of the measurement, then recovery of the fluorescence intensity is detected for 130 seconds.

4.6. Antibodies

Antibody 528 against ErbB1 was prepared from the supernatant of the corresponding hybridoma line (catalog no. HB-8509, American Type Culture Collection, Rockville, MD, USA). Against ErbB2, we have used trastuzumab, 2C4 (both from Genentech Inc., South San Fransisco, CA), and Ab3/OP15, that binds to the intracellular domain (Calbiochem-Merck Biosciences, Schwalbach, Germany). Activated form of ErbB1 was labeled with clone74 (Transduction Laboratories, Lexington, KY, USA). Phosphorylated ErbB2 was labeled with Ab18 (clone PN2A, Dianova, Hamburg, Germany), but in some experiments, we used PY99 antibody against phosphotyrosine (cs-7020, Canta Cruz Biotechnology). MUC4 was detected using 1G8 antibody that binds to the membrane associated β subunit (kind gift of Kermit L. Carraway). Antibodies were used at final concentrations of 1-10μg/ml diluted in PBS. Antibodies were conjugated with AlexaFluor488, AlexaFluor543, AlexaFluor633 (Molecular Probes, Leiden, The Netherlands), Cy3, Cy5 (Amersham Biosciences, Freiburg, Germany) for direct labeling, according to the manufacturers instructions. Indirect immunofluorescence was performed by applying fluorophore conjugated goat anti mouse polyclonal antibodies (Dianova, Hamburg, Germany, or Jackson ImmunoResearch, West Grove, PA, USA).

4.7. Determination of receptor numbers and trastuzumab dissociation constants

SKBR-3, JIMT-1, and A4-ErbB2-mYFP cells were harvested upon reaching half confluence, washed once in ice-cold PBS, and resuspended at 5×10^5 cells in 100 µl PBS. Cells were incubated for 10 minutes on ice with Alexa-488 conjugated antibodies. Kd values were determined using concentrations of 2.5 to 50 µg/ml; for determining expression levels, saturating concentrations of 50 µg/ml were used. After staining, cells were centrifuged for 4 min at 800g, washed in PBS, and fixed with 1% formaldehyde. Intensity histograms of 2×10^4 cells were measured with a Becton Dickinson (Franklin Lakes, NJ, USA) FACScan flow cytometer taking FL1 data. Surface expression of ErbB2 on SKBR-3 was quantified using QIFIKIT (DakoCytomation, Glostrup, Denmark) according to the manufacturer's instructions and was found to be 1.1×10^6 molecules per cell. The relative numbers of cell surface proteins on other cells were calculated by comparing the FL1 fluorescence intensities with that of ErbB2 on SKBR-3, taking the dye/protein labeling ratios of the antibodies into consideration. For determining Kd-s, background corrected histogram means, normalized to the maximal intensities were used from each sample. The bound fraction was estimated from the relative labeling intensities and known total receptor numbers. Scatchard plots with bound/free ratio against bound antibodies were used to calculate the Kd-s.

4.8. Immunofluorescent labeling

Cells were seeded onto 12 mm cover slips or Nunc chamber slides, and used at sub-confluence. Before the experiments, cultures were washed once with ice cold PBS, then incubated with fluorescently labeled trastuzumab or 2C4 for 30 minutes on ice to avoid internalization. After fixation with 4% paraformaldehyde (PFA) for 20 minutes on ice and washing, the samples were flipped into Mowiol (0.1 M Tris-HCl, pH 8.5, 25 w/v % glycerol, 10% Mowiol 4-88, Hoechst Pharmaceuticals, Frankfurt, Germany).

For intracellular labeling, sub-confluent cultures grown on cover slips were fixed with 100% methanol at -20°C for 20 minutes. After rehydrating the samples with PBS, cells were blocked and permeabilized for 20 min at room temperature using 1 mg/ml BSA (Sigma) and 0.1% Triton X-100 (Fluka, Buchs, Switzerland) in PBS. Primary antibodies against phospho-ErbB1, phospho-ErbB2, phosphotyrosine (PY) or 1G8 antibodies were diluted in 100 µl PBS

with 1mg/ml BSA and 0.1% Triton X-100 to a final concentration of 1µg/ml. After 30 min at RT, cells were washed three times with 1 mg/ml BSA and 0.1% Triton X-100 in PBS for 5 min. Incubation with secondary Cy3-goat anti mouse immunoglobulin (GAMIG) was performed as with the primary ones. Samples were washed again and mounted in 5 µl Mowiol on pre-cleaned microscopic slides.

Flow cytometry samples were labeled according to a similar protocol, the but the cells were harvested before labeling by incubation with trypsin-EDTA solution, then washed once in ice cold PBS, and pelleted by centrifugation at 600× g. Cell number per sample was 50000, and labeling was performed in 50 µl PBS. We have previously verified that the labeled cell surface entities are resistant to trypsin digestion.

4.9. Preparation of chemically coupled trastuzumab and EGF microspheres

Natural murine EGF was obtained from IC Chemikalien (Ismaning, Germany). Carboxy-functionalized superparamagnetic 1µm microspheres (SERA-MAG, Seradyn, IN, USA) were activated with 0.1 M sulpho-N-hydroxysulphosuccinimide (Pierce, Rockfort, IL, USA), 0.1 M 1-ethyl(-3-[3-dimethyl-aminopropyl])carbodiimide hydrochloride (Pierce) in 0.1 M 2-(N-morpholino)ethane sulfonic acid (MOPS; Sigma) buffer, at pH 6, for 1 h at room temperature. After two washes in 0.1 M MOPS, the microspheres were equilibrated in coupling buffer (0.1 M Na-phosphate, pH 8). The coupling reaction was carried out overnight at 4°C with 50 µg EGF or 250 µg trastuzumab in 150 µl of coupling buffer for 30 µl of the 5% microsphere slurry with constant agitation. The microspheres were then washed twice with coupling buffer and thoroughly with PBS. The remaining reactive groups were capped with 1 M ethanolamine for 2 h at room temperature followed by further washings in PBS. The microspheres were aliquoted and stored in PBS with 0.1% Na-azide. The presence of trastuzumab on the surface of microspheres was confirmed using fluorescently labeled polyclonal goat anti-human antibody. Uncoupled microspheres showed no staining.

4.10. Cell stimulation with derivatized paramagnetic microbeads

To avoid nonspecific interaction of the microspheres, they were blocked with 1 mg/ml bovine serum albumin (BSA; Sigma) in Tyrode's buffer or PBS. Cells were washed in Tyrode's buffer containing 0.01 M glucose and 0.1-1 mg/ml BSA and maintained in this buffer in a

humid chamber. For stimulation, the magnetic microspheres or free ligand were diluted in 50 µl PBS; the final concentration was approximately 10 to 30 microspheres per cell. To provide a specific time of interaction and initiation of stimulation, the cover slips were positioned on a magnet at time 0. Control experiments were performed without the magnet. After a specified reaction time, between 2 and 45 min at 37°C, cells were rinsed with PBS and fixed with ice-cold methanol for 20 min at -20°C. Uncoupled, EGF-linked, and trastuzumab-linked magnetic microspheres or free trastuzumab, dye-conjugated trastuzumab or EGF in solution were used as stimulating ligands.

4.11. Confocal Laser Scanning Microscopy

For confocal laser scanning microscopy, a Zeiss (Göttingen, Germany) LSM 510 systems with Plan-Apochromat 63×/1.4 NA, oil objective were used. AlexaFluor488 and YFP were excited with 488 and 514 nm Ar ion laser lines and detected through 505-550 nm and 530±15 nm bandpass filter. Cy3 and AlexaFluor543 were excited with a 543-nm HeNe laser and detected through an 560 longpass or 560-615 nm bandpass filter. Cy5 and AlexaFluor647 were excited with a 633-nm HeNe laser and detected through a 650 longpass filter. Pinholes were set to obtain 1 µm optical slices except for high Z-resolution sectioning (Fig. 10.) where 0.5 µm slices were acquired in 0.4 µm steps. Reflection images of the microsphere distribution were taken using a 633 nm HeNe laser without filtering the reflected light, and the pinhole set to 10.3 Airy units. 512 × 512 pixel images were taken with pixel times of 6.4 µs and averaging 2 lines in the case of high-resolution images. All images were obtained in multi-track mode to avoid crosstalk with other channels. With the settings used, channel crosstalk was negligible as determined using single labeled samples.

4.12. Image Analysis

Reconstruction of orthogonal sections was done using the LSM system software (version 3.2). The cross-correlation coefficient characterizing the coincidence of signals in two channels of an image was calculated with a program custom written in the LabView environment [186] using the equation below. Briefly, for a pair of images x and y, the cross-correlation coefficient is defined as

$$C = \frac{\sum_i \sum_j (x_{i,j} - \bar{x})(y_{i,j} - \bar{y})}{\sqrt{\sum_i \sum_j (x_{i,j} - \bar{x})^2 \sum_i \sum_j (y_{i,j} - \bar{y})^2}} \quad (12)$$

where $x_{i,j}$ and $y_{i,j}$ are fluorescence pixel values at coordinates i,j in images x and y. Only those pixels were used for the summation that were above detection threshold in both images. Threshold values were determined as the highest histogram values from images of unlabeled samples taken with identical instrument parameters. The theoretical maximum is C=1 for identical images, and a value close to 0 implies random spatial localization of the two labels relative to each other.

Other image processing tasks were performed using SCIL-Image (TNO, Delft, The Netherlands). For determining ErbB phosphorylation in stimulated and nonstimulated areas of cells, background-corrected fluorescence of immunolabeled phospho-ErbB was used as an input channel. The histogram mean of cells from images of unlabeled samples taken with identical instrument parameters were taken as background values. Binary masks on cells were created by thresholding reflection images. Threshold values were chosen manually to exclude all background pixels; occasional holes in cell masks were filled with dilation-erosion cycles using a 3 × 3 mask and a connectivity of 8 pixels. Additional binary masks for separating stimulated and nonstimulated areas were generated by thresholding reflection images of microspheres when microsphere-coupled ligands were used and by thresholding Cy5-trastuzumab images when trastuzumab in solution was used as stimulus. For calculating the proportion of pixels above the resting level of phosphorylation, overall maximum values from corresponding nonstimulated but equivalently labeled cells were used as threshold.

5. Results and Discussion

5.1. Fluorescence correlation spectroscopy gives new insight into the activation mechanism of ErbB1

For studying how EGF binding alters the mobility and aggregation state of ErbB1, we have used as model system the ErbB1-eGFP chimeric protein stably transfected into CHO cells [181]. Although GFP derivates have a tendency for spontaneous dimerization, these aggregates are not stable (Kd = 100μM) [187], and thus eGFP-fusion proteins are amenable to fluorescence correlation spectroscopy measurements. The presence of endogenous fluorescent label was intended to obviate unwanted artifacts of antibody labeling, however, it also required that the functionality of the construct is confirmed.

5.1.1. The ErbB1-eGFP fluorescent chimera created for FCS measurements is functionally active

Signal transduction through ErbB1 is initiated by activation of the tyrosine kinase and subsequent phosphorylation of tyrosine residues in the receptor C-terminal domain and down-stream substrates. Lysates of ligand-treated and control cells were probed for tyrosine phosphorylated proteins by Western blot (Fig. 6.). The human epidermoid carcinoma cell line A431 served as a positive control. In A431 cells, as well as F1-10 cells, ligand-induced tyrosine phosphorylation of bands with ~170-190 kDa molecular weight, corresponding to ErbB1 was dose-dependent. Due to its larger molecular weight, the mobility of the ErbB1-eGFP fusion protein was smaller than that of the native EGF receptor. Other proteins at ~60, 65, 90 and 100 kDa were also phosphorylated in a dose-dependent manner. In non-transfected CHO cells only two weak bands with 100 and 110 kDa molecular weight were present, and although these were also present in A431 and F1-10 cells, their phosphorylation state did not change upon EGF treatment. The F1-10 cell line expresses only 2×10^4 copies of the ErbB1-eGFP fusion protein on average compared to 2×10^6 EGF receptors in A431 cells. For this reason, the intensity of the band corresponding to the receptor was much weaker in F1-10 than in A431 cells and for better visibility a contrast-enhanced image is also show (Fig. 6b.)

Phospholipase Cγ is one of the early down-stream effectors of EGF receptor signaling. Activation of this enzyme by binding to phosphotyrosine residues of EGFR leads

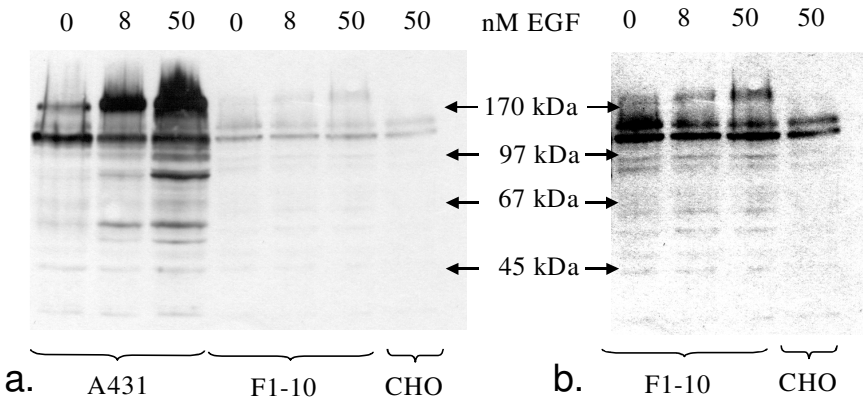

Fig. 6. Elevated tyrosine phosphorylation upon EGF treatment
(a) Anti-phosphotyrosine Western blot of A431, F1-10 and CHO cells in rest, and stimulated with 8 or 50 nM EGF. (b) Contrast-enhanced image of the lanes for F1-10 and CHO from the blot in A. In A431 cells phosphotyrosine immunoreactivity increases in a dose-dependent manner upon EGF treatment. In F1-10 cells, this dose-dependent elevation is less prominent, but still detectable. Untransfected CHO cells served as negative control.

to the generation of diacylglycerol and release of inositol-trisphosphate, eliciting an increase of intracellular calcium concentration [188]. The aim of the Ca^{2+} measurements was not an absolute determination of Ca^{2+} concentration, but the mere demonstration of the presence of Ca^{2+} responses and illustration of their relative magnitude for different cells and different conditions. Changes in intracellular calcium were detected by ratiometric imaging of the fluorescence of the Ca-indicator dye Fura-2 excited at 340 and 380 nm. Resting intracellular Ca^{2+} levels of 80-120 nM and F340/F380 ratios around 1 were characteristic of all three cell lines. Positive control A431 cells showed prominent Ca^{2+} elevation upon 50 nM EGF, in comparison, F1-10 cells expressing ErbB1-eGFP produced definitely lower but still measurable Ca^{2+} peaks (Fig. 7.). At 8 nM EGF a calcium response was detectable in A431 cells only. CHO negative controls did not exhibit an increase in intracellular calcium at any EGF concentration. Similarly to tyrosine phosphorylation, the background of the weaker calcium response in the case of F1-10 is likely the order of magnitude lower level of receptor expression. This is not a disadvantage, however, if one wants to examine the process of receptor activation at more physiological expression levels.

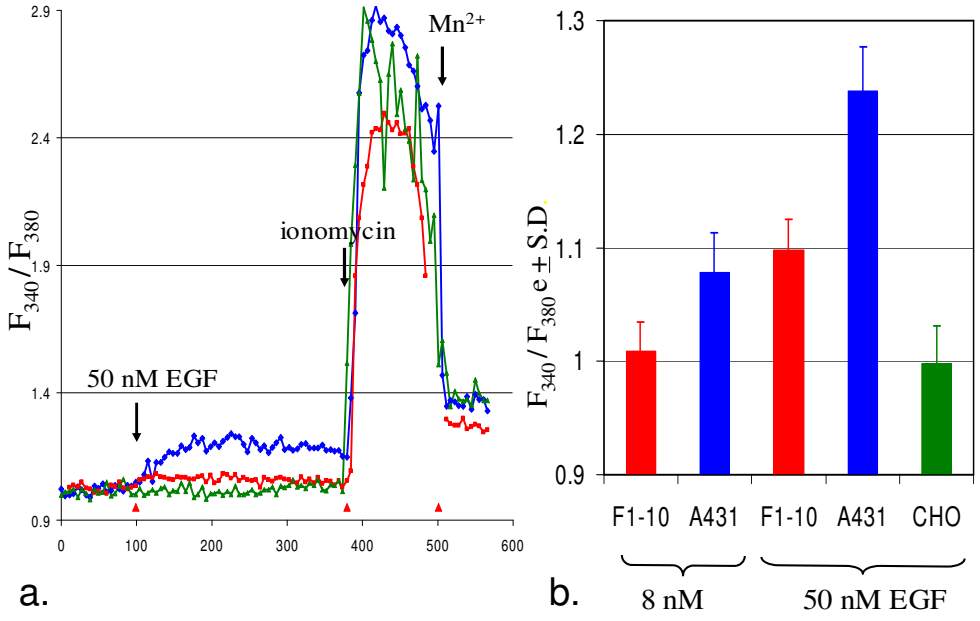

Fig. 7. Calcium responses upon EGF simulation
(a) A typical calcium responses to EGF stimulation are shown – red trace: F1-10, blue trace: A431, green trace: CHO. Resting F340/380 ratios were around 1 in all the cell lines. EGF stimulation, calibration with ionomycin and quenching by Mn are also indicated on the curve. (b) Averaged peak calcium responses of 10-30 cells are presented. A431 cells have responded to both 8 and 50 nM EGF, whereas in the case of F1-10, the elevation was only significant after stimulation with 50nM EGF. Control CHO cells were not stimulated by EGF.

5.1.2 Diffusion rate of ErbB1 decreases upon EGF stimulation

FCS measurements imply the continuous illumination of fluorophores in a sub-micron sized spot. During the initial part of this illumination, we have experienced photobleaching of a fraction of ErbB1-eGFP fluorescence (Fig. 8a.). This exponential decay of intensity with a time constant of 1-2 s has contributed an additional slow component to the autocorrelation curve and thus hindered the correct fitting of ErbB1 diffusion times. In order to avoid the continuous decrease of intensity during autocorrelation measurements, the fluorescence of the fraction of molecules with low mobility was photobleached by illuminating the sample using an intensity of 10 kW/cm^2 for 30-60 seconds, until the fluorescence was constant. The remaining intensity was 26 ± 16 % SD (n=21) of the original one. We can assume that in the first period of the measurements we have photobleached the immobile, anchored fraction of ErbB1-eGFP that was not, or just slowly substituted by diffusion, and thus unable to escape

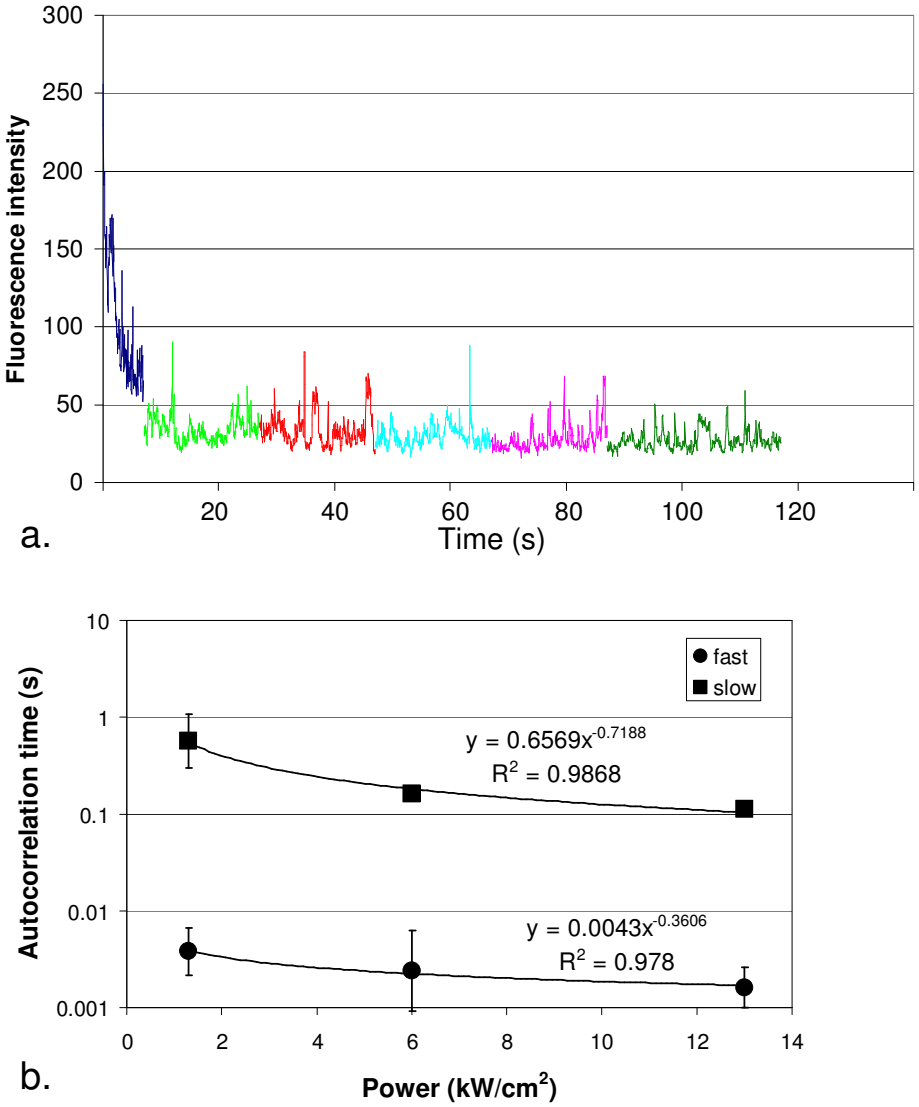

Fig. 8. Photobleaching of the immobile ErbB1 fraction
(a) Fluorescence intensity fluctuation traces taken consecutively at the same place of the cell membrane are shown in different color. Initially, the fluorescence of immobile eGFP-ErbB1 fraction is bleached, leading to a prominent decrease of fluorescence intensity. Including this time range into the fit adds a slow component to the autocorrelation function which is unrelated to slow diffusion in the membrane. To avoid related artifacts, we have analyzed the fluorescent intensity fluctuations after bleaching the immobile fraction.(b) Apparent diffusion autocorrelation times of ErbB1-eGFP as a function of illumination power. A fast and a slow autocorrelation time was determined for each cell. Both values are gradually underestimated with increasing laser power, but the slow, membrane component is more affected (please not the log scale). Mean ± S.D. for 4-6 independent experiments.

photobleaching or light-driven blinking. The bleachable fraction was proportional to the initial fluorescence intensity of the cell. The non-bleached fraction exhibited a steady average fluorescence in time indicating that its diffusion is fast enough to exchange the illuminated population before it is irreversibly bleached. We must note, however, that this strategy

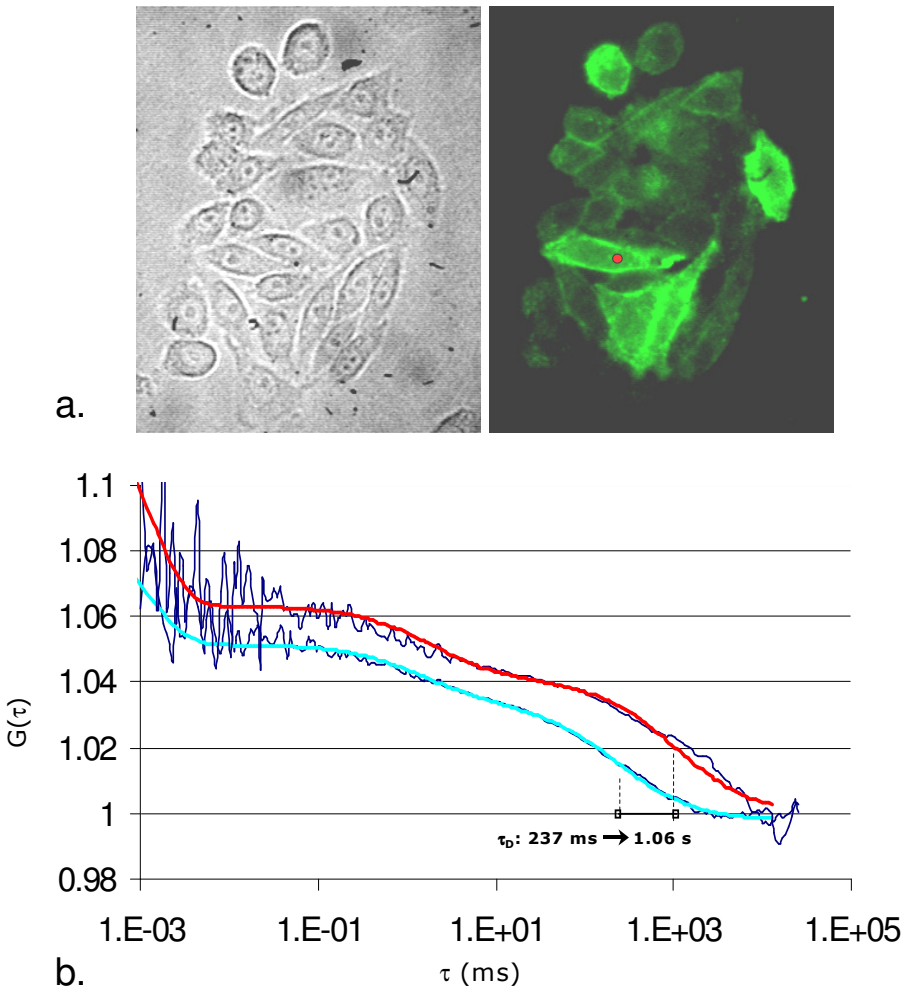

Fig. 9. FCS shows slowed down diffusion upon EGF treatment
(a) transmission and fluorescent images of F1-10 cells. A red dot indicates the localization of the confocal volume. (b) Fitted autocorrelation curves taken before (blue) and after (red) EGF stimulation. The autocorrelation time characteristic of the slower diffusion component has increased form 237 ms to 1.06s upon EGF stimulation as it is indicated by right shifting of the curves.

restricts FCS measurements to reasonably rapidly diffusing species, or at least hinders the exact determination of proportions among species with varying diffusion constants. In fact, in a separate series of experiments we have determined that at higher laser powers, where more of the slowly diffusing species are photobleached, the overall diffusion determined in FCS appears to be faster, and if more components are differentiated, the slower components will be more affected (Fig 8b.).

Result of a fluorescence correlation spectroscopy measurement can be seen on Fig. 9. with the transmission and fluorescence images of F1-10 cells (Fig. 9a.), and autocorrelation

curves before and after EGF treatment (Fig. 9b.). Using the general mathematical model in eq. 3., we have tested five different approaches and found that the autocorrelation curves can be best fitted, on the grounds of minimum number of necessary components and lowest mean square error, by a four-component model. This model takes into account a fast and a slow diffusion component (n=2 in eq. 3), in addition to triplet state formation ($G_{triplet}$), and a blinking component (G_{blink}) that apparently covers both protonation dependent blinking terms as well as light induced blinking. Of the diffusion terms, the fast one is a 3 dimensional diffusion, originating mostly from the cytoplasm [181], whereas the slow one is proposed to be a 2D motion in the plane of the membrane. In this model, we allowed for the possibility of anomalous subdiffusion or obstructed diffusion for both diffusing species. The anomaly parameter d_w (see eq. 3.) expresses the degree of non-linearity. For free Brownian diffusion this value equals 2, while for obstructed diffusion this value is larger than 2. Data obtained from 12 independent experiments for cells that were measured on the same membrane spot before and after stimulation with 50 nM EGF are shown in Table 1.

Table 1

Fit Parameter	Before EGF	After EGF
D_1 (10^{-7} cm^2/s)	1.97±0.83	1.63±0.94
D_2 (10^{-9} cm^2/s)	1.17±0.51*	0.66±0.30*
W_1	0.30±0.06	0.36±0.12
$d_{w,1}$	2.12±0.38	2.43±0.35**
$d_{w,2}$	2.02±0.14	1.96±0.16
Θ_c	0.09±0.01	0.09±0.01
τ_c (10^{-4} s)	1.81±0.21	1.87±0.22
T	0.47±0.08	0.51±0.14
τ_{tr} (10^{-6} s)	2.3±0.5	2.5±0.9
Mse	3.5	3.5

Diffusion properties of ErbB1-eGFP fusion protein revealed by FCS

Data are presented as means ± S.D. from twelve independent experiments with autocorrelation recorded immediately before and after stimulation with 50 nM EGF.
D: diffusion constant, w: weight of diffusion component, d_w: anomaly parameter, T: triplet fraction, τ_{tr}: triplet lifetime, Θ_c: fraction of dark species, τ_c: chemical relaxation time of the protonation process, mse: mean squared error of nonlinear fits.
* D_2 changed significantly after EGF stimulation (two-tailed paired t-tests p=0.0016); D_1 has not changed significantly.
** $d_{w,1}$ differed significantly from 2 after EGF stimulation (p=0.00004), i.e. the diffusion of the fast cytoplasmic component can be described by a model of obstructed diffusion. $d_{w,2}$ has not changed significantly.

The faster diffusion was characterized by a diffusion constant of $1.97\pm0.83 \times 10^{-7}$ cm^2/s. The cytoplasmic nature of this fast component was confirmed by the position dependence of the relative contribution of this component to the autocorrelation function. In the cytoplasm of resting cells, the fast component contributed 59 ± 8% to the autocorrelation function, compared to only 33 ± 5% when the beam waist was placed on the plasma membrane. This component could be attributed to ErbB1-eGFP fusion proteins being transported in vesicles, to free cytoplasmic ErbB1-eGFP that had lost its signal sequence, proteolytic release of GFP into the cytoplasm, GFP transcribed alone owing to the strong promoter of the plasmid, or other fluorescent molecules native to the cytoplasm. Of these possibilities the first can probably be excluded as the diffusion constant of integral membrane proteins in intracellular membranes is comparable to that in the cytoplasm membrane [189-191] and the speed of vesicular traffic is even slower than that [192]. The other possibilities are supported by earlier data on the diffusion constant of free cytoplasmic GFP also obtained using FCS ($D = 1.7 \pm 0.4 \times 10^{-7}$ cm^2/s [181] and $1.25 \pm 0.13 \times 10^{-7}$ cm^2/s [179]). The failure to detect free GFP in Western blots of F1-10 cell lysates may signify that the fast diffusing species is the cytoplasmic fusion protein, but it also could be attributed to too low concentrations of this proteolytic fragment. As this molecular species will largely escape photobleaching, analysis of the autocorrelation functions will overestimate the relative fraction of these molecules compared to the full length receptors.

The slow diffusion term gave rise to a diffusion constant of $1.17\pm0.51\times 10^{-9}$ cm^2/s. Control measurements have indicated co-diffusion of the intracellular GFP tag on ErbB1 and AlexaFluor647 labeled 528-Fab attached to the extracellular domain of ErbB1 on F1-10 cells, confirming that this component of the autocorrelation spectrum originates from movement of receptors in the plane of the cell membrane. The diffusion constant derived was consistent with a relatively freely diffusible transmembrane protein [193]. In coherence with this, for the membrane diffusion component the anomaly parameter was 2, which hints that in the small area examined by FCS, overall there are no obstacles to diffusion. Upon EGF stimulation, the most obvious change occurred in the slow membrane diffusion component D_2, which on average slowed to about half of the original value immediately upon EGF stimulation. The most extreme example of this is plotted on Fig. 9b., where the characteristic diffusion time shifts from 237 ms to 1065 ms. This observation is coherent with the predicted di- and oligomerization of the ErbB1 receptors during their activation, but does not exclude the possibility that ErbB1 exists also in the form of pre-associated dimers that upon EGF

stimulation associate to larger aggregates, other proteins, or cytoskeletal elements, leading to their decreased lateral mobility.

The only other parameter that has changed was the anomaly parameter of intracellular fast diffusion, which increased after EGF treatment. This observation hints that diffusion of the cytoplasmic ErbB1-eGFP (or free eGFP) becomes hindered upon cell stimulation. This is best explained by allocating this component to free ErbB1-eGFP, which upon ErbB1 activation can transiently interact with the intracellular domains of membrane-localized receptors. However, it must be noted that the shape of the autocorrelation function has a weak dependence on the anomaly parameter d_w, implying that the fitted value of this parameter may carry considerable error and the degree of its alteration upon stimulus could easily be overestimated.

5.1.3 ErbB1 could exist also as pre-formed di- or oligomers

In resting cells, the ErbB1-eGFP fusion proteins showed a relatively uniform distribution (Fig. 10a). Stimulation with EGF led to receptor aggregation and internalization within 5 min, which was still apparent even 30 min after stimulation (Fig. 10b). Parameters derived from autocorrelation measurements acquired directly before and after adding 50 nM EGF to the cells are shown in Table 1., and on a cell-by-cell basis on Fig. 11. As discussed above, the diffusion constants on average decreased upon stimulation with EGF, and this was indeed the case for each cell that could be measured before and after stimulus on the same membrane patch (Fig. 11a). In addition, EGF caused a decrease of the number of molecules N in the detection volume in most of the cases (Fig. 11b.). The average ratio of the apparent number of molecules after and before EGF incubation was 0.78. These two observations so far are consistent with the more widely accepted theory that upon EGF stimulation, EGF receptors aggregate.

Receptor oligomerization was further evaluated by calculating the fluorescence per molecule normalized to laser power (*fpm*). The *fpm* is obtained by dividing the background corrected fluorescence F by the background corrected number of molecules N and the laser power P:

$$fpm = FN^{-1}P^{-1} \qquad (13)$$

The background fluorescence was corrected for with the following formula [194]:

$$G_{corr}(\tau) = \left(1 - \frac{I_B}{I_{tot}}\right)^2 \left[G(\tau) - a_0\right] + a_0 \qquad (14)$$

where I_B is the uncorrelated background intensity (cellular autofluorescence and dark current of the photodiodes), I_{tot} is the total intensity including the signal and the background, $G(\tau)$ is the autocorrelation and a_0 is the offset term as described in eq. 3.

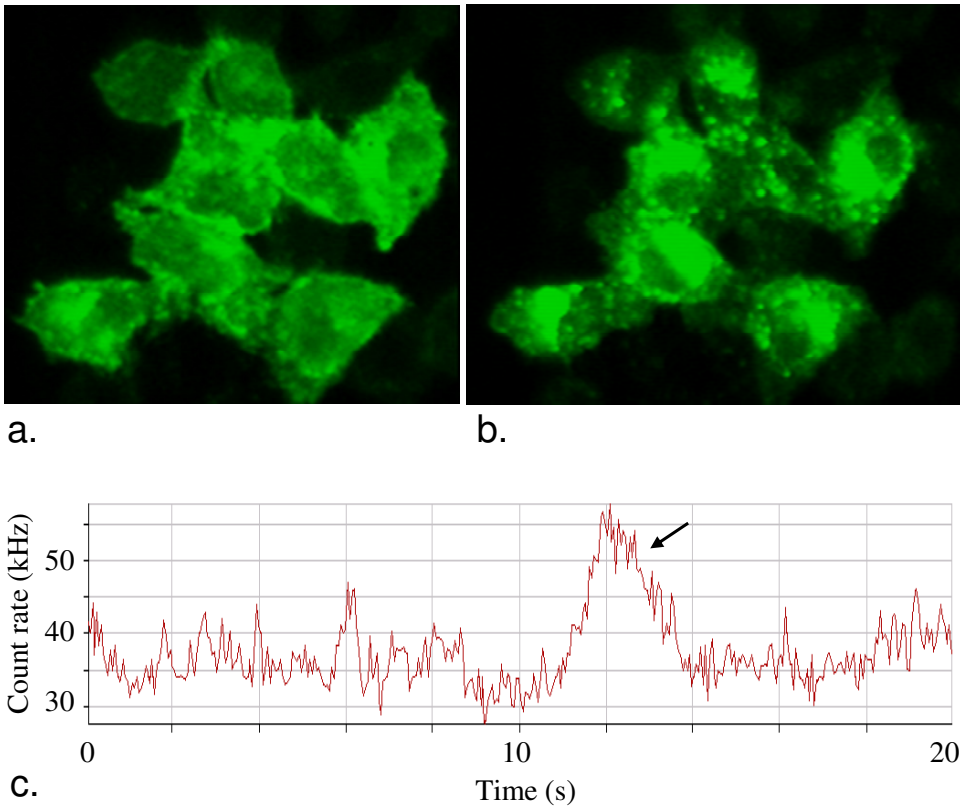

Fig. 10. GFP-ErbB1 distribution before and after EGF stimulation
Fluorescence images of F1-10 cells were taken before (a) and ~30 minutes after (b) EGF stimulation. In resting cells, the distribution of receptors is more uniform than in stimulated cells, where it is more granular. (c) After stimulation, diffusion of sizeable aggregates across the observation volume can be observed with FCS (arrow).

The mean fluorescence decreased after stimulation, but only to the same extent as the number of molecules *N*; consequently, the mean fluorescence per molecule was unaffected (Fig. 11c.), and the ratio of the *fpm* values after and before stimulation was close to 1 (0.94±0.36) (Fig. 11d.). These findings may reflect activation of the receptors according to the conformational

activation model (not involving a change in the aggregation state of the receptor) rather than by induced receptor dimerization or oligomerization. In fact, in a very recent study applying a modified fluorescence intensity distribution analysis (FIDA) approach for use in a two-dimensional system with quantal brightnesses, the degree of EGF receptor clustering on the surface of transfected CHO cells has been quantified, and the analysis has demonstrated that under physiological conditions, the EGF receptor exists in a complex equilibrium involving single molecules and clusters of two or more receptors [195].

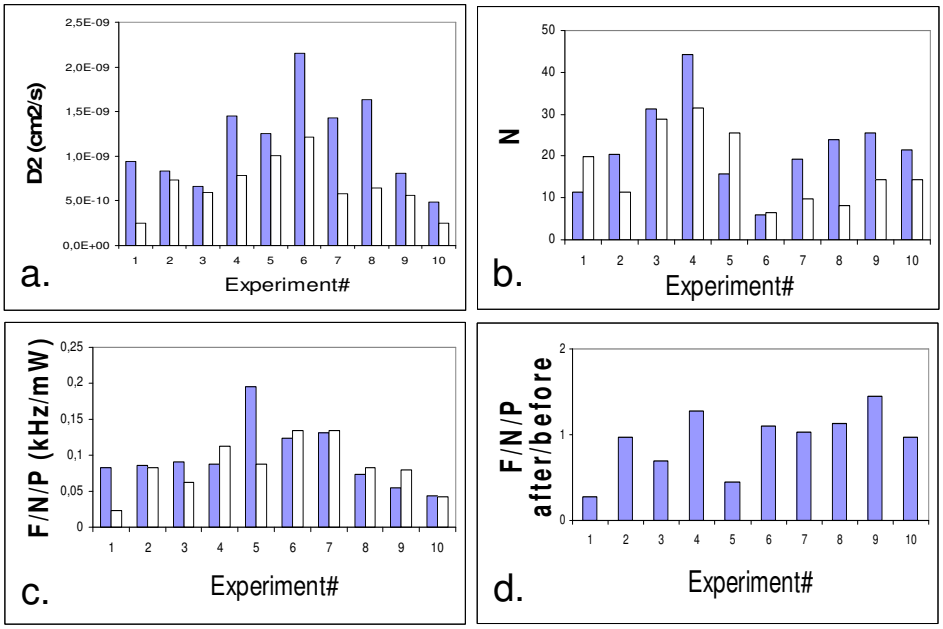

Fig. 11. Effect of EGF stimulation on ErbB1 dynamics and membrane distribution
Filled (blue) bars: before treatment, open bars: after treatment. (a) the change of *D2,* the longer, intra-membrane diffusion component upon stimulation by 50 nM EGF. (b) the change of the apparent number of independently moving particles in the detection volume, *N*. (c) effect of EGF treatment on the normalized specific fluorescence per independently moving particle. F is the fluorescence intensity in kHz, N is the average number of molecules in the detection volume and P is the laser power. (d) ratio of F/N/P values after and before stimulation.

On the other hand, the two-fold decrease of *D* even exceeds the theoretically predictable value for dimerization (assuming spherical molecules this would be by a factor of $\sim\sqrt[3]{2}=1.26$). A higher order oligomerization of the receptors could explain the drastic decrease of D but is inconsistent with the meek 22% decrease of the number of independently diffusing species. The constancy of the normalized fluorescence per molecule also indicates

that, in the first few minutes of activation, the aggregate size of EGF receptors does not change significantly.

This discrepancy is best resolved by hypothesizing the immobilization or at least hindrance of the motion of the ErbB1-eGFP fusion proteins by interaction with static structures such as the underlying cytoskeleton [196]. However, we have to keep in mind that the chromophore of a large fraction of the receptors is bleached and therefore not subject of the FCS studies. Thus, it is equally plausible that receptor aggregation / dimerization also occurs, but it is only reflected by the decrease in diffusion constant, as the detected ErbB1-eGFP molecules, or preformed dimers adhere to the more slowly moving higher order clusters that are already photobleached in the pre-bleach period and thus do not contribute to the specific fluorescence per particle value. Most recent single-wavelength fluorescence cross-correlation and fluorescence resonance energy transfer (FRET) data actually support the idea that the EGF receptor exhibits preformed homodimeric structures on the cell surface which further aggregate upon EGF stimulation. In fact, we also have observed that within half an hour of stimulation receptor clusters become more prominent (Fig. 10b.), and these cluster could be seen diffusing across the FCS observation volume (Fig. 10c.).

5.1.4. Complementarity of Fluorescence Recovery After Photobleaching and FCS in resolving the mobility of ErbB1

Our fluorescence recovery after photobleaching (FRAP) experiments in resting cells yielded diffusion coefficients of 0.7-0.9×10^{-10} cm^2/s (Table 2.).

Table 2.

	FCS	FRAP	
model	anomalous	anomalous	generic
D ($cm^2/s \times 10^{-10}$)	10.70	0.90	0.71
S.D.	4.00	0.33	0.31
No. of cells	26	51	51
d_w	2.02	-	-
α	-	0.6	0.8

Diffusion constants determined for the EGFR-GFP fusion protein using FCS and FRAP on resting cells

FCS data from F1-10 cells were evaluated according to eq. 3. (a fast and a slow species with anomalous diffusion, one blinking term plus triplet correction; in the table the slow diffusion coefficient is given). FRAP recovery curves on F1-4 cells were fitted to the anomalous diffusion model either fixing $f_\infty = f^0$ (termed anomalous) or leaving the value of f_∞ free (generic).

Earlier reports on the lateral diffusion coefficients of EGF receptors determined by FRAP are available for several cell types: $D = 4.5\text{-}8.2 \times 10^{-10}$ cm^2/s at 15-37 °C on A431 cells [197], $D = 1.8 \times 10^{-10}$ cm^2/s, on fibroblasts and $D = 4.1 \times 10^{-10}$ cm^2/s on keratinocytes [198]. The common feature of these measurements was the application of fluorescently labeled EGF which obviates the possibility to obtain data on resting cells. The lower range of these data converge to our diffusion constants obtained by FRAP, while the higher range reaches the lower diffusion constants we have measured using FCS after stimulation. Some of these discrepancy can easily explained by the use of different cell types and experimental conditions, as well as the possibly biased nature of FRAP measurements using the ligand EGF as a label. However, the difference of one order of magnitude in our data obtained with similar resting cells needs to be interpreted further.

To understand this discrepancy, the different nature of the experiments must be considered: in FCS, the local environment of a relatively small area of the membrane is probed, which may be smaller than the diameter of a membrane domain. Therefore mainly diffusion inside a membrane microdomain determines the diffusion correlation time. In FRAP, the long-range diffusion rate of unbleached molecules arriving from more distant areas and having to cross domain boundaries is also examined. Thus, the rate of long-range receptor motion is not only affected by the intradomain diffusion rate, but also by the rate of crossing domain boundaries [199,200]. It also has to be kept in mind that in the FCS measurements receptors with low mobility were pre-bleached to avoid artifacts in the autocorrelation function, so the motion of this fraction of the molecules was not subject of the FCS studies.

When the autocorrelation functions were fitted with models including a blinking term and two anomalous diffusion components, the average anomaly parameter of the membrane diffusion term was close to two, corresponding to free Brownian diffusion. In contrast, for FRAP measurements the anomaly parameter lesser than unity (α=0.6 or 0.8 depending on the model used) hints at the possibility of obstructed diffusion. Anomalous diffusion can result from either molecular interactions (binding to immobile structures or large complexes), frequent collisions with densely packed obstacles or corralling due to boundaries between distinct membrane domains [184,201,202].

The uncertainty of detecting anomalous diffusion in the FCS measurements may originate from the fact that fluctuations resulting from molecular movements in the immediate vicinity of the detection volume are detected. In contrast, in FRAP the recovery of fluorescence results from diffusion of molecules over both short and longer distances. Molecules therefore may encounter a large number of diffusion barriers. Thus the short-range

diffusion of molecules in FCS will be hardly affected by boundaries and heterogeneities in membrane organization. Only if a diffusion barrier lies within the detection volume, or if membrane microdomains are comparable in size with the detection volume, may anomalous diffusion be observed. The diffusion constant and anomaly parameter may also depend on the size of the membrane domain and the position of the detection volume with respect to the domain boundaries: inside a larger domain, observed diffusion may occur faster than in the case of smaller ones, where domain boundaries need to be crossed to observe mobility (hop diffusion) [203-205]. The large standard deviation of the slow diffusion constant and the anomaly parameter in the FCS measurements may reflect such factors of microheterogeneity of the plasma membrane.

Thus FCS can be said to be an adequate probe of local diffusion rates and molecular mechanisms. However, the large fraction of receptors with low mobility demonstrates a practical limitation of FCS in cellular studies set forth by the sensitivity of the method to the displacement of the membrane with respect to the detection volume. These factors prevent measurements of diffusion times as slow, or slower than a few seconds (in our case τ_ds longer than a few seconds). For investigating such slow diffusion processes FRAP may be a more adequate approach.

5.2. Derivatized microbeads as a novel tool for assessing ErbB activation

Microspheres covered with ligands or antibodies are used in many fields of biochemistry, biophysics and cell biology. Immunomagnetic microsphere separation and microparticle based flow cytometry play an important role in experimental protocols and analytical procedures [206,207]. Recently, microspheres have also served as powerful tools for studying complex cell biological phenomena such as collagen phagocytosis in fibroblasts [208,209], viscoelastic responses of endothelial cells upon thrombin stimulation measured by magnetic microsphere-based microrheology [210], and re-organization of lipid rafts and signaling complexes upon various stimuli [211-217]. Microsphere-based techniques also allow localized stimulation of cells with precise control of timing and location, providing a versatile tool for kinetic assays of signal spreading and downstream propagation. In our studies, we used EGF and trastuzumab coupled paramagnetic microspheres to explore the activation properties of ErbB1 and ErbB2 *in situ*.

5.2.1. EGF and trastuzumab conjugated microspheres efficiently evoke ErbB autophosphorylation

To test the functionality of trastuzumab- and EGF coupled microspheres, we first used a cell line derived from the A431 epidermoid carcinoma by stably transfecting it with the ErbB2-mYFP chimera gene. Native A431 cells express 2×10^6 ErbB1 and 4×10^4 ErbB2 receptors as measured by flow cytometry. The transfected line A4-ErbB2-mYFP exhibits a somewhat downregulated expression of ErbB1 (1.2×10^6) and 9.5×10^5 ErbB2 per cell. Applying EGF microspheres, ErbB1 could be focally activated (Fig. 12.) as previously described for these microspheres [25,26]. Activation was detected as total tyrosine phosphorylation (Mab PY99) [26] and as specific phosphorylation of ErbB1 (Mab clone74). The correlation between the phosphorylation signal and location of microspheres was high, as characterized by the cross-correlation coefficients C = 0.68 and C = 0.57 for phospho-ErbB1 and phosphotyrosine, respectively. (Not all microspheres lay in the same plane as the confocal immunofluorescence images show. Thus, activation signals coincided with a subset of microsphere loci in this case, whereas the correlation coefficients were calculated from stacks of confocal images through the cells.) Trastuzumab microspheres on the same cells also evoked local total tyrosine phosphorylation (Mab PY99) and specific ErbB2 phosphorylation (Mab 18). The correlation of microsphere position with ErbB2 and generic tyrosine phosphorylation was high, as indicated by the cross-correlation coefficients 0.68 and 0.47, respectively. When uncoupled microspheres were used as control, no activation above the level of baseline phosphorylation was detected. It is noteworthy that the correlation between microspheres and specific ErbB phosphorylation was always higher than that between microspheres and generic phosphotyrosine labeling, implying that signal spreading from the activated receptors may be attributed to other molecular species, including adapters like Shc, but possibly also to other downstream effectors such as Ras.

5.2.2. Focal stimulation by EGF and trastuzumab microspheres yields a well-localized activation process without lateral signal spreading

As shown in Fig. 12., trastuzumab- and EGF-coupled microspheres caused a local activation of ErbB receptors, which was evident also from the high degree of correlation between microsphere position and receptor phosphorylation. We observed only highly localized activation of the receptors in the immediate proximity of the microspheres. There was no spreading of phospho-ErbB1 activation over the plasma membrane in any cell line expressing ErbB1 and stimulated with EGF-linked magnetic microspheres regardless of

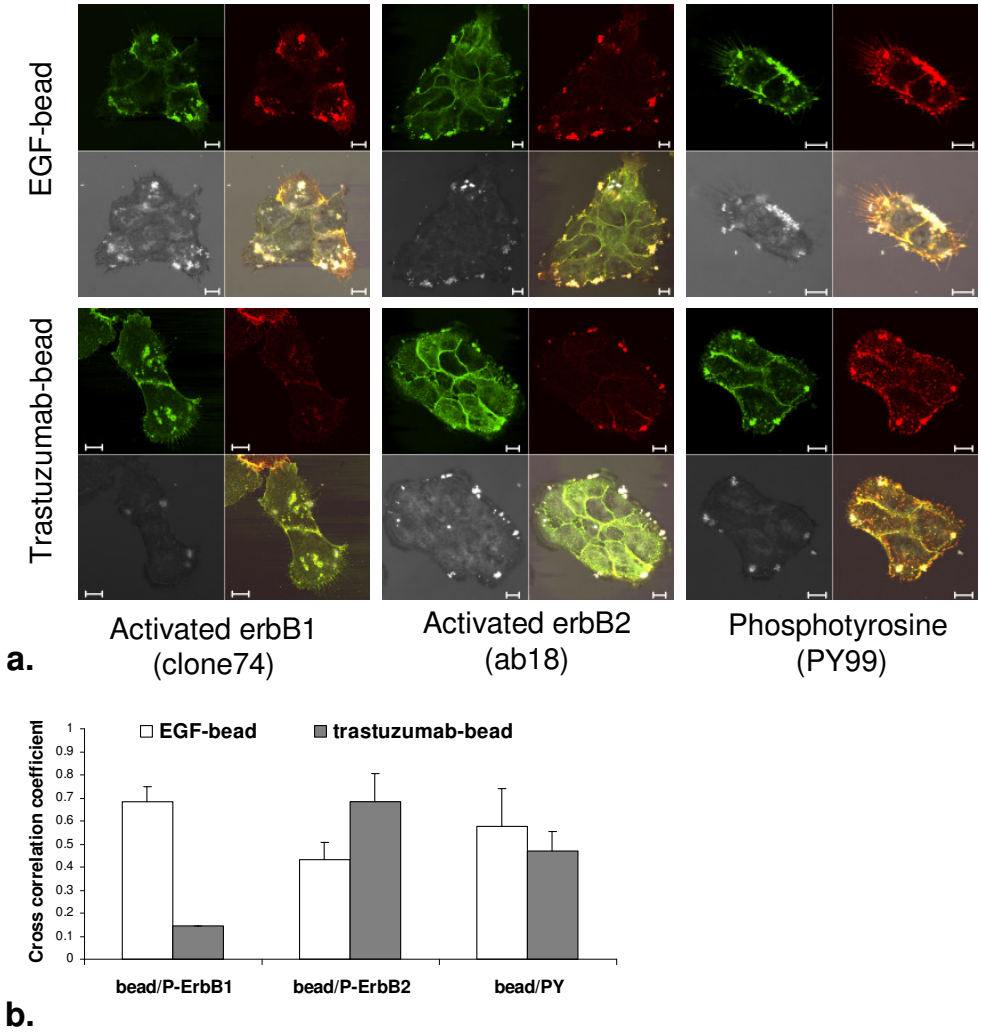

Fig. 12. Signaling efficiency of derivatized microspheres and transactivation of ErbB receptors

(a) Images of A431 cells, stably transfected with an erbB2-mYFP construct, are shown after 10 min of stimulation with EGF- or trastuzumab-coupled microspheres. Green images, YFP signal; red images, activated erbB1 (left), activated erbB2 (middle), and tyrosine phosphorylation (right). Reflection gray-scale images show the location of individual and clustered microspheres as bright spots. On the overlay images, only overlap of the microspheres localized in the confocal fluorescence plane can show coincidence. Scale bar, 10µm. Upper row, EGF-coupled microspheres, lower row, trastuzumab-coupled microspheres. (b) Cross-correlation values (± S.D.) for EGF- (open columns) and trastuzumab- (gray columns) microsphere-covered areas and phosphorylation of erbB1 (left), erbB2 (middle), and tyrosine residues (right).

whether the microspheres were applied with or without a magnet. Transactivation of ErbB2 induced by EGF-linked magnetic microspheres was also well localized spatially. ErbB2-mYFP was recruited with ErbB1 to EGF microspheres from the surrounding membrane, but

phospho-ErbB2 was almost exclusively around the EGF microspheres. Similarly, trastuzumab microspheres recruited ErbB2-mYFP to their neighborhood and initiated phosphorylation of the receptor, which was then followed by apparent efforts to internalize the microspheres (Fig. 13.). The co-localization of red (phosphotyrosine) and green (ErbB2-mYFP) signals was almost complete around the microspheres. The ErbB2-mYFP molecules and the surrounding membrane concentrated around the microspheres, with a signal-free area corresponding to the interior of the microsphere (see the orthogonal sections in Fig. 13). Clusters of ErbB2-mYFP were also observed outside the microsphere-covered areas (arrows in Fig. 13) but there was no sign of phosphorylation in these clusters. Stated quantitatively, in microsphere-covered areas the ratio of background corrected YFP/phosphotyrosine signal was 1.2 ± 0.2, whereas in areas outside the microspheres that were above background for YFP, the corresponding ratio was 6.8 ± 1.4.

Verveer et al. [24] experienced that after focal stimulation, ErbB1 activation has spread rapidly to the unstimulated areas of the cell membrane suggesting further associations and secondary dimer formation after ligand binding. In contrast, others have detected local patches of stimulation [25,26,218] Even under conditions of receptor overexpression, only downstream activation of intracellular elements of the ErbB1 signaling pathways and localized polymerization of actin [218] could be seen. We have confirmed these latter observations using several cell lines, and extended then also to trastuzumab microspheres, that exhibited only local activation and induced internalization similarly to EGF-coupled magnetic microspheres. The absence of lateral spreading confirms the notion derived from FCS measurements that preformed ErbB1 di- or oligomers could be instrumental in EGF-based signaling. The observation that EGF-evoked signals do not spread laterally even at high ligand densities gains importance in light of most anti-ErbB1 therapeutic antibodies relying on blocking EGF binding. On cells with pre-formed signaling units and lacking lateral signal spreading, such blocking mechanism can be more effective.

5.2.3. EGF-bound ErbB1 transactivates ErbB2 but trastuzumab-bound ErbB2 does not transactivate ErbB1

Measuring the activation of ErbB1 and ErbB2 upon stimulation allowed the assessment of the degree of transactivation of ErbB1 to ErbB2 and of ErbB2 to ErbB1. In the latter case, trastuzumab-coupled microspheres provided a unique new tool because ErbB2 has no physiological ligand, but trastuzumab is able to induce specific ErbB2 phosphorylation. We have observed quite strong ErbB2 phosphorylation upon EGF-microsphere stimulation, for

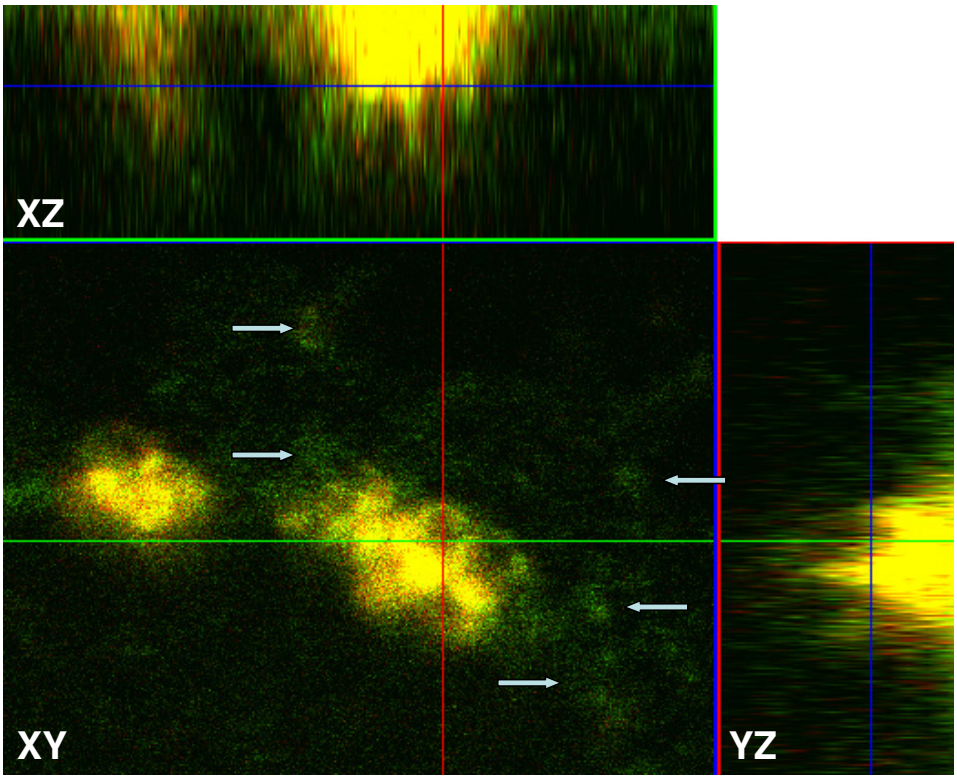

Fig. 13. Trastuzumab microspheres are internalized after erbB2 activation
Stimulation with Herceptin microspheres for 10 min resulted in focal aggregation and phosphorylation of erbB2 molecules. Orthogonal reconstruction of the image stacks shows microspheres engulfed by the membrane. Orthogonal sections of a part of an A4-erbB2-mYFP cell are shown. The x-y section, as indicated by the blue lines in the x-z and y-z projections, shows the membrane surface of the cell where the microspheres were bound. Green channel, erbB2-mYFP; red channel, phosphotyrosine immunofluorescence. Microspheres are surrounded by aggregated erbB2-mYFP receptors, overlapping completely with the phosphotyrosine signal. Membrane areas void of microspheres contain clusters of erbB2-mYFP that are negative for phosphotyrosine (PY) and therefore appear as faint green patches (arrows). The hollow area indicated by the cross-hairs is the center of the nonfluorescent microsphere. Image dimensions (x, y, z) are 16.2 × 16.2 × 0.4 μm per optical slice.

which the cross-correlation between microsphere locus and phospho-ErbB2 was C = 0.43 (Fig. 12b.). In the reverse direction, however, very little activation of ErbB1 was seen upon trastuzumab-microsphere stimulation. A phospho-ErbB1 specific immunofluorescent signal was not observed above the level in starved, resting cells, and correlated poorly with microsphere location (C = 0.13, Fig. 12b.). In a few random cells, ErbB1 was spontaneously activated without added ligand (see membrane of a cell at the top of the panel of Fig. 10a.), a property characteristic of A431 cells. Because on these cells ErbB1 and ErbB2 were

expressed at roughly the same levels, the asymmetric results indicate a much higher affinity of EGF bound ErbB1 for ErbB2 than that of the trastuzumab bound ErbB2 for ErbB1. A possible explanation could be that bivalent trastuzumab binding to ErbB2 favors ErbB2 dimer formation and sterically hinders its association with ErbB1, although probably not by obstructing the dimerization loop, but rather by preventing the formation of a multimer of at least one ErbB1 and an active ErbB2 dimer [219].

5.2.4. Transactivation of ErbB2 via ligand bound ErbB1 depends on receptor density

We have, as a next step, exploited the possibility that both ErbB2 activation with trastuzumab linked microspheres and ErbB1 activation with EGF-microspheres was feasible only on A4ErbB2-mYPF but also on SKBR-3 and JIMT-1 cells and examined whether transactivation of ErbB1 and ErbB2 occurred on these cell lines. A lack of specific ErbB1 phosphorylation in SKBR-3 and JIMT-1 cell lines indicated that trastuzumab microspheres did not activate ErbB1 (Fig. 14.), a result consistent with that obtained on A4ErbB2-mYPF cells. The cross-correlations of bead location and P-ErbB1 signal in the images shown were 0.26 and 0.16 for SKBR-3 and JIMT-1, respectively. Trastuzumab in solution was also unable to evoke ErbB1 phosphorylation, where EGF-linked microspheres were effective in directly activating ErbB1 on SKBR-3 and JIMT-1, albeit at very low levels. The signal intensity of phospho-ErbB1 immunofluorescence was roughly proportional to the level of ErbB1 expression on the two cell lines, whereas the fraction of pixels under EGF microspheres that showed ErbB1 phosphorylation above resting levels were 59 ± 22% and 43 ± 19% ($n > 10$) for SKBR-3 and JIMT-1 respectively, comparable to the results with trastuzumab microspheres. The very high degree of phospho-ErbB2 activation seen in the case of A4ErbB2-mYFP cells could not be detected at the EGF-linked microsphere loci on SKBR-3 and JIMT-1 cells. Nevertheless, phospho-ErbB2 was generated underneath these microspheres (Fig. 14.) and the phospho-ErbB2 signal intensity in SKBR-3 and JIMT-1 reached 40% and 25%, respectively, of the hypothetical maximum stimulation that was generated by trastuzumab microspheres (Fig. 15a.). In addition, the proportion of pixels under EGF-microspheres that exhibited ErbB2 phosphorylation above resting levels was significantly higher than outside the microspheres (Fig. 15b.). The differences in the activation of ErbB2 through ErbB1 in the cell lines examined appeared to be proportional to the differences in ErbB1 expression levels. We conclude that ErbB2 transactivation in cells with similar ErbB2 levels is dependent on the expression level of ErbB1.

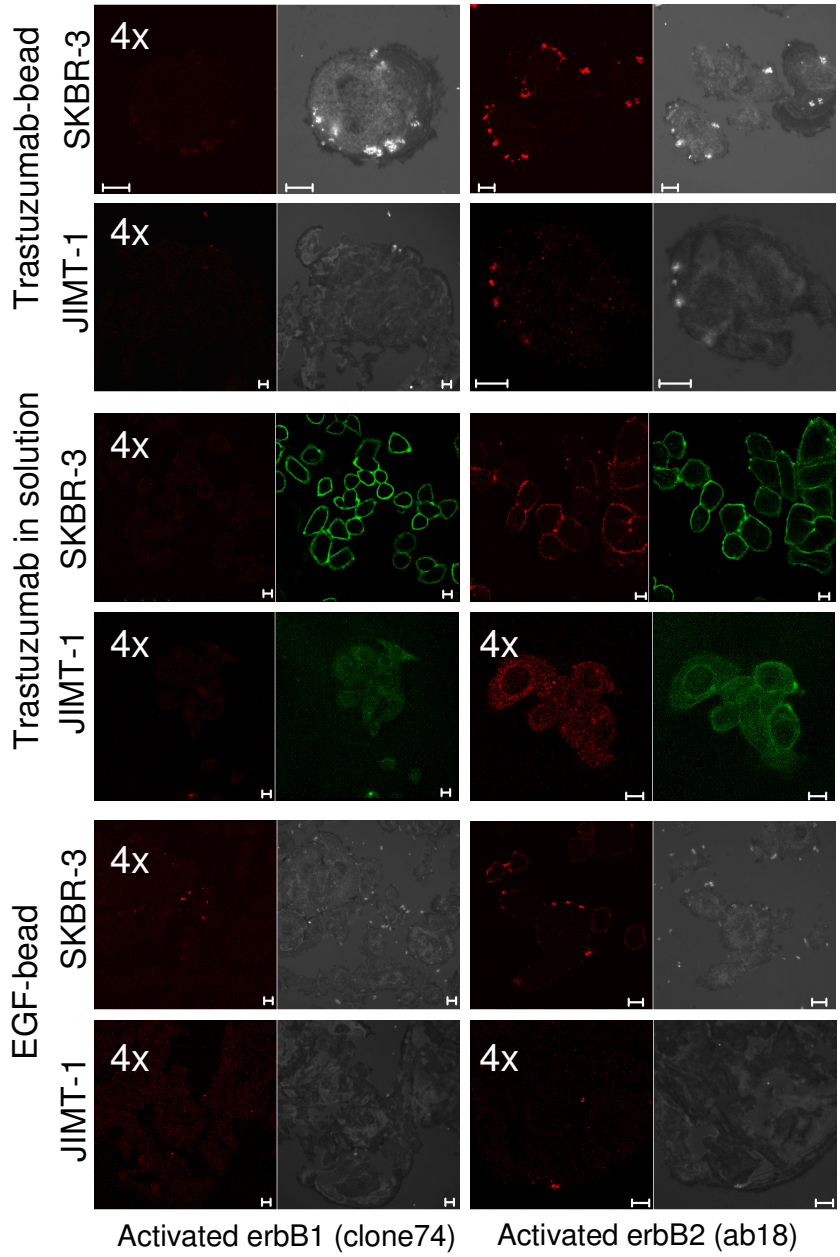

Fig. 14. Activation of erbB1 and erbB2 by trastuzumab- and EGF-coupled microspheres and trastuzumab in solution on SKBR-3 and JIMT-1 cells

SKBR-3 and JIMT-1 cells were stimulated with trastuzumab-coupled microspheres, trastuzumab in solution, or EGF-coupled microspheres for 10 min. Red channel, activated erbB1 (left) or activated erbB2 (right). Reflection gray-scale images show distribution of the microspheres as bright spots. Green channel, trastuzumab in solution binding to the cells. The P-erbB1 signal in all panels and the P-erbB2 in the case of JIMT-1 cells stimulated with trastuzumab in solution or EGF microspheres are displayed at four times amplification. Scale bar, 10 µm.

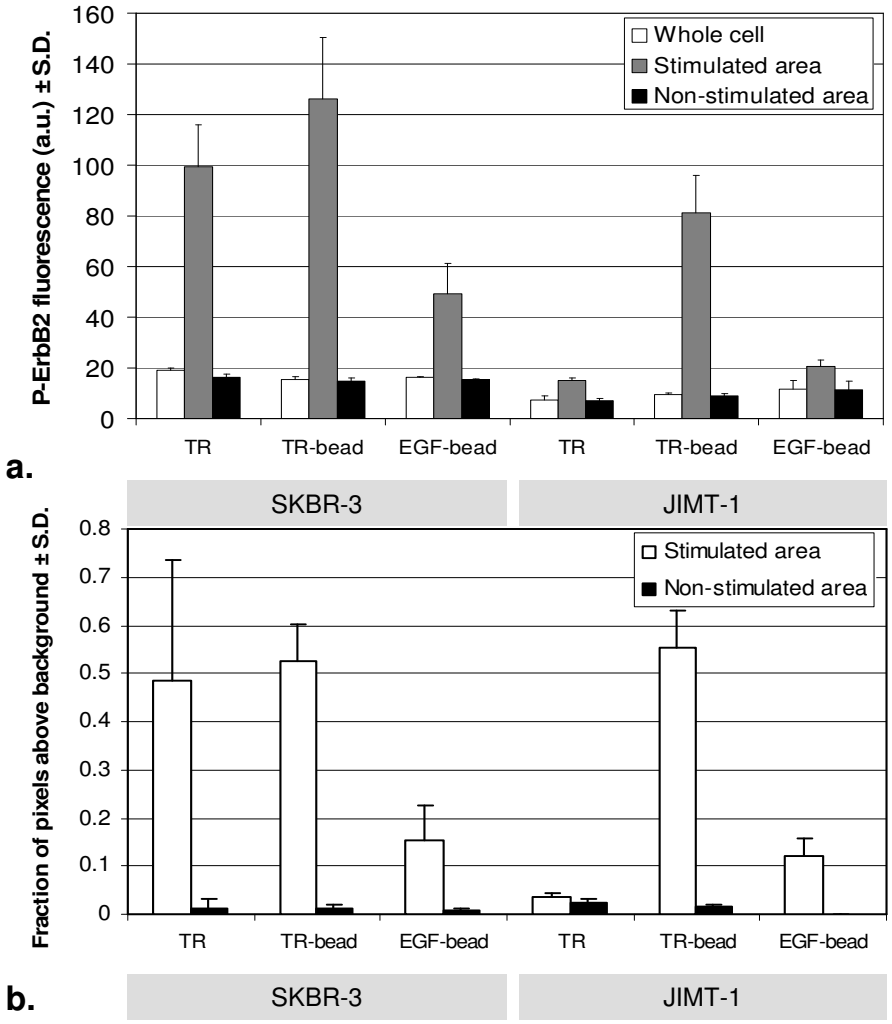

Fig. 15. Activation and transactivation of erbB2 on SKBR-3 and JIMT-1 cells quantitated by digital image processing

(a) ErbB2 phosphorylation quantitated by immunofluorescence and compared for SKBR-3 and JIMT-1 cells stimulated with trastuzumab coupled to microspheres, trastuzumab in solution, and EGF microspheres. The total background-corrected signal was averaged and plotted for the whole cell (white columns) and for areas under (gray columns) and outside (black columns) the microspheres or fluorescence signal from directly labeled trastuzumab.

(b) Proportion of pixels above resting ErbB2 phosphorylation levels determined for trastuzumab- or microsphere-covered areas (white columns) and for areas outside the stimulated regions (black columns). For comparison of cells treated with soluble trastuzumab, maximal resting P-ErbB2 levels were determined from nonstimulated cells and from cells treated with non-coupled microspheres for comparing microsphere-stimulated cells. Averages from at least 10 cells from three independent experiments are plotted with standard deviations represented as error bars.

5.3. Steric hindrance: a possible trastuzumab resistance mechanism

The SKBR-3 cell line is a well-known trastuzumab sensitive model of ErbB2 overexpressing mammary carcinoma. This cell line expresses 1.9×10^5 ErbB1 and 1.1×10^6 ErbB2 molecules per cell as measured by flow cytometry. While *in vitro* proliferation of SKBR-3 and several other breast tumor lines are inhibited by trastuzumab, good *in vitro* models of trastuzumab resistance were unavailable until the recent establishment of the JIMT-1 line [162].

5.3.1. ErbB2 expression and affinity for trastuzumab in trastuzumab sensitive and resistant cell lines

Although JIMT-1 cells express about half of the amount of ErbB2 as SKBR-3 cells do (0.62 and 1.1 million receptor per cell, respectively [162], trastuzumab binds much weaker to them (Fig. 16.). If binding of fluorescently labeled trastuzumab to ErbB2 on JIMT-1 is quantified in flow cytometry using Qifikit, the apparent expression level of ErbB2 is considerably lower, ~8×10^4. We have extended this measurement to trastuzumab Fab and two other ErbB2 targeting antibodies, 2C4 and OP15 (Fig. 17b.). OP-15 binds to the intracellular domain of the ErbB2 (Fig. 17a.), thus, its labeling intensity truly represent ErbB2 expression; accordingly, proportion of ErbB2 on JIMT-1 to SKBR-3 was ~ 0,5. The antibody 2C4, which binds to the dimerization arm of ErbB2, gave similar results. The same ratio for trastuzumab was ~ 0.1, however, it could be increased to ~ 0.4 by treating the cells with Triton X-100, and trastuzumab Fab fragments could also bind 2.5 times better to JIMT-1 cells than the whole trastuzumab antibody.

Dissociation constant of trastuzumab was determined on JIMT-1 and SKBR-3 cells in Scatchard experiments (Fig. 17c.). On JIMT-1, dissociation constant was 2.5×10^{-8} M, one order of magnitude greater than on SKBR-3. This latter, 2.5×10^{-9} M, is still over and order of magnitude greater than the 0.1 nM dissociation constant of trastuzumab determined by ELISA for expressed ErbB2 extracellular domain in solution [101], which draws the attention to the highly important role of local molecular environment in actually experienced by therapeutic antibodies at the surface of living cells. In line with this, it is reasonable to propose, that in JIMT-1 cells, the reason of the resistance could be decreased trastuzumab binding.

Together with these experiments, microscopic fluorescence resonance energy transfer (FRET) measurements were also done in our group and have shown that the level of ErbB1/ErbB2 heteroassociation, and ErbB2/ErbB2 homoassociation is much lower on JIMT-1 than on SKBR-3 cells [30]. In the case of JIMT-1 cells, hetero- or homoassociation has not changed when the cells were stimulated with EGF, whereas on SKBR-3 cells, EGF

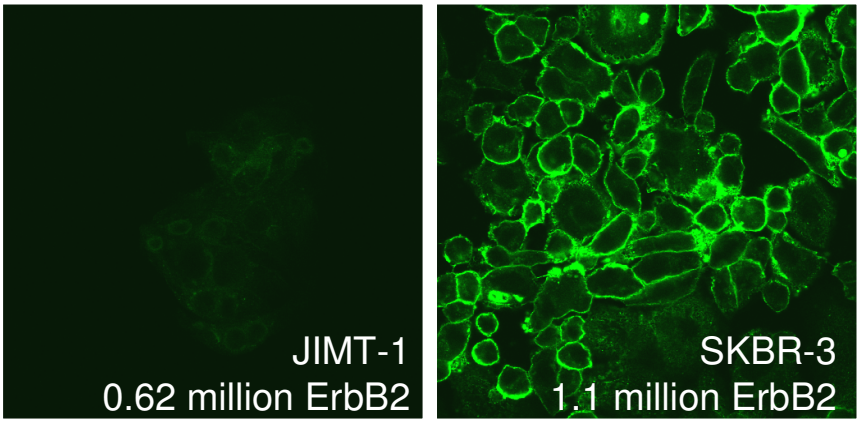

Fig. 16. Trastuzumab binds less on the surface of JIMT-1 cells
JIMT-1 cells express less ErbB2 compared to SKBR-3, but still a significant level. In contrast to the presence of 0.62 million ErbB2 on its cell surface, JIMT-1 almost does not show trastuzumab binding. The images were taken with the same instrument settings from 200 × 200 µm fields of view.

stimulation resulted in enhanced homo- and heteroassociation of ErbB2. In the same series of experiments, we also showed that trastuzumab in solution cannot activate ErbB2 on JIMT-1 cells. Western blot studies, as well as *in situ* immunofluorescent labeling of phospho-ErbB2 followed by flow cytometry suggested that basic phosphorylation level of ErbB2 on JIMT-1 is also lower than that on SKBR-3, but by stimulation with trastuzumab it can be elevated to a small extent. This raises the possibility, that ErbB2 on JIMT-1 may be functionally intact, but sterically hindered in binding to putative association partners and trastuzumab, which would result in trastuzumab resistance.

5.3.2. Trastuzumab microspheres are effective even if trastuzumab in solution has no effect

To elucidate whether our theory of a functionally intact, but sterically hindered ErbB2 on JIMT-1 could be valid, we have made use of the derivatized paramagnetic microspheres characterized earlier. Stimulation of JIMT-1 cells with trastuzumab-coupled microspheres led to pronounced phosphorylation of ErbB2, similarly to the case of SKBR-3 (Fig. 14.). The cross-correlation between microspheres and phospho-ErbB2 specific immunofluorescence signal in the images shown was quantitated and found to be C = 0.73 and C = 0.57 for SKBR-3 and JIMT-1, respectively. Increased phosphorylation was confirmed using generic anti-posphotyrosine staining (not shown). As expected, the application of trastuzumab in solution led to hardly any activation of ErbB2 (Fig. 14.; note that for JIMT-1, the phospho-

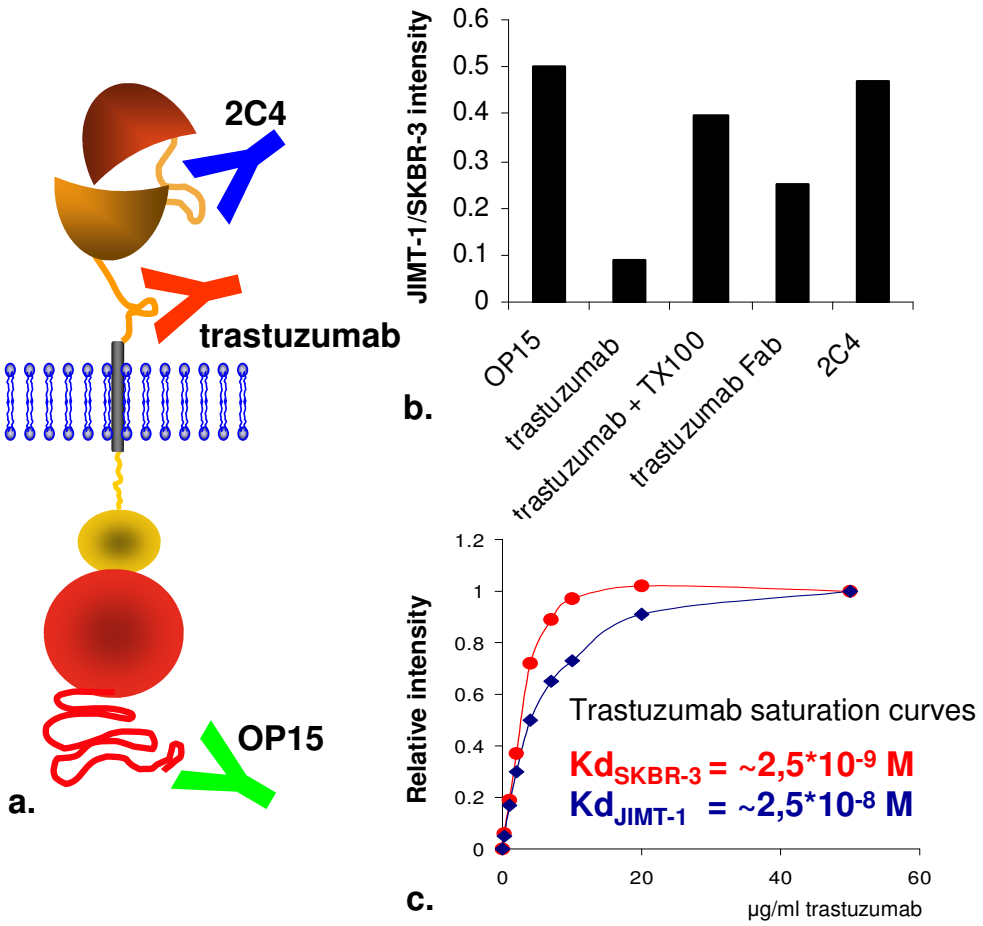

Fig. 17. Trastuzumab binding on SKBR-3 and JIMT-1 cells
(a) The drawing on the left shows the binding sites of different ErbB2 targeted antibodies. OP15 binding to the intracellular domain ideally labels every ErbB2 molecule. Trastuzumab binds to a membrane adjacent region; 2C4 to the dimerization arm. (b) Ratio of labeling intensities on JIMT-1 versus SKBR-3 for various antibodies. OP15 and 2C4 ratios are close to the expression ratio (~0.5), whereas trastuzumab binds much less TO JIMT-1 cells. TX-100 treatment can enhance trastuzumab binding, but the labeling intensity does not reach that of OP15. Fab fragments also bind better than whole trastuzumab. (c) Trastuzumab dose - saturation curveson SKBR-3 (red) and JIMT-1 (blue). The dissociation constant determined from the curves was a magnitude higher for JIMT-1 than for SKBR-3.

ErbB2 signal is displayed at four times amplification). To further quantitate the information from experiments visualized in Fig. 14., In SKBR-3 cells, the level of ErbB2 phosphorylation increased in areas where trastuzumab or trastuzumab microspheres were bound, as opposed to nonstimulated areas of the plasma membrane (Fig. 15a.), and the number of pixels above the maximal resting ErbB2 phosphorylation level also increased (Fig. 15b.). In the case of JIMT-1, trastuzumab in solution increased ErbB2 phosphorylation, albeit to a much lesser

extent than trastuzumab microspheres (Fig. 15a.). The same conclusion was derived from the increased number of pixels above resting activation levels (Fig. 15b.), and was consistent with the level of binding of trastuzumab that could be demonstrated by flow cytometry (Fig. 17b). JIMT-1 cells can also internalize soluble trastuzumab to some extent which may correspond to the small degree of activation and phosphorylation of ErbB2 that we observed. This inhibition can apparently be overridden by applying a higher density of ligand and, possibly, as a result of the steric effects arising from the microspheres. A general finding was that the application of trastuzumab in solution led to less intensive activation (smaller local density of phospho-ErbB2) in all cell lines than that achieved by trastuzumab microspheres, which we attribute to the higher local ligand concentration.

5.3.3. Membrane-associated mucin, MUC4, can be one cause of decreased trastuzumab binding and efficiency

It had been reported previously that overexpression of rat Muc4 results in reduced binding of antibodies against the extracellular region of ErbB2 [164] Fluorescence microscopy, showed that MUC4 was expressed at a substantially higher level in JIMT-1 (Fig. 18a.) than in the trastuzumab-sensitive SKBR-3 cells (Fig. 18b.). JIMT-1 cells labeled with 1G8 against MUC4 and with trastuzumab showed an inverse correlation between the local density of MUC4 and trastuzumab binding implying that high MUC4 expression may interfere with the binding of trastuzumab.

As mentioned previously, 2C4, an antibody targeting the dimerization loop, and also the Fab fragment of trastuzumab could more efficiently bind to ErbB2 on JIMT-1 cells than the whole IgG1 trastuzumab; and treatment of the cells with Triton X-100 before trastuzumab labeling could also increase antibody binding. This latter phenomenon can be well explained by the molecular structure of the MUC4 complex. The large O-glycosylated ascites sialoglycoprotein 1 (ASGP1) domain is connected non-covalently to the smaller ASGP2 domain, thus, its removal helps trastuzumab binding (Fig. 18c.). Inevitably, using Triton X-100 also makes intracellular ErbB2 epitopes available, which could be yet another reason for increased ErbB2 labeling on JIMT-1 after this pre-treatment. Nonetheless, assuming a roughly similar proportion of intra and extracellular ErbB2 in JIMT-1 and SKBR-3, the increased JIMT-1/SKBR-3 ratio of ErbB2 accessibility by trastuzumab upon Triton X-100 treatment (Fig. 17b.) is coherent with the idea of liberating ASGP1 domains by the detergent.

The rat homologue of MUC4 can activate ErbB2 via its pair of EGF-like domains within its ASGP2 region [220]. Human MUC4 also contains EGF homologue domains [221], and

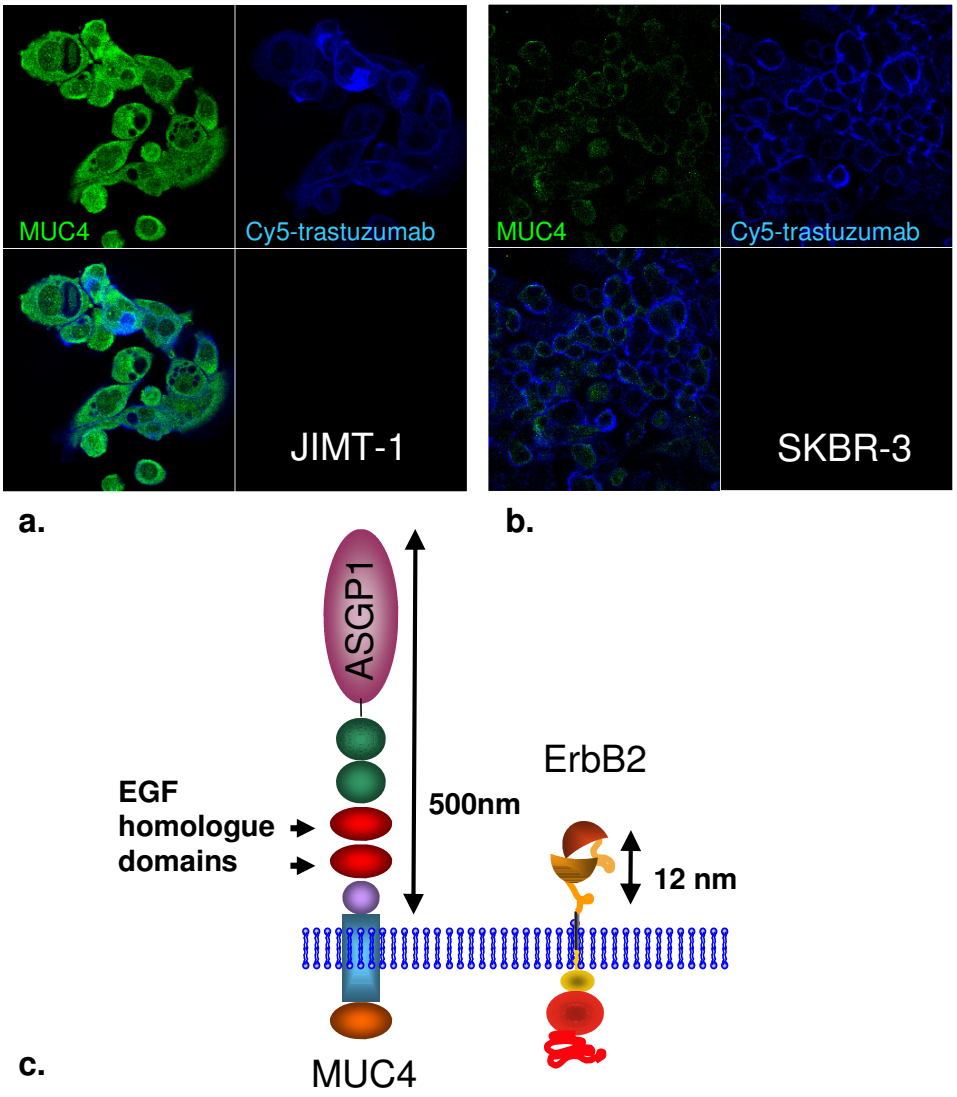

Fig. 18. MUC4 overexpression and anticorrelaion with trastuzumab labeling pattern
(a) On JIMT-1 cells, MUC4 labeling was strong and its pattern was largely complementary to trastuzumab positive areas. (b) On SKBR-3 MUC4 labeling is week while trastuzumab binds more strongly. Images were taken with identical instrument settings. The images were taken with the same instrument settings from 200 × 200 µm fields of view. (c) The dawing below shows the extracellular domain structure of MUC4 and demonstrates that a molecule of this size could prevent access to ErbB2 from the extracellular space. The large ascites sialoglycoprotein 1 (ASGP1) domain is thought to have a major role in steric hindrance.

J

IMT-1 expresses both MUC4 and ErbB2 at a high level; nevertheless, phosphorylation level of ErbB2 is low. One reason for this could be a different conformation of human MUC4, but the much greater size of the human form [222] can also hinder ErbB2 from binding to the adjacent molecules. We have demonstrated applying paramagnetic microspheres that the MUC4 coat on the surface of JIMT-1 cells can be perturbed so that ErbB2 can become activated, whereas trastuzumab in solution was ineffective. The importance of MUC4 in the

trastuzumab resistance of JIMT-1 cells was further studied by our group. RNA interference experiments were performed to depress MUC4 expression. MUC4 siRNA proved to be an efficient suppressor of MUC4 expression when transfected into JIMT-1, and although the fraction of cells successfully transfected with the siRNA was low (15%), the suppression efficiency was almost 100% in these cells. Flow cytometric separation of siRNA treated cells based on trastuzumab binding capacity yielded a dim and a bright population that showed high and low MUC4 expression (normalized to total actin), respectively, in Western blot. This confirmed the complementarity of MUC4 expression and ability of ErbB2 to bind trastuzumab. As MUC4 expression is routinely not yet tested, its precise role in big populations cannot be estimated. However, based on our findings it appears to be important to investigate this aspect of trastuzumab resistance further as it might be a good prognostic factor, and a possible indication that tyrosine kinase inhibitors might be better applied than ErbB2-targeted antibodies.

6. Conclusions

- ErbB1-eGFP chimeric molecules are functionally intact, and can serve as a good model system for mobility measurements when stably expressed in CHO cells. Fluorescence correlation spectroscopy (FCS) could resolve a slow, $1.17\pm0.51\times 10^{-9}$ cm^2/s intramembrane diffusion component of the fused receptor in addition to fast cytoplasmic diffusion and photochemical processes in the eGFP tag. FCS measurements were selective for diffusible molecular species as not or very slowly diffusing eGFP tags needed to be photobleached for average fluorescence to stabilize.
- Stimulation with EGF resulted in a reduction by 50% of ErbB1 membrane diffusion and by 25% of the concentration of diffusing particles, coherent with the idea of ligand induced aggregation. However, this would also cause an increase of the relative fluorescence per particle, but this parameter did not change. Consequently, it is likely that pre-formed ErbB1 dimers are present on the cell surface, that upon EGF binding get conformationally activated and associate with less mobile ErbB1 clusters that have already been photobleached, or interact with the cytoskeleton yielding slower average diffusion.
- FCS disclosed ErbB1 diffusion rates an order of magnitude faster than FRAP measurements for the same ErbB1-eGFP chimera. Also, diffusion resolved by FCS exhibited no anomaly (spatial hindrance) within the small sub-micron detection spot, while FRAP showed that influx of fluorescent species from distal areas into the bleached spot is a result of anomalous diffusion. Thus FCS and FRAP are complementary both in terms of assessing local and larger range diffusion, as well as being selective to faster and slower fluctuations, respectively.
- In various cell lines expressing ErbB1 and ErbB2 at different quantities, EGF and trastuzumab coated paramagnetic microspheres proved to be functional and stimulated local phosphorylation of the targeted ErbB1 or ErbB2 receptors. The signaling events remained laterally localized, and activated the internalization machinery.
- EGF coated microspheres transactivated also ErbB2, while trastuzumab coated ones did not transactivate ErbB1, indicating that trastuzumab binding favors ErbB2 homodimers. The extent of ErbB2 transactivation by EGF beads was directly proportional to increasing surface density of ErbB1, implying that in the presence of activated ErbB1, formation of ErbB1-ErbB2 heterodimers is favorable.

- Trastuzumab binds less on the surface of JIMT-1 cells, its dissociation constant is a magnitude higher than on SKBR-3. ErbB2 phosphorylation is low on JIMT-1 and is not enhanced substantially by trastuzumab. However, ErbB2 on these cells is functional, since high ligand density on trastuzumab-coated microspheres could evoke local ErbB2 activation. The steric effect likely exerted by the beads also hints at the possibility of hindered trastuzumab binding on JIMT-1.
- The mucosialoprotein MUC4 was found to be overexpressed on JIMT-1 cells and its expression was negatively correlated with trastuzumab binding. Given the large size and abundance of MUC4, it could well play a role in sterically hindering trastuzumab binding, and as such, might be a useful predictor of the success of ErbB2-directed antibody therapies.

7. References

[1] Downward J, Yarden Y, Mayes E, Scrace G, Totty N, Stockwell P, et al. Close similarity of epidermal growth factor receptor and v-erb-B oncogene protein sequences. Nature 1984;307:521-527.

[2] Schechter AL, Stern DF, Vaidyanathan L, Decker SJ, Drebin JA, Greene MI, et al. The neu oncogene: an erb-B-related gene encoding a 185,000-Mr tumour antigen. Nature 1984;312:513-516.

[3] Shih C, Padhy LC, Murray M, Weinberg RA. Transforming genes of carcinomas and neuroblastomas introduced into mouse fibroblasts. Nature 1981;290:261-264.

[4] Coussens L, Yang-Feng TL, Liao YC, Chen E, Gray A, McGrath J, et al. Tyrosine kinase receptor with extensive homology to EGF receptor shares chromosomal location with neu oncogene. Science 1985;230:1132-1139.

[5] Semba K, Kamata N, Toyoshima K, Yamamoto T. A v-erbB-related protooncogene, c-erbB-2, is distinct from the c-erbB-1/epidermal growth factor-receptor gene and is amplified in a human salivary gland adenocarcinoma. Proc Natl Acad Sci U S A 1985;82:6497-6501.

[6] King CR, Kraus MH, Aaronson SA. Amplification of a novel v-erbB-related gene in a human mammary carcinoma. Science 1985;229:974-976.

[7] Yamamoto T, Ikawa S, Akiyama T, Semba K, Nomura N, Miyajima N, et al. Similarity of protein encoded by the human c-erb-B-2 gene to epidermal growth factor receptor. Nature 1986;319:230-234.

[8] Ward CW, Hoyne PA, Flegg RH. Insulin and epidermal growth factor receptors contain the cysteine repeat motif found in the tumor necrosis factor receptor. Proteins 1995;22:141-153.

[9] Garrett TP, McKern NM, Lou M, Elleman TC, Adams TE, Lovrecz GO, et al. Crystal structure of a truncated epidermal growth factor receptor extracellular domain bound to transforming growth factor alpha. Cell 2002;110:763-773.

[10] Cho HS, Leahy DJ. Structure of the extracellular region of HER3 reveals an interdomain tether. Science 2002;297:1330-1333.

[11] Ferguson KM, Berger MB, Mendrola JM, Cho HS, Leahy DJ, Lemmon MA. EGF activates its receptor by removing interactions that autoinhibit ectodomain dimerization. Mol Cell 2003;11:507-517.

[12] Schlessinger J. Signal transduction. Autoinhibition control. Science 2003;300:750-752.

[13] Burgess AW, Cho HS, Eigenbrot C, Ferguson KM, Garrett TP, Leahy DJ, et al. An open-and-shut case? Recent insights into the activation of EGF/ErbB receptors. Mol Cell 2003;12:541-552.

[14] Schlessinger J. The epidermal growth factor receptor as a multifunctional allosteric protein. Biochemistry 1988;27:3119-3123.

[15] Citri A, Skaria KB, Yarden Y. The deaf and the dumb: the biology of ErbB-2 and ErbB-3. Exp Cell Res 2003;284:54-65.

[16] Gadella TW, Jr., Jovin TM. Oligomerization of epidermal growth factor receptors on A431 cells studied by time-resolved fluorescence imaging microscopy. A stereochemical model for tyrosine kinase receptor activation. J Cell Biol 1995;129:1543-1558.

[17] Stern DF, Kamps MP. EGF-stimulated tyrosine phosphorylation of p185neu: a potential model for receptor interactions. Embo J 1988;7:995-1001.

[18] Carpenter G. Receptors for epidermal growth factor and other polypeptide mitogens. Annu Rev Biochem 1987;56:881-914.

[19] Yarden Y, Schlessinger J. Epidermal growth factor induces rapid, reversible aggregation of the purified epidermal growth factor receptor. Biochemistry 1987;26:1443-1451.

[20] Yarden Y, Schlessinger J. Self-phosphorylation of epidermal growth factor receptor: evidence for a model of intermolecular allosteric activation. Biochemistry 1987;26:1434-1442.

[21] van Belzen N, Rijken PJ, Hage WJ, de Laat SW, Verkleij AJ, Boonstra J. Direct visualization and quantitative analysis of epidermal growth factor-induced receptor clustering. J Cell Physiol 1988;134:413-420.

[22] Spaargaren M, Defize LH, Boonstra J, de Laat SW. Antibody-induced dimerization activates the epidermal growth factor receptor tyrosine kinase. J Biol Chem 1991;266:1733-1739.

[23] Cochet C, Kashles O, Chambaz EM, Borrello I, King CR, Schlessinger J. Demonstration of epidermal growth factor-induced receptor dimerization in living cells using a chemical covalent cross-linking agent. J Biol Chem 1988;263:3290-3295.

[24] Verveer PJ, Wouters FS, Reynolds AR, Bastiaens PI. Quantitative imaging of lateral ErbB1 receptor signal propagation in the plasma membrane. Science 2000;290:1567-1570.

[25] Brock R, Jovin TM. Heterogeneity of signal transduction at the subcellular level: microsphere-based focal EGF receptor activation and stimulation of Shc translocation. J Cell Sci 2001;114:2437-2447.

[26] Brock R, Jovin TM. Quantitative image analysis of cellular protein translocation induced by magnetic microspheres: application to the EGF receptor. Cytometry A 2003;52:1-11.

[27] Nagy P, Vereb G, Sebestyen Z, Horvath G, Lockett SJ, Damjanovich S, et al. Lipid rafts and the local density of ErbB proteins influence the biological role of homo- and heteroassociations of ErbB2. J Cell Sci 2002;115:4251-4262.

[28] Yarden Y, Sliwkowski MX. Untangling the ErbB signalling network. Nat Rev Mol Cell Biol 2001;2:127-137.

[29] Ferguson KM, Darling PJ, Mohan MJ, Macatee TL, Lemmon MA. Extracellular domains drive homo- but not hetero-dimerization of erbB receptors. Embo J 2000;19:4632-4643.

[30] Zsebik B, Citri A, Isola J, Yarden Y, Szollosi J, Vereb G. Hsp90 inhibitor 17-AAG reduces ErbB2 levels and inhibits proliferation of the trastuzumab resistant breast tumor cell line JIMT-1. Immunol Lett 2006;104:146-155.

[31] Guo L, Abraham J, Flynn DC, Castranova V, Shi X, Qian Y. Individualized survival and treatment response predictions for breast cancers using phospho-EGFR, phospho-ER, phospho-HER2/neu, phospho-IGF-IR/In, phospho-MAPK, and phospho-p70S6K proteins. Int J Biol Markers 2007;22:1-11.

[32] Gamett DC, Pearson G, Cerione RA, Friedberg I. Secondary dimerization between members of the epidermal growth factor receptor family. J Biol Chem 1997;272:12052-12056.

[33] Alroy I, Yarden Y. The ErbB signaling network in embryogenesis and oncogenesis: signal diversification through combinatorial ligand-receptor interactions. FEBS Lett 1997;410:83-86.

[34] Harari D, Yarden Y. Molecular mechanisms underlying ErbB2/HER2 action in breast cancer. Oncogene 2000;19:6102-6114.

[35] Weiner DB, Liu J, Cohen JA, Williams WV, Greene MI. A point mutation in the neu oncogene mimics ligand induction of receptor aggregation. Nature 1989;339:230-231.

[36] Waterman H, Alroy I, Strano S, Seger R, Yarden Y. The C-terminus of the kinase-defective neuregulin receptor ErbB-3 confers mitogenic superiority and dictates endocytic routing. Embo J 1999;18:3348-3358.

[37] Stamos J, Sliwkowski MX, Eigenbrot C. Structure of the epidermal growth factor receptor kinase domain alone and in complex with a 4-anilinoquinazoline inhibitor. J Biol Chem 2002;277:46265-46272.

[38] Hubbard SR, Till JH. Protein tyrosine kinase structure and function. Annu Rev Biochem 2000;69:373-398.

[39] Lenferink AE, Pinkas-Kramarski R, van de Poll ML, van Vugt MJ, Klapper LN, Tzahar E, et al. Differential endocytic routing of homo- and hetero-dimeric ErbB tyrosine kinases confers signaling superiority to receptor heterodimers. Embo J 1998;17:3385-3397.

[40] Levkowitz G, Waterman H, Zamir E, Kam Z, Oved S, Langdon WY, et al. c-Cbl/Sli-1 regulates endocytic sorting and ubiquitination of the epidermal growth factor receptor. Genes Dev 1998;12:3663-3674.

[41] Mosesson Y, Shtiegman K, Katz M, Zwang Y, Vereb G, Szollosi J, et al. Endocytosis of receptor tyrosine kinases is driven by monoubiquitylation, not polyubiquitylation. J Biol Chem 2003;278:21323-21326.

[42] Hommelgaard AM, Lerdrup M, van Deurs B. Association with membrane protrusions makes ErbB2 an internalization-resistant receptor. Mol Biol Cell 2004;15:1557-1567.

[43] Xu W, Yuan X, Beebe K, Xiang Z, Neckers L. Loss of Hsp90 association up-regulates Src-dependent ErbB2 activity. Mol Cell Biol 2007;27:220-228.

[44] Le Boeuf F, Houle F, Sussman M, Huot J. Phosphorylation of focal adhesion kinase (FAK) on Ser732 is induced by rho-dependent kinase and is essential for proline-rich tyrosine kinase-2-mediated phosphorylation of FAK on Tyr407 in response to vascular endothelial growth factor. Mol Biol Cell 2006;17:3508-3520.

[45] Kuramochi Y, Guo X, Sawyer DB. Neuregulin activates erbB2-dependent src/FAK signaling and cytoskeletal remodeling in isolated adult rat cardiac myocytes. J Mol Cell Cardiol 2006;41:228-235.

[46] Liebmann C. Regulation of MAP kinase activity by peptide receptor signalling pathway: paradigms of multiplicity. Cell Signal 2001;13:777-785.

[47] Vivanco I, Sawyers CL. The phosphatidylinositol 3-Kinase AKT pathway in human cancer. Nat Rev Cancer 2002;2:489-501.

[48] Hemi R, Paz K, Wertheim N, Karasik A, Zick Y, Kanety H. Transactivation of ErbB2 and ErbB3 by tumor necrosis factor-alpha and anisomycin leads to impaired insulin signaling through serine/threonine phosphorylation of IRS proteins. J Biol Chem 2002;277:8961-8969.

[49] Di Cristofano A, Pandolfi PP. The multiple roles of PTEN in tumor suppression. Cell 2000;100:387-390.

[50] Nahta R, Yu D, Hung MC, Hortobagyi GN, Esteva FJ. Mechanisms of disease: understanding resistance to HER2-targeted therapy in human breast cancer. Nat Clin Pract Oncol 2006;3:269-280.

[51] Patterson RL, van Rossum DB, Nikolaidis N, Gill DL, Snyder SH. Phospholipase C-gamma: diverse roles in receptor-mediated calcium signaling. Trends Biochem Sci 2005;30:688-697.

[52] Griner EM, Kazanietz MG. Protein kinase C and other diacylglycerol effectors in cancer. Nat Rev Cancer 2007;7:281-294.

[53] Haura EB, Turkson J, Jove R. Mechanisms of disease: Insights into the emerging role of signal transducers and activators of transcription in cancer. Nat Clin Pract Oncol 2005;2:315-324.

[54] Bromberg J, Darnell JE, Jr. The role of STATs in transcriptional control and their impact on cellular function. Oncogene 2000;19:2468-2473.

[55] Grandis JR, Drenning SD, Zeng Q, Watkins SC, Melhem MF, Endo S, et al. Constitutive activation of Stat3 signaling abrogates apoptosis in squamous cell carcinogenesis in vivo. Proc Natl Acad Sci U S A 2000;97:4227-4232.

[56] Frame MC. Src in cancer: deregulation and consequences for cell behaviour. Biochim Biophys Acta 2002;1602:114-130.

[57] Frame MC. Newest findings on the oldest oncogene; how activated src does it. J Cell Sci 2004;117:989-998.

[58] Hiscox S, Morgan L, Green TP, Barrow D, Gee J, Nicholson RI. Elevated Src activity promotes cellular invasion and motility in tamoxifen resistant breast cancer cells. Breast Cancer Res Treat 2006;97:263-274.

[59] Kolibaba KS, Druker BJ. Protein tyrosine kinases and cancer. Biochim Biophys Acta 1997;1333:F217-248.

[60] Fischer-Colbrie J, Witt A, Heinzl H, Speiser P, Czerwenka K, Sevelda P, et al. EGFR and steroid receptors in ovarian carcinoma: comparison with prognostic parameters and outcome of patients. Anticancer Res 1997;17:613-619.

[61] Kersemaekers AM, Fleuren GJ, Kenter GG, Van den Broek LJ, Uljee SM, Hermans J, et al. Oncogene alterations in carcinomas of the uterine cervix: overexpression of the epidermal growth factor receptor is associated with poor prognosis. Clin Cancer Res 1999;5:577-586.

[62] Inada S, Koto T, Futami K, Arima S, Iwashita A. Evaluation of malignancy and the prognosis of esophageal cancer based on an immunohistochemical study (p53, E-cadherin, epidermal growth factor receptor). Surg Today 1999;29:493-503.

[63] Kramer C, Klasmeyer K, Bojar H, Schulz WA, Ackermann R, Grimm MO. Heparin-binding epidermal growth factor-like growth factor isoforms and epidermal growth factor receptor/ErbB1 expression in bladder cancer and their relation to clinical outcome. Cancer 2007;109:2016-2024.

[64] Brabender J, Danenberg KD, Metzger R, Schneider PM, Park J, Salonga D, et al. Epidermal growth factor receptor and HER2-neu mRNA expression in non-small cell lung cancer Is correlated with survival. Clin Cancer Res 2001;7:1850-1855.

[65] Klijn JG, Berns PM, Schmitz PI, Foekens JA. The clinical significance of epidermal growth factor receptor (EGF-R) in human breast cancer: a review on 5232 patients. Endocr Rev 1992;13:3-17.

[66] Li D, Ji H, Zaghlul S, McNamara K, Liang MC, Shimamura T, et al. Therapeutic anti-EGFR antibody 806 generates responses in murine de novo EGFR mutant-dependent lung carcinomas. J Clin Invest 2007;117:346-352.

[67] Yamazaki H, Ohba Y, Tamaoki N, Shibuya M. A deletion mutation within the ligand binding domain is responsible for activation of epidermal growth factor receptor gene in human brain tumors. Jpn J Cancer Res 1990;81:773-779.

[68] Wikstrand CJ, McLendon RE, Friedman AH, Bigner DD. Cell surface localization and density of the tumor-associated variant of the epidermal growth factor receptor, EGFRvIII. Cancer Res 1997;57:4130-4140.

[69] Halatsch ME, Schmidt U, Behnke-Mursch J, Unterberg A, Wirtz CR. Epidermal growth factor receptor inhibition for the treatment of glioblastoma multiforme and other malignant brain tumours. Cancer Treat Rev 2006;32:74-89.

[70] Frederick L, Wang XY, Eley G, James CD. Diversity and frequency of epidermal growth factor receptor mutations in human glioblastomas. Cancer Res 2000;60:1383-1387.

[71] Sartor CI. Epidermal growth factor family receptors and inhibitors: radiation response modulators. Semin Radiat Oncol 2003;13:22-30.

[72] Slamon DJ, Godolphin W, Jones LA, Holt JA, Wong SG, Keith DE, et al. Studies of the HER-2/neu proto-oncogene in human breast and ovarian cancer. Science 1989;244:707-712.

[73] Prost S, Le MG, Douc-Rasy S, Ahomadegbe JC, Spielmann M, Guerin M, et al. Association of c-erbB2-gene amplification with poor prognosis in non-inflammatory breast carcinomas but not in carcinomas of the inflammatory type. Int J Cancer 1994;58:763-768.

[74] Menard S, Pupa SM, Campiglio M, Tagliabue E. Biologic and therapeutic role of HER2 in cancer. Oncogene 2003;22:6570-6578.

[75] Shiga H, Rasmussen AA, Johnston PG, Langmacher M, Baylor A, Lee M, et al. Prognostic value of c-erbB2 and other markers in patients treated with chemotherapy for recurrent head and neck cancer. Head Neck 2000;22:599-608.

[76] Silva SD, Agostini M, Nishimoto IN, Coletta RD, Alves FA, Lopes MA, et al. Expression of fatty acid synthase, ErbB2 and Ki-67 in head and neck squamous cell carcinoma. A clinicopathological study. Oral Oncol 2004;40:688-696.

[77] Turken O, Kunter E, Cermik H, Isitmangil T, Kandemir G, Yaylaci M, et al. Prevalence and prognostic value of c-erbB2 expression in non-small cell lung cancer (NSCLC). Neoplasma 2003;50:257-261.

[78] Goji J, Nakamura H, Ito H, Mabuchi O, Hashimoto K, Sano K. Expression of c-ErbB2 in human neuroblastoma tissues, adrenal medulla adjacent to tumor, and developing mouse neural crest cells. Am J Pathol 1995;146:660-672.

[79] Fallon KB, Havlioglu N, Hamilton LH, Cheng TP, Carroll SL. Constitutive activation of the neuregulin-1/erbB signaling pathway promotes the proliferation of a human peripheral neuroepithelioma cell line. J Neurooncol 2004;66:273-284.

[80] Gollamudi M, Nethery D, Liu J, Kern JA. Autocrine activation of ErbB2/ErbB3 receptor complex by NRG-1 in non-small cell lung cancer cell lines. Lung Cancer 2004;43:135-143.

[81] Perez-Nadales E, Lloyd AC. Essential function for ErbB3 in breast cancer proliferation. Breast Cancer Res 2004;6:137-139.

[82] Latta EK, Tjan S, Parkes RK, O'Malley FP. The role of HER2/neu overexpression/amplification in the progression of ductal carcinoma in situ to invasive carcinoma of the breast. Mod Pathol 2002;15:1318-1325.

[83] Ho GH, Calvano JE, Bisogna M, Borgen PI, Rosen PP, Tan LK, et al. In microdissected ductal carcinoma in situ, HER-2/neu amplification, but not p53 mutation, is associated with high nuclear grade and comedo histology. Cancer 2000;89:2153-2160.

[84] Yi ES, Harclerode D, Gondo M, Stephenson M, Brown RW, Younes M, et al. High c-erbB-3 protein expression is associated with shorter survival in advanced non-small cell lung carcinomas. Mod Pathol 1997;10:142-148.

[85] Zhou H, Liu L, Lee K, Qin X, Grasso AW, Kung HJ, et al. Lung tumorigenesis associated with erb-B-2 and erb-B-3 overexpression in human erb-B-3 transgenic mice is enhanced by methylnitrosourea. Oncogene 2002;21:8732-8740.

[86] Reinmuth N, Brandt B, Kunze WP, Junker K, Thomas M, Achatzy R, et al. Ploidy, expression of erbB1, erbB2, P53 and amplification of erbB1, erbB2 and erbB3 in non-small cell lung cancer. Eur Respir J 2000;16:991-996.

[87] Vakar-Lopez F, Cheng CJ, Kim J, Shi GG, Troncoso P, Tu SM, et al. Up-regulation of MDA-BF-1, a secreted isoform of ErbB3, in metastatic prostate cancer cells and activated osteoblasts in bone marrow. J Pathol 2004;203:688-695.

[88] Maurer CA, Friess H, Kretschmann B, Zimmermann A, Stauffer A, Baer HU, et al. Increased expression of erbB3 in colorectal cancer is associated with concomitant increase in the level of erbB2. Hum Pathol 1998;29:771-777.

[89] Knowlden JM, Gee JM, Seery LT, Farrow L, Gullick WJ, Ellis IO, et al. c-erbB3 and c-erbB4 expression is a feature of the endocrine responsive phenotype in clinical breast cancer. Oncogene 1998;17:1949-1957.

[90] Junttila TT, Laato M, Vahlberg T, Soderstrom KO, Visakorpi T, Isola J, et al. Identification of patients with transitional cell carcinoma of the bladder

overexpressing ErbB2, ErbB3, or specific ErbB4 isoforms: real-time reverse transcription-PCR analysis in estimation of ErbB receptor status from cancer patients. Clin Cancer Res 2003;9:5346-5357.

[91] Sato JD, Kawamoto T, Le AD, Mendelsohn J, Polikoff J, Sato GH. Biological effects in vitro of monoclonal antibodies to human epidermal growth factor receptors. Mol Biol Med 1983;1:511-529.

[92] Natali PG, Nicotra MR, Bigotti A, Venturo I, Slamon DJ, Fendly BM, et al. Expression of the p185 encoded by HER2 oncogene in normal and transformed human tissues. Int J Cancer 1990;45:457-461.

[93] Harwerth IM, Wels W, Marte BM, Hynes NE. Monoclonal antibodies against the extracellular domain of the erbB-2 receptor function as partial ligand agonists. J Biol Chem 1992;267:15160-15167.

[94] Xu F, Lupu R, Rodriguez GC, Whitaker RS, Boente MP, Berchuck A, et al. Antibody-induced growth inhibition is mediated through immunochemically and functionally distinct epitopes on the extracellular domain of the c-erbB-2 (HER-2/neu) gene product p185. Int J Cancer 1993;53:401-408.

[95] Hurwitz E, Stancovski I, Sela M, Yarden Y. Suppression and promotion of tumor growth by monoclonal antibodies to ErbB-2 differentially correlate with cellular uptake. Proc Natl Acad Sci U S A 1995;92:3353-3357.

[96] Stancovski I, Hurwitz E, Leitner O, Ullrich A, Yarden Y, Sela M. Mechanistic aspects of the opposing effects of monoclonal antibodies to the ERBB2 receptor on tumor growth. Proc Natl Acad Sci U S A 1991;88:8691-8695.

[97] Yip YL, Smith G, Koch J, Dubel S, Ward RL. Identification of epitope regions recognized by tumor inhibitory and stimulatory anti-ErbB-2 monoclonal antibodies: implications for vaccine design. J Immunol 2001;166:5271-5278.

[98] Landgraf R. HER2 therapy. HER2 (ERBB2): functional diversity from structurally conserved building blocks. Breast Cancer Res 2007;9:202.

[99] De Santes K, Slamon D, Anderson SK, Shepard M, Fendly B, Maneval D, et al. Radiolabeled antibody targeting of the HER-2/neu oncoprotein. Cancer Res 1992;52:1916-1923.

[100] Sarup JC, Johnson RM, King KL, Fendly BM, Lipari MT, Napier MA, et al. Characterization of an anti-p185HER2 monoclonal antibody that stimulates receptor function and inhibits tumor cell growth. Growth Regul 1991;1:72-82.

[101] Carter P, Presta L, Gorman CM, Ridgway JB, Henner D, Wong WL, et al. Humanization of an anti-p185HER2 antibody for human cancer therapy. Proc Natl Acad Sci U S A 1992;89:4285-4289.

[102] Bookman MA, Darcy KM, Clarke-Pearson D, Boothby RA, Horowitz IR. Evaluation of monoclonal humanized anti-HER2 antibody, trastuzumab, in patients with recurrent or refractory ovarian or primary peritoneal carcinoma with overexpression of HER2: a phase II trial of the Gynecologic Oncology Group. J Clin Oncol 2003;21:283-290.

[103] Gatzemeier U, Groth G, Butts C, Van Zandwijk N, Shepherd F, Ardizzoni A, et al. Randomized phase II trial of gemcitabine-cisplatin with or without trastuzumab in HER2-positive non-small-cell lung cancer. Ann Oncol 2004;15:19-27.

[104] Ziada A, Barqawi A, Glode LM, Varella-Garcia M, Crighton F, Majeski S, et al. The use of trastuzumab in the treatment of hormone refractory prostate cancer; phase II trial. Prostate 2004;60:332-337.

[105] Fujimoto-Ouchi K, Sekiguchi F, Yasuno H, Moriya Y, Mori K, Tanaka Y. Antitumor activity of trastuzumab in combination with chemotherapy in human gastric cancer xenograft models. Cancer Chemother Pharmacol 2007;59:795-805.

[106] Kim SY, Kim HP, Kim YJ, Oh do Y, Im SA, Lee D, et al. Trastuzumab inhibits the growth of human gastric cancer cell lines with HER2 amplification synergistically with cisplatin. Int J Oncol 2008;32:89-95.

[107] Cuello M, Ettenberg SA, Clark AS, Keane MM, Posner RH, Nau MM, et al. Down-regulation of the erbB-2 receptor by trastuzumab (herceptin) enhances tumor necrosis factor-related apoptosis-inducing ligand-mediated apoptosis in breast and ovarian cancer cell lines that overexpress erbB-2. Cancer Res 2001;61:4892-4900.

[108] Baselga J, Albanell J. Mechanism of action of anti-HER2 monoclonal antibodies. Ann Oncol 2001;12 Suppl 1:S35-41.

[109] Klapper LN, Waterman H, Sela M, Yarden Y. Tumor-inhibitory antibodies to HER-2/ErbB-2 may act by recruiting c-Cbl and enhancing ubiquitination of HER-2. Cancer Res 2000;60:3384-3388.

[110] Levkowitz G, Oved S, Klapper LN, Harari D, Lavi S, Sela M, et al. c-Cbl is a suppressor of the neu oncogene. J Biol Chem 2000;275:35532-35539.

[111] Zhou P, Fernandes N, Dodge IL, Reddi AL, Rao N, Safran H, et al. ErbB2 degradation mediated by the co-chaperone protein CHIP. J Biol Chem 2003;278:13829-13837.

[112] Austin CD, De Maziere AM, Pisacane PI, van Dijk SM, Eigenbrot C, Sliwkowski MX, et al. Endocytosis and sorting of ErbB2 and the site of action of cancer therapeutics trastuzumab and geldanamycin. Mol Biol Cell 2004;15:5268-5282.

[113] Barok M, Isola J, Palyi-Krekk Z, Nagy P, Juhasz I, Vereb G, et al. Trastuzumab causes antibody-dependent cellular cytotoxicity-mediated growth inhibition of submacroscopic JIMT-1 breast cancer xenografts despite intrinsic drug resistance. Mol Cancer Ther 2007;6:2065-2072.

[114] Clynes RA, Towers TL, Presta LG, Ravetch JV. Inhibitory Fc receptors modulate in vivo cytoxicity against tumor targets. Nat Med 2000;6:443-446.

[115] Yakes FM, Chinratanalab W, Ritter CA, King W, Seelig S, Arteaga CL. Herceptin-induced inhibition of phosphatidylinositol-3 kinase and Akt Is required for antibody-mediated effects on p27, cyclin D1, and antitumor action. Cancer Res 2002;62:4132-4141.

[116] Lenferink AE, Busse D, Flanagan WM, Yakes FM, Arteaga CL. ErbB2/neu kinase modulates cellular p27(Kip1) and cyclin D1 through multiple signaling pathways. Cancer Res 2001;61:6583-6591.

[117] Nahta R, Takahashi T, Ueno NT, Hung MC, Esteva FJ. P27(kip1) down-regulation is associated with trastuzumab resistance in breast cancer cells. Cancer Res 2004;64:3981-3986.

[118] Wen XF, Yang G, Mao W, Thornton A, Liu J, Bast RC, Jr., et al. HER2 signaling modulates the equilibrium between pro- and antiangiogenic factors via distinct

pathways: implications for HER2-targeted antibody therapy. Oncogene 2006;25:6986-6996.

[119] Izumi Y, Xu L, di Tomaso E, Fukumura D, Jain RK. Tumour biology: herceptin acts as an anti-angiogenic cocktail. Nature 2002;416:279-280.

[120] Carter WB. HER2 signaling--induced microvessel dismantling. Surgery 2001;130:382-387.

[121] Niu G, Carter WB. Human epidermal growth factor receptor 2 regulates angiopoietin-2 expression in breast cancer via AKT and mitogen-activated protein kinase pathways. Cancer Res 2007;67:1487-1493.

[122] Klos KS, Zhou X, Lee S, Zhang L, Yang W, Nagata Y, et al. Combined trastuzumab and paclitaxel treatment better inhibits ErbB-2-mediated angiogenesis in breast carcinoma through a more effective inhibition of Akt than either treatment alone. Cancer 2003;98:1377-1385.

[123] Li S, Schmitz KR, Jeffrey PD, Wiltzius JJ, Kussie P, Ferguson KM. Structural basis for inhibition of the epidermal growth factor receptor by cetuximab. Cancer Cell 2005;7:301-311.

[124] Rocha-Lima CM, Soares HP, Raez LE, Singal R. EGFR targeting of solid tumors. Cancer Control 2007;14:295-304.

[125] Dittmann K, Mayer C, Rodemann HP. Inhibition of radiation-induced EGFR nuclear import by C225 (Cetuximab) suppresses DNA-PK activity. Radiother Oncol 2005;76:157-161.

[126] Seiden MV, Burris HA, Matulonis U, Hall JB, Armstrong DK, Speyer J, et al. A phase II trial of EMD72000 (matuzumab), a humanized anti-EGFR monoclonal antibody, in patients with platinum-resistant ovarian and primary peritoneal malignancies. Gynecol Oncol 2007;104:727-731.

[127] Crombet-Ramos T, Rak J, Perez R, Viloria-Petit A. Antiproliferative, antiangiogenic and proapoptotic activity of h-R3: A humanized anti-EGFR antibody. Int J Cancer 2002;101:567-575.

[128] Yang XD, Jia XC, Corvalan JR, Wang P, Davis CG. Development of ABX-EGF, a fully human anti-EGF receptor monoclonal antibody, for cancer therapy. Crit Rev Oncol Hematol 2001;38:17-23.

[129] Foon KA, Yang XD, Weiner LM, Belldegrun AS, Figlin RA, Crawford J, et al. Preclinical and clinical evaluations of ABX-EGF, a fully human anti-epidermal growth factor receptor antibody. Int J Radiat Oncol Biol Phys 2004;58:984-990.

[130] Tyagi P. Recent results and ongoing trials with panitumumab (ABX-EGF), a fully human anti-epidermal growth factor receptor antibody, in metastatic colorectal cancer. Clin Colorectal Cancer 2005;5:21-23.

[131] Agus DB, Akita RW, Fox WD, Lewis GD, Higgins B, Pisacane PI, et al. Targeting ligand-activated ErbB2 signaling inhibits breast and prostate tumor growth. Cancer Cell 2002;2:127-137.

[132] Molina MA, Codony-Servat J, Albanell J, Rojo F, Arribas J, Baselga J. Trastuzumab (herceptin), a humanized anti-Her2 receptor monoclonal antibody, inhibits basal and activated Her2 ectodomain cleavage in breast cancer cells. Cancer Res 2001;61:4744-4749.

[133] Franklin MC, Carey KD, Vajdos FF, Leahy DJ, de Vos AM, Sliwkowski MX. Insights into ErbB signaling from the structure of the ErbB2-pertuzumab complex. Cancer Cell 2004;5:317-328.

[134] Dalken B, Giesubel U, Knauer SK, Wels WS. Targeted induction of apoptosis by chimeric granzyme B fusion proteins carrying antibody and growth factor domains for cell recognition. Cell Death Differ 2006;13:576-585.

[135] Schmidt M, Vakalopoulou E, Schneider DW, Wels W. Construction and functional characterization of scFv(14E1)-ETA - a novel, highly potent antibody-toxin specific for the EGF receptor. Br J Cancer 1997;75:1575-1584.

[136] Nielsen UB, Kirpotin DB, Pickering EM, Hong K, Park JW, Refaat Shalaby M, et al. Therapeutic efficacy of anti-ErbB2 immunoliposomes targeted by a phage antibody selected for cellular endocytosis. Biochim Biophys Acta 2002;1591:109-118.

[137] Jonker DJ, O'Callaghan CJ, Karapetis CS, Zalcberg JR, Tu D, Au HJ, et al. Cetuximab for the treatment of colorectal cancer. N Engl J Med 2007;357:2040-2048.

[138] Rosell R, Robinet G, Szczesna A, Ramlau R, Constenla M, Mennecier BC, et al. Randomized phase II study of cetuximab plus cisplatin/vinorelbine compared with cisplatin/vinorelbine alone as first-line therapy in EGFR-expressing advanced non-small-cell lung cancer. Ann Oncol 2007.

[139] Harari PM. Stepwise progress in epidermal growth factor receptor/radiation studies for head and neck cancer. Int J Radiat Oncol Biol Phys 2007;69:S25-27.

[140] Krempien R, Muenter MW, Huber PE, Nill S, Friess H, Timke C, et al. Randomized phase II--study evaluating EGFR targeting therapy with cetuximab in combination with radiotherapy and chemotherapy for patients with locally advanced pancreatic cancer--PARC: study protocol [ISRCTN56652283]. BMC Cancer 2005;5:131.

[141] Gholam D, Chebib A, Hauteville D, Bralet MP, Jasmin C. Combined paclitaxel and cetuximab achieved a major response on the skin metastases of a patient with epidermal growth factor receptor-positive, estrogen receptor-negative, progesterone receptor-negative and human epidermal growth factor receptor-2-negative (triple-negative) breast cancer. Anticancer Drugs 2007;18:835-837.

[142] Bellone S, Frera G, Landolfi G, Romani C, Bandiera E, Tognon G, et al. Overexpression of epidermal growth factor type-1 receptor (EGF-R1) in cervical cancer: implications for Cetuximab-mediated therapy in recurrent/metastatic disease. Gynecol Oncol 2007;106:513-520.

[143] Modjtahedi H, Moscatello DK, Box G, Green M, Shotton C, Lamb DJ, et al. Targeting of cells expressing wild-type EGFR and type-III mutant EGFR (EGFRvIII) by anti-EGFR MAb ICR62: a two-pronged attack for tumour therapy. Int J Cancer 2003;105:273-280.

[144] Cunningham MP, Thomas H, Fan Z, Modjtahedi H. Responses of human colorectal tumor cells to treatment with the anti-epidermal growth factor receptor monoclonal antibody ICR62 used alone and in combination with the EGFR tyrosine kinase inhibitor gefitinib. Cancer Res 2006;66:7708-7715.

[145] Giusti RM, Shastri KA, Cohen MH, Keegan P, Pazdur R. FDA drug approval summary: panitumumab (Vectibix). Oncologist 2007;12:577-583.

[146] Socinski MA. Antibodies to the epidermal growth factor receptor in non small cell lung cancer: current status of matuzumab and panitumumab. Clin Cancer Res 2007;13:s4597-4601.

[147] Arteaga ME, Ledon N, Casaco A, Pardo B, Garcia M, Boleda M, et al. Systemic and Skin Toxicity in Cercopithecus aethiops sabaeus Monkeys Treated During 26 Weeks with a High Intravenous Dose of the Anti- Epidermal Growth Factor Receptor Monoclonal Antibody Nimotuzumab. Cancer Biol Ther 2007;6.

[148] Scott AM, Lee FT, Tebbutt N, Herbertson R, Gill SS, Liu Z, et al. A phase I clinical trial with monoclonal antibody ch806 targeting transitional state and mutant epidermal growth factor receptors. Proc Natl Acad Sci U S A 2007;104:4071-4076.

[149] Yang W, Barth RF, Wu G, Kawabata S, Sferra TJ, Bandyopadhyaya AK, et al. Molecular targeting and treatment of EGFRvIII-positive gliomas using boronated monoclonal antibody L8A4. Clin Cancer Res 2006;12:3792-3802.

[150] Fury MG, Lipton A, Smith KM, Winston CB, Pfister DG. A phase-I trial of the epidermal growth factor receptor directed bispecific antibody MDX-447 without and with recombinant human granulocyte-colony stimulating factor in patients with advanced solid tumors. Cancer Immunol Immunother 2007.

[151] Nahta R, Esteva FJ. Trastuzumab: triumphs and tribulations. Oncogene 2007;26:3637-3643.

[152] Herbst RS, Davies AM, Natale RB, Dang TP, Schiller JH, Garland LL, et al. Efficacy and safety of single-agent pertuzumab, a human epidermal receptor dimerization inhibitor, in patients with non small cell lung cancer. Clin Cancer Res 2007;13:6175-6181.

[153] Gordon MS, Matei D, Aghajanian C, Matulonis UA, Brewer M, Fleming GF, et al. Clinical activity of pertuzumab (rhuMAb 2C4), a HER dimerization inhibitor, in advanced ovarian cancer: potential predictive relationship with tumor HER2 activation status. J Clin Oncol 2006;24:4324-4332.

[154] Engel RH, Kaklamani VG. HER2-positive breast cancer: current and future treatment strategies. Drugs 2007;67:1329-1341.

[155] Johnson BE, Janne PA. Rationale for a phase II trial of pertuzumab, a HER-2 dimerization inhibitor, in patients with non-small cell lung cancer. Clin Cancer Res 2006;12:4436s-4440s.

[156] Repp R, van Ojik HH, Valerius T, Groenewegen G, Wieland G, Oetzel C, et al. Phase I clinical trial of the bispecific antibody MDX-H210 (anti-FcgammaRI x anti-HER-2/neu) in combination with Filgrastim (G-CSF) for treatment of advanced breast cancer. Br J Cancer 2003;89:2234-2243.

[157] Weiner LM, Clark JI, Davey M, Li WS, Garcia de Palazzo I, Ring DB, et al. Phase I trial of 2B1, a bispecific monoclonal antibody targeting c-erbB-2 and Fc gamma RIII. Cancer Res 1995;55:4586-4593.

[158] McCall AM, Adams GP, Amoroso AR, Nielsen UB, Zhang L, Horak E, et al. Isolation and characterization of an anti-CD16 single-chain Fv fragment and construction of an anti-HER2/neu/anti-CD16 bispecific scFv that triggers CD16-dependent tumor cytolysis. Mol Immunol 1999;36:433-445.

[159] Kiewe P, Hasmuller S, Kahlert S, Heinrigs M, Rack B, Marme A, et al. Phase I trial of the trifunctional anti-HER2 x anti-CD3 antibody ertumaxomab in metastatic breast cancer. Clin Cancer Res 2006;12:3085-3091.

[160] Azemar M, Djahansouzi S, Jager E, Solbach C, Schmidt M, Maurer AB, et al. Regression of cutaneous tumor lesions in patients intratumorally injected with a recombinant single-chain antibody-toxin targeted to ErbB2/HER2. Breast Cancer Res Treat 2003;82:155-164.

[161] Dinh P, de Azambuja E, Piccart-Gebhart MJ. Trastuzumab for early breast cancer: current status and future directions. Clin Adv Hematol Oncol 2007;5:707-717.

[162] Tanner M, Kapanen AI, Junttila T, Raheem O, Grenman S, Elo J, et al. Characterization of a novel cell line established from a patient with Herceptin-resistant breast cancer. Mol Cancer Ther 2004;3:1585-1592.

[163] Carraway KL, Carvajal ME, Li P, Carraway CA. ErbB2 and its ligand Muc4 (sialomucin complex) in rat lacrimal gland. Adv Exp Med Biol 2002;506:289-295.

[164] Price-Schiavi SA, Jepson S, Li P, Arango M, Rudland PS, Yee L, et al. Rat Muc4 (sialomucin complex) reduces binding of anti-ErbB2 antibodies to tumor cell surfaces, a potential mechanism for herceptin resistance. Int J Cancer 2002;99:783-791.

[165] Ghatak S, Misra S, Toole BP. Hyaluronan constitutively regulates ErbB2 phosphorylation and signaling complex formation in carcinoma cells. J Biol Chem 2005;280:8875-8883.

[166] Ghatak S, Misra S, Toole BP. Hyaluronan oligosaccharides inhibit anchorage-independent growth of tumor cells by suppressing the phosphoinositide 3-kinase/Akt cell survival pathway. J Biol Chem 2002;277:38013-38020.

[167] Marhaba R, Zoller M. CD44 in cancer progression: adhesion, migration and growth regulation. J Mol Histol 2004;35:211-231.

[168] Palyi-Krekk Z, Barok M, Isola J, Tammi M, Szollo si J, Nagy P. Hyaluronan-induced masking of ErbB2 and CD44-enhanced trastuzumab internalisation in trastuzumab resistant breast cancer. Eur J Cancer 2007;43:2423-2433.

[169] Nahta R, Yuan LX, Zhang B, Kobayashi R, Esteva FJ. Insulin-like growth factor-I receptor/human epidermal growth factor receptor 2 heterodimerization contributes to trastuzumab resistance of breast cancer cells. Cancer Res 2005;65:11118-11128.

[170] Nagata Y, Lan KH, Zhou X, Tan M, Esteva FJ, Sahin AA, et al. PTEN activation contributes to tumor inhibition by trastuzumab, and loss of PTEN predicts trastuzumab resistance in patients. Cancer Cell 2004;6:117-127.

[171] Diermeier S, Horvath G, Knuechel-Clarke R, Hofstaedter F, Szollosi J, Brockhoff G. Epidermal growth factor receptor coexpression modulates susceptibility to Herceptin in HER2/neu overexpressing breast cancer cells via specific erbB-receptor interaction and activation. Exp Cell Res 2005;304:604-619.

[172] Brockhoff G, Heckel B, Schmidt-Bruecken E, Plander M, Hofstaedter F, Vollmann A, et al. Differential impact of Cetuximab, Pertuzumab and Trastuzumab on BT474 and SK-BR-3 breast cancer cell proliferation. Cell Prolif 2007;40:488-507.

[173] Mimura K, Kono K, Hanawa M, Kanzaki M, Nakao A, Ooi A, et al. Trastuzumab-mediated antibody-dependent cellular cytotoxicity against esophageal squamous cell carcinoma. Clin Cancer Res 2005;11:4898-4904.

[174] Kono K, Takahashi A, Ichihara F, Sugai H, Fujii H, Matsumoto Y. Impaired antibody-dependent cellular cytotoxicity mediated by herceptin in patients with gastric cancer. Cancer Res 2002;62:5813-5817.

[175] Barok M, Balázs M, Nagy P, Rákosy Z, Treszl A, Tóth E, et al. Trastuzumab decreases the number of circulating and disseminated tumor

cells despite trastuzumab resistance of the primary tumor. Cancer Lett 2007;in press.

[176] Laemmli UK. Cleavage of structural proteins during the assembly of the head of bacteriophage T4. Nature 1970;227:680-685.

[177] Grynkiewicz G, Poenie M, Tsien RY. A new generation of Ca2+ indicators with greatly improved fluorescence properties. J Biol Chem 1985;260:3440-3450.

[178] Haupts U, Maiti S, Schwille P, Webb WW. Dynamics of fluorescence fluctuations in green fluorescent protein observed by fluorescence correlation spectroscopy. Proc Natl Acad Sci U S A 1998;95:13573-13578.

[179] Wachsmuth M, Waldeck W, Langowski J. Anomalous diffusion of fluorescent probes inside living cell nuclei investigated by spatially-resolved fluorescence correlation spectroscopy. J Mol Biol 2000;298:677-689.

[180] Widengren J, Mets U, Rigler R. Photodynamic properties of green fluorescent proteins investigated by fluorescence correlation spectroscopy. Chemical Physics 1999;250:171-186.

[181] Brock R, Vamosi G, Vereb G, Jovin TM. Rapid characterization of green fluorescent protein fusion proteins on the molecular and cellular level by fluorescence correlation microscopy. Proc Natl Acad Sci U S A 1999;96:10123-10128.

[182] Brock R, Jovin TM. Fluorescence correlation microscopy (FCM)-fluorescence correlation spectroscopy (FCS) taken into the cell. Cell Mol Biol (Noisy-le-grand) 1998;44:847-856.

[183] Brock R, Hink MA, Jovin TM. Fluorescence correlation microscopy of cells in the presence of autofluorescence. Biophys J 1998;75:2547-2557.

[184] Feder TJ, Brust-Mascher I, Slattery JP, Baird B, Webb WW. Constrained diffusion or immobile fraction on cell surfaces: a new interpretation. Biophys J 1996;70:2767-2773.

[185] Wolf DE, Edidin M. Methods of Measuring Diffusion and Mobility of Molicules in Surface membranes. In: Baker PF, editor. Techniques in Cellular Physiology. Elsevier: Amsterdam, 1981: 1-14.

[186] Vereb G, Jr., Matkó J, Vámosi G, Ibrahim SM, Magyar E, Varga S, et al. Cholesterol-dependent clustering of IL-2Ralpha and its colocalization with HLA and CD48 on T lymphoma cells suggest their functional association with lipid rafts. Proc Natl Acad Sci USA 2000;97:6013-6018.

[187] Green Fluorescence Protein properties, applications and protocols. Wiley-Liss: New York, Chichester, Weinheim, Brisbane,Singapore,Toronto,2000.

[188] Margolis B, Rhee SG, Felder S, Mervic M, Lyall R, Levitzki A, et al. EGF induces tyrosine phosphorylation of phospholipase C-II: a potential mechanism for EGF receptor signaling. Cell 1989;57:1101-1107.

[189] Cole NB, Smith CL, Sciaky N, Terasaki M, Edidin M, Lippincott-Schwartz J. Diffusional mobility of Golgi proteins in membranes of living cells. Science 1996;273:797-801.

[190] Wagner ML, Tamm LK. Reconstituted syntaxin1a/SNAP25 interacts with negatively charged lipids as measured by lateral diffusion in planar supported bilayers. Biophys J 2001;81:266-275.

[191] Roberts RL, Barbieri MA, Pryse KM, Chua M, Morisaki JH, Stahl PD. Endosome fusion in living cells overexpressing GFP-rab5. J Cell Sci 1999;112 (Pt 21):3667-3675.

[192] Oheim M, Stuhmer W. Tracking chromaffin granules on their way through the actin cortex. Eur Biophys J 2000;29:67-89.

[193] Adkins EM, Samuvel DJ, Fog JU, Eriksen J, Jayanthi LD, Vaegter CB, et al. Membrane mobility and microdomain association of the dopamine transporter studied with fluorescence correlation spectroscopy and fluorescence recovery after photobleaching. Biochemistry 2007;46:10484-10497.

[194] Koppel DE, Axelrod D, Schlessinger J, Elson EL, Webb WW. Dynamics of fluorescence marker concentration as a probe of mobility. Biophys J 1976;16:1315-1329.

[195] Saffarian S, Li Y, Elson EL, Pike LJ. Oligomerization of the EGF receptor investigated by live cell fluorescence intensity distribution analysis. Biophys J 2007;93:1021-1031.

[196] van Bergen en Henegouwen PM, Defize LH, de Kroon J, van Damme H, Verkleij AJ, Boonstra J. Ligand-induced association of epidermal growth factor receptor to the cytoskeleton of A431 cells. Journal of Cellular Biochemistry 1989;39:455-465.

[197] Schlessinger J. Lateral and rotational diffusion of EGF-receptor complex: relationship to receptor-mediated endocytosis. Biopolymers 1983;22:347-353.

[198] Lirvall M, Ljungqvist-Hoddelius P, Wasteson A, Magnusson KE. UVB radiation affects the mobility of epidermal growth factor receptors in human keratinocytes and fibroblasts. Biosci Rep 1996;16:227-238.

[199] Edidin M, Zuniga MC, Sheetz MP. Truncation mutants define and locate cytoplasmic barriers to lateral mobility of membrane glycoproteins. Proc Natl Acad Sci U S A 1994;91:3378-3382.

[200] Kusumi A, Sako Y. Cell surface organization by the membrane skeleton. Curr Opin Cell Biol 1996;8:566-574.

[201] Edidin M. Patches and fences: probing for plasma membrane domains. J Cell Sci Suppl 1993;17:165-169.

[202] Dietrich C, Yang B, Fujiwara T, Kusumi A, Jacobson K. Relationship of lipid rafts to transient confinement zones detected by single particle tracking. Biophys J 2002;82:274-284.

[203] Sako Y, Kusumi A. Barriers for lateral diffusion of transferrin receptor in the plasma membrane as characterized by receptor dragging by laser tweezers: fence versus tether. J Cell Biol 1995;129:1559-1574.

[204] Tomishige M, Sako Y, Kusumi A. Regulation mechanism of the lateral diffusion of band 3 in erythrocyte membranes by the membrane skeleton. J Cell Biol 1998;142:989-1000.

[205] Kusumi A, Nakada C, Ritchie K, Murase K, Suzuki K, Murakoshi H, et al. Paradigm shift of the plasma membrane concept from the two-dimensional continuum fluid to the partitioned fluid: high-speed single-molecule tracking of membrane molecules. Annu Rev Biophys Biomol Struct 2005;34:351-378.

[206] Greenfield LJ, Jr., Sun F, Neelands TR, Burgard EC, Donnelly JL, MacDonald RL. Expression of functional GABAA receptors in transfected L929 cells isolated by immunomagnetic bead separation. Neuropharmacology 1997;36:63-73.

[207] Cook EB, Stahl JL, Lowe L, Chen R, Morgan E, Wilson J, et al. Simultaneous measurement of six cytokines in a single sample of human tears using microparticle-based flow cytometry: allergics vs. non-allergics. J Immunol Methods 2001;254:109-118.

[208] Segal G, Lee W, Arora PD, McKee M, Downey G, McCulloch CA. Involvement of actin filaments and integrins in the binding step in collagen phagocytosis by human fibroblasts. J Cell Sci 2001;114:119-129.

[209] Arora PD, Silvestri L, Ganss B, Sodek J, McCulloch CA. Mechanism of cyclosporin-induced inhibition of intracellular collagen degradation. J Biol Chem 2001;276:14100-14109.

[210] Bausch AR, Ziemann F, Boulbitch AA, Jacobson K, Sackmann E. Local measurements of viscoelastic parameters of adherent cell surfaces by magnetic bead microrheometry. Biophys J 1998;75:2038-2049.

[211] Tanimura N, Nagafuku M, Minaki Y, Umeda Y, Hayashi F, Sakakura J, et al. Dynamic changes in the mobility of LAT in aggregated lipid rafts upon T cell activation. J Cell Biol 2003;160:125-135.

[212] Kovacs B, Maus MV, Riley JL, Derimanov GS, Koretzky GA, June CH, et al. Human CD8+ T cells do not require the polarization of lipid rafts for activation and proliferation. Proc Natl Acad Sci U S A 2002;99:15006-15011.

[213] Shah M, Patel K, Fried VA, Sehgal PB. Interactions of STAT3 with caveolin-1 and heat shock protein 90 in plasma membrane raft and cytosolic complexes. Preservation of cytokine signaling during fever. J Biol Chem 2002;277:45662-45669.

[214] Ko KS, Arora PD, McCulloch CA. Cadherins mediate intercellular mechanical signaling in fibroblasts by activation of stretch-sensitive calcium-permeable channels. J Biol Chem 2001;276:35967-35977.

[215] Dai Z, Luo X, Xie H, Peng HB. The actin-driven movement and formation of acetylcholine receptor clusters. J Cell Biol 2000;150:1321-1334.

[216] MacGillivray MK, Cruz TF, McCulloch CA. The recruitment of the interleukin-1 (IL-1) receptor-associated kinase (IRAK) into focal adhesion complexes is required for IL-1beta -induced ERK activation. J Biol Chem 2000;275:23509-23515.

[217] Wiederkehr-Adam M, Ernst P, Muller K, Bieck E, Gombert FO, Ottl J, et al. Characterization of phosphopeptide motifs specific for the Src homology 2 domains of signal transducer and activator of transcription 1 (STAT1) and STAT3. J Biol Chem 2003;278:16117-16128.

[218] Kempiak SJ, Yip SC, Backer JM, Segall JE. Local signaling by the EGF receptor. J Cell Biol 2003;162:781-787.

[219] Bagossi P, Horvath G, Vereb G, Szollosi J, Tozser J. Molecular modeling of nearly full-length ErbB2 receptor. Biophys J 2005;88:1354-1363.

[220] Carraway KL, 3rd, Rossi EA, Komatsu M, Price-Schiavi SA, Huang D, Guy PM, et al. An intramembrane modulator of the ErbB2 receptor tyrosine kinase that potentiates neuregulin signaling. J Biol Chem 1999;274:5263-5266.

[221] Moniaux N, Nollet S, Porchet N, Degand P, Laine A, Aubert JP. Complete sequence of the human mucin MUC4: a putative cell membrane-associated mucin. Biochem J 1999;338 (Pt 2):325-333.

[222] Sheng Z, Wu K, Carraway KL, Fregien N. Molecular cloning of the transmembrane component of the 13762 mammary adenocarcinoma sialomucin complex. A new member of the epidermal growth factor superfamily. J Biol Chem 1992;267:16341-16346.

8. Acknowledgements

I gratefully acknowledge the help of György Vereb, János Szöllősi, Péter Nagy, György Vámosi and György Vereb Sr. during the experiments and in preparing my thesis, as well as the skillful technical assistance of Tünde Pálné Terdik, Hajnalka Vágóné Toldi, Anikó Harangi and Júlia Hunyadi. I would also like to say thanks to Thomas M. Jovin and Donna Arndt-Jovin (Max Planck Intitute for Biochemical Chemistry, Göttingen, Germany) and the members of our group and our department: Márk Barok, János Roszik, László Ujlaky-Nagy, Gábor Horváth, Ákos Fábián, Zsuzsanna Pályi-Krekk, Zsolt Fazekas, Ágnes Szabó, Tamás Lajtos and Éva Pálfi. Last but not least, thanks go to my family and all my friends for their support and patience.

10. Publications

10.1. Related In extenso publications

1. **Friedländer E**, Arndt-Jovin DJ, Nagy P, Jovin TM, Szöllősi J, Vereb G. Signal transduction of erbB receptors in trastuzumab (Herceptin) sensitive and resistant cell lines: Local stimulation using magnetic microspheres as assessed by quantitative digital microscopy. Cytometry A 2005;67A:161-171. IF: 3.293

2. Nagy P, **Friedländer E**, Tanner M, Kapanen AI, Carraway KL, Isola J, Jovin TM. Decreased accessibility and lack of activation of ErbB2 in JIMT-1, a herceptin-resistant, MUC4-expressing breast cancer cell line. Cancer Res 2005;65:473-82. IF: 7.656

3. **Friedländer E**, Barok M, Szöllősi J, Vereb G. ErbB-directed immunotherapy: Antibodies in current practice and promising new agents. Immunol Lett 2007. IF: 2.352

4. Vereb G, Ujlaky-Nagy L, **Friedländer E**, Vámosi G, Szöllősi J. Fluorescence Correlation Spectroscopy of Living Cells. In: Mendez-Vilas A, Labajos-Broncano L, editors. Modern Research and Educational Topics in Microscopy. Volume 2, Formatex Microscopy Book Series 3. Badajoz, Spain: Formatex; 2007. p 848-54.

5. Vámosi G, **Friedländer E**, Ibrahim SM, Brock R, Damjanovich S, Szöllősi J, Jovin TM, Vereb G. Activation of pre-formed oligomers of EGF receptors and their diffusion over short and long distances – complementarity of fluorescence correlation microscopy and FRAP in cellular diffusion measurements. In preparation / Submitted

10.2. Other publications

1. Krasznai ZT, **Friedländer E**, Nagy A, Szabó G, Vereb G, Goda K, Hernádi Z. Quantitative and functional assay of MDR1/P170-mediated MDR in ascites cells of patients with ovarian cancer. Anticancer Res 2005;25:1187-92. IF: 1.479

2. Kakuk A, **Friedländer E**, Vereb G, Jr., Kása A, Balla A, Balla T, Heilmeyer LM, Jr., Gergely P, Vereb G. Nucleolar localization of phosphatidylinositol 4-kinase PI4K230 in various mammalian cells. Cytometry A 2006;69:1174-83. IF: 3.293

3. Márián T, Szabó-Péli J, Németh E, Trón L, **Friedländer E**, Szabó A, Balkay L, Veress G, Krasznai Z. Na+/Ca2+ exchanger inhibitors modify the accumulation of tumor-diagnostic PET tracers in cancer cells. Eur J Pharm Sci 2007;30:56-63. IF: 2.482

Cumulated impact factor (SCI 2006): 20.555

10.3. Lectures and posters

1. Boda J, **Friedländer E**: Role of lipid rafts in the submicron cell- surface distribution and signal- transduction of the IL-2 receptor (11th European Students' Conference Berlin, 2000)

2. Vámosi G, Ibrahim SM, **Friedländer E,** Brock R, Jovin TM, Vereb G: Mobility and co-mobility of cell surface receptors studied by fluorescence correlation microscopy (XI. Symposium on the signals and signal processing in the immun system EFIS Pécs, 2001)

3. **Friedländer E,** Vámosi G, Ibrahim SM, Brock R, Jovin TM, Damjanovich S, Vereb G: Analysis of the function of the epidermal growth factor receptor-GFP fused protein (a Román Biofizikai Társaság Nagygyűlése Szováta, 2001)

4. Vámosi G, Ibrahim SM., **Friedländer E**, Brock R, Jovin TM, Vereb G: Epidermális növekedési faktor receptor- GFP fúziós fehérje membrán diffúziójának és működésének jellemzése (XI. Sejt - és Fejlődésbiológiai Napok Debrecen, 2001)

5. Nagy L, Boda J, **Friedländer E**, Szöllősi J, Vereb G: Gap junction kommunikáció gliblasztóma sejtekben és szerepe a PDGFR jelátvitelében (XI. Sejt - és Fejlődésbiológiai Napok Debrecen, 2001)

6. Vámosi G, Ibrahim SM, **Friedländer E**, Brock R, Jovin TM, Vereb G: EGF receptor - GFP fúziós fehérje működésének és diffúziójának fluoreszcencia korrelációs spektroszkópiás vizsgálata (Magyar Biofizikai Társaság XX. Vándorgyűlése Budapest, 2001)

7. Veress G, **Friedländer E**, Antal M, Vereb G: A CB1 kannabinoid receptor immunreaktív struktúrák karakterizálása patkány gerincvelőben (III. Magyar Sejtanalitikai Konferencia, Budapest, 2002)

8. Vámosi G, Ibrahim SM, Brock R, Majewski V, **Friedländer E,** Jovin TM, Vereb G: Fluorescence correlation microscopy of epidermal growth factor receptor stimulation (III. Magyar Sejtanalitikai Konferencia, Budapest, 2002)

9. **Friedländer E**, Kakuk A, Madarász E, Vereb G, Vereb G: A foszfatidil-inozitol 4-kináz PI4K230 izoformájának lokalizációja neurális sejtekben (III. Magyar Sejtanalitikai Konferencia, Budapest, 2002)

10. Krasznai ZT, Nagy A, Szabó G, **Friedländer E,** Hernádi Z: Multidrog rezisztencia kimutatása ovárium tumoros betegek aszciteszéből származó sejteken (Magyar Onkológus Vándorgyűlés, Budapest, 2002)

11. Vámosi G, Brock R, Ibrahim SM, **Friedländer E**, Majewski V, Damjanovich S, Arndt-Jovin D, Jovin TM and Vereb G: Fluorescent correlation microscopy of EGF receptor stimulation (2nd congress of the European Life Science Organization, Nice, 2002)

12. Veress G , Makkai B, **Friedländer E,** Holló K, Vereb G, Mackie K, Antal M.: Characterisation Of Cannabinoid Receptor 1 Immunoreactivity In The Spinal Cord Of The Rat (IBRO International Workshop on Signalling Mechanisms in the Central and Peripherial Nervous System, Debrecen, 2002)

13. **Friedländer E**, Vámosi G, Brock R, Ibrahim SM, Majewski V, Jovin T M and Vereb G: Mobility and compartmentation of epidermal growth factor receptor studied by FRAP and FCS (Methods and Applications of Fluorescence: Spectroscopy and Imaging and Probes, Prague, 2003)

14. Ujlaki-Nagy L, Petrás M, **Friedländer E**, Szöllősi J, Vereb Gy: Lipid raftok integritásának szerepe glioblasztoma sejtek PDGF receptorainak sejtfelszíni mintázatában) Magyar Biofizikai Társaság XXI. Kongresszusa, Szeged, 2003)

15. Vereb G, Nagy P, Vámosi G, Bodnár A, Zsebik B, Ujlaki-Nagy L, **Friedländer E**, Bacsó Z, Gombos I, Damjanovich S, Szöllősi J, Matkó J: Flow and Imaging Cytometric Analysis of Membrane Microdomains (Rafts) in Living Cells (Methods and Applications of Fluorescence: Spectroscopy and Imaging and Probes, Prague, 2003)

16. Krasznai, ZT, **Friedländer E**, Nagy A, Szabó G, Vereb G, Hernádi Z: Parallel functional and immunofluortescent detection of MDR1 P170 mediated multidrug resistance in tumour cells from ascites fluid of patients with ovarian cancer. (4th Congress in Characteristics in Obstetrics and gynecology and Infertility Berlin, 2003)

17. Veress G, **Friedländer E**, Vereb G, Antal M: Immunohystochemical Properties of the CB1 Cannabinoid Receptor Immunoreactive Structures in the Drosal Horn of the Spinal Chord of the Rat (Magyar Idegtudományi Társaság IX: Konferenciája, Balatonfüred, 2003)

18. **Friedländer E**, Vámosi G, Brock R, Ibrahim SM, Majewski V, Jovin TM, Vereb G.: Mobility and compartmentation of epidermal growth factor receptor studied by FRAP

and FCS (Summer School “Advanced Immunological techniques”, EPONA and University of Debrecen, 2003)

19. **Friedländer E**, Lidke D, Arndt-Jovin D, Jovin T, Szöllősi J, Vereb G: Cell stimulation using Herceptin® covered magnetic beads (International School of Biophysics, Non-Invasive Biophysical Methods and their application in Biology and medicine, Gaiser, 2003)

20. **Friedländer E**, Zsebik B, Nagy P , Arndt-Jovin D, Szöllősi J, Vereb G: Az ErbB2 receptorok molekuláris környezetének szerepe trastuzumab rezisztencia kialakulásában: lokális stimuláció mikrogyöngyökkel és kvantitatív digitális mikroszkópia (IV. Magyar Sejtanalitikai Konferencia, Budapest, 2004)

21. Orosz Á, **Friedländer E**, Tóth E. Juhász J, Juhász A, Berta A, Vereb G, Takács L: Primer sejtkultúrák létrehozása normál és 5q31-hez kapcsolt dystrophiás humán szaruhártyákból (IV. Magyar Sejtanalitikai Konferencia, Budapest, 2004)

22. **Friedländer E**, Lidke D, Arndt-Jovin D, Jovin T, Szöllősi J, Vereb G: Cell stimulation using Herceptin©-covered magnetic beads (XXII. ISAC International congress, Montpellier, 2004)

23. Juhász J, Miklóssy G, Fehér A, **Friedländer E**, Horváth G, Bagossi P, Tőzsér J, Vereb G, Szöllősi J: ErbB2 „shedding” mutánst expresszáló CHO sejtvonal előállítása és jellemzése (IV. Magyar Sejtanalitikai Konferencia, Budapest, 2004)

24. Vereb G, Nagy P, Zsebik B, **Friedländer E**, Isola J, Jovin T, Park J, Szöllõsi J: Molecular interactions of ErbB2: implications for cancer therapy (XXII. ISAC International congress,. Montpellier, 2004)